Deep Sea Research Part II: Topical Studies in Oceanography
May 2021, Volume 186-188, Pages 104936 (22p.)
https://doi.org/10.1016/j.dsr2.2021.104936
https://archimer.ifremer.fr/doc/00696/80831/

Distribution and long-term change of the sea surface carbonate system in the Mozambique Channel (1963–2019)

Lo Monaco Claire [1] , Metzl Nicolas [1, *], Fin Jonathan [1], Mignon Claude [1], Cuet Pascale [2], Douville Eric [3], Gehlen Marion [3], Tuyet Trang Chau Thi [3], Tribollet Aline [1]

[1] Laboratoire LOCEAN/IPSL, Sorbonne Université-CNRS-IRD-MNHN, Paris, 75005, France
[2] Laboratoire ENTROPIE and Laboratoire d'Excellence CORAIL, Université de La Réunion-IRD- CNRS-IFREMER-Université de la Nouvelle-Calédonie, Saint-Denis, La Réunion, 97744, France
[3] Laboratoire LSCE/IPSL, CEA-CNRS-UVSQ, Université Paris-Saclay Gif-sur-Yvette, 91191, France

* Corresponding author : Nicolas Metzl, email address : nicolas.metzl@locean.ipsl.fr

Abstract :

We report new oceanic carbonate system observations obtained during two cruises conducted in January 2004 (OISO-11) and April 2019 (CLIM-EPARSES) in the Mozambique Channel and estimate the long-term trend of sea surface fugacity of CO2 (fCO2) and pH using historical data. While in January 2004 the region was a large CO2 source, the ocean was near equilibrium in April 2019. Although this region experienced a dramatic cyclone event "Idai" in March 2019 leading to low salinity and low dissolved inorganic carbon (CT) and total alkalinity (AT) concentrations in the central channel, salinity normalized AT were unchanged and CT concentrations were higher in 2019 compared to 2004 by about 12 µmol.kg-1, likely due to anthropogenic CO2 uptake over 15 years. Compared to fCO2 observations of 1963 in the channel, the oceanic fCO2 was higher in 2004/2019 by about 100 µatm, an increase close to that observed in the atmosphere (90 ppm). A part of the fCO2 increase from 1963 to 2019 (about +10 µatm) is due to the long-term ocean warming in this region (+0.011 °C.decade-1). We estimated a mean decrease of −0.087 (±0.007) pH unit between 1963 and 2019, typical of the preindustrial versus modern change in the global ocean. Using other observations in the southern part of the Mozambique Channel (around 25°S) we estimated a pH trend of −0.0129.decade-1 (±0.0042) for 1963–1995 and −0.0227.decade-1 (±0.0048) for 1995–2019 suggesting a strengthening of acidification trend in the Mozambique Channel in agreement with the anthropogenic CO2 forcing. For the recent period, these rates were confirmed by reconstructed fCO2 and pH monthly fields using a neural network model. We noted however that the pH trend in the Mozambique Channel appeared lower than previous estimates at the scale of the Indian Ocean. Based on historical atmospheric CO2 data we estimated that pH in the Mozambique Channel was about 8.18 (±0.014) in the year 1800, i.e. 0.13 higher than in 2019. The concentration of CT in the year 1800 was likely around 1915 (±10) µmol.kg-1. These results will contribute to a better understanding of the impacts of ocean acidification on coral reefs since the industrial revolution by (1) providing a reference level for the reconstruction of pH from coral core samples that were collected at different locations in this region in 2019 and (2) by informing environmental authorities aiming at preserving and protecting those threatened ecosystems.

Highlights

► New observations of the marine carbonate system in the Mozambique Channel. ► First evaluation of long-term trends of sea surface fCO_2 and pH in the Mozambique Channel. ► The fCO_2 increase and pH decrease are mainly attributed to anthropogenic CO_2 uptake. ► Results suggest a strengthening of acidification trend in the Mozambique Channel since the mid-90s.

Keywords : Mozambique Channel, Ocean CO2, Acidification, Long-term trends

1 Introduction:

Since the industrial revolution, about 675 GtC of anthropogenic carbon dioxide (CO_2) has been emitted into the atmosphere (Friedlingstein et al, 2019) leading to an unprecedented growth of atmospheric CO_2 concentrations that reached on average 410 ppm in 2019 (Dlugokencky and Tans, 2020). Since 1750 about 25 % of anthropogenic CO_2 has been absorbed by the ocean (Friedlingstein et al, 2019) and about 31% during the period 1994-2007 (Gruber et al., 2019a). This absorption helps to mitigate global warming but induces ocean acidification (Doney et al 2009; Feely et al., 2009; Wu et al. 2018). The latter is a major threat to marine ecosystems (Fabry et al., 2008; Gattuso et al 2015). It impacts both calcifying organisms such as coccolithophores (Riebesell et al 2000; Beaufort et al., 2011), foraminifera (de Moel et al 2009), bivalves (Waldbusser et al, 2015; Tan and Zheng, 2020), and corals (Kleypas et al., 1999; Mollica et al. 2018), and major agents of carbonate dissolution, the bioeroding microflora and sponges (Schönberg et al. 2017). The accumulation of anthropogenic CO_2 in the ocean has led to a global decrease in pH in surface waters by on average -0.1 units since the industrial revolution (Jiang et al., 2019). It is projected to further decrease by on average -0.2 to -0.4 units by the end of the century depending on the anthropogenic emission scenario and locations (Orr et al., 2005; Jiang et al., 2019; IPCC, 2019). Although future pH changes appear to be more pronounced in the cold and high latitudes (especially in the Arctic) compared to equatorial upwelling areas, significant pH changes are also likely to occur in the tropics and subtropics (Jiang et al, 2019; Ono et al, 2019).

Long-term observations at fixed open ocean monitoring stations since the 1980s or the 1990s show that ocean pH declined between -0.0013 and -0.0026 units per year depending on the location (Bates et al., 2014). High rates of surface ocean acidification are reported for coastal zones, ranging from $-0.0020.yr^{-1}$ (± 0.0007) off the south coast of Japan (Ishii et al 2011) to $-0.0028.yr^{-1}$ (±0.0003) in the Mediterranean Sea (Kapsenberg et al, 2017). In coral reef areas, high-frequency variability (e.g. Hofmann et al, 2011; Cyronak et al., 2020) confounds the assessment of the long-term pH trend by direct measurements. However, pH time series reconstructed based on coral boron isotopic ratio ($\delta^{11}B$) allow to identify a prominent ocean acidification trend in the recent decades (e.g. Liu et al 2014; Wu et al, 2018; D'Olivo et al., 2019). A compilation of direct pCO_2 observations at several coral reef locations (Cyronak et al 2014) suggests that over 1992-2012 sea water pCO_2 increased at a rate of +6.6 (± 1.4) $\mu atm.yr^{-1}$, i.e. up to times 3.5 faster than in the atmosphere and the open ocean. At constant temperature and alkalinity this would lead to a fast pH decline of $-0.0055.yr^{-1}$ in coral reef areas against $-0.0018.yr^{-1}$ on average in the open ocean (Feely et al., 2009; Lauvset et al 2015; Iida et al, 2020) ultimately triggering net dissolution of reef structures (Eyre et al. 2018; Tribollet et al. 2019). At global scale, based on high quality surface ocean fCO_2 data compiled in the SOCAT data product version 2 (Bakker et al 2014; Pfeil et al 2013), and combined with regional alkalinity/salinity relationships (Lee et al 2006), Lauvset et al (2015) estimated rates of pH declines ranging from $-0.0010.yr^{-1}$ to $-0.0027.yr^{-1}$ in different basins over the period 1991-2011. The fastest pH decline of $-0.0024.yr^{-1}$ (± 0.0004) for the period 1981-2011 and of -

0.0027.yr^{-1} (± 0.0005) over 1991-2011 occurred in the Indian Ocean. In addition to ocean warming, such a rapid pH change, if confirmed by independent measurements and correlated to a rapid change of the carbonate saturation state, might put Indian Ocean coral reef ecosystems at risk, including many of those in the Mozambique Channel (e.g. Eparses Islands). In this oceanic region, *in situ* observations remain scarce as very few oceanographic campaigns have been conducted.

Here we present the first temporal observations of the sea surface carbonate system in the Mozambique Channel (including fugacity of CO_2, fCO_2, total alkalinity, A_T and dissolved inorganic carbon, C_T) measured during two cruises conducted in January 2004 and April 2019. We also use historical fCO_2 observations to explore the long-term change in fCO_2 and pH in this region over the period 1963-2019 and compare these variations with estimates of regional anthropogenic CO_2 concentrations and with reconstructed monthly pCO2 and pH fields derived from a neural network model (Denvil-Sommer et al, 2019; Chau et al, 2020).

2 Data collection and methods

2.1 Observations during the 2004 and 2019 cruises

In January 2004 (Cruise OISO-11, 8-Jan/7-Feb 2004) and April 2019 (project CLIM-EPARSES, 5-30 April 2019) we conducted two cruises in the Mozambique Channel on-board R.V. Marion-Dufresne (Figure 1, Table 1). During these cruises, underway continuous surface ocean measurements were made for temperature (SST), salinity (SSS), fugacity of CO_2 (fCO_2), total alkalinity (A_T) and total dissolved inorganic carbon (C_T). In addition, discrete sea surface samples were taken for the analysis of Chl-a and nutrients. In April 2019, the sampling scheme was completed by hydrocasts at selected stations (0-200m in coastal waters nearby the Eparses Islands, and 0-1000m in open waters between islands). With the exception of Chl-a, analytical methods follow the protocol used since 1998 during OISO cruises onboard R.V. Marion-Dufresne in the Southern Indian Ocean. They have been previously described (Jabaud-Jan et al., 2004; Metzl et al 2006; Metzl, 2009).

Sea surface temperature (SST) and salinity (SSS) were measured continuously using a SBE45 thermosalinograph. Salinity data were controlled by regular sampling and conductivity measurements (Guildline Autosal 8400B and using IAPSO standard/OSIL). Sea surface temperature and salinity were also checked against CTD's surface records. Accuracies of SST and SSS are about 0.005 °C and 0.01.

In addition to the continuous underway measurements, we regularly sampled surface water for Chlorophyll-a (Chl-a) and nutrients (Nitrate and Silicate). The Chl-a samples were stored at -80°C on-board after filtration and measured back in the laboratory using a fluorometric method (Aminot and Kerouel, 2004). Nitrate and silicate were measured onboard in January 2004 with an automatic colorimetric Technicon analyser following the methods described by Tréguer and Le Corre (1975).

Total alkalinity (A_T) and total dissolved inorganic carbon (C_T) were measured on-board for both underway continuous surface and water-column samples using a potentiometric titration method (Edmond, 1970) in a closed cell. The system is automatic for sampling continuously surface seawater and transferring it into the cell. For water-column measurements, samples were collected from Niskin bottles in 500 ml glass bottles for analysis within 4h or by adding 300 µl of saturated mercuric chloride solution before storage in a cool place for subsequent analysis. For calibration, we used the Certified Referenced Materials (CRMs, Batch #52, 58 and 62 for OISO-11 and Batch #173 for CLIM-EPARSES) provided by Pr. A. Dickson (SIO, University of California). For both cruises, we estimated the accuracy at about 3 µmol.kg^{-1} for both A_T and C_T (based on CRMs measurements). During CLIM-EPARSES standard errors of 122 replicates for surface samples were ±2.6 µmol.kg^{-1} for A_T and ±2.4 µmol.kg^{-1} for C_T. For OISO-11, a cruise that took place in January-February 2004 in the Mozambique Channel and the Southern Indian ocean (including 15 stations), errors of replicates for deep samples (n=19) was ±2.7 µmol.kg^{-1} for A_T and ±3.3 µmol.kg^{-1} for C_T. Errors of 31 replicates for surface samples were ±1.5 µmol.kg^{-1} for A_T and ±1.8 µmol.kg^{-1} for C_T. The water column data for OISO-11 have been quality controlled in CARINA (Lo Monaco et al., 2010) and revisited in GLODAPv2 (Key et al., 2015; Olsen et al., 2016) with no corrections applied for A_T and C_T. Surface underway A_T and C_T data for OISO-11 and CLIM-EPARSES are both available at NCEID/OCADS (Metzl and Lo Monaco, 2018; Lo Monaco et al, 2020b).

During CLIM-EPARSES in April 2019, one station located at 22.30°S/40.40°E was sampled near Europa Island. At 1000m, our measurements for A_T and C_T data are respectively 2334 µmol.kg^{-1} and 2247 µmol.kg^{-1}. We are not aware of any biogeochemical stations (including A_T and C_T data) in the central Mozambique Channel. However a WOCE line was sampled in the southern part at 25°S in June 1995 (Sabine et al., 1999) and reoccupied in December 2003 (Murata et al., 2010). These data are part of the GLODAPv2.2019 data product (Olsen et al., 2019). At 25°S around 1000m GLODAPv2.2019 data were in a range of 2310-2340 µmol.kg^{-1} for A_T and 2200-2255 µmol.kg^{-1} for C_T. Our measurements at 1000m at 22.30°S in 2019 are thus in the higher range of concentrations observed at 25°S in 1995 or 2003, not taking into account the natural variability and anthropogenic signals.

For fCO_2 measurements, sea-surface water was continuously equilibrated with a "thin film" type equilibrator thermostated with surface seawater (Poisson *et al.*, 1993). The CO_2 in the dried gas was measured with a non-dispersive infrared analyser (NDIR, Siemens Ultramat 5F or 6F). Standard gases for calibration (around 270, 350 and 480 ppm) and atmospheric CO_2 were measured every 6 hours. To correct xCO_2 dry measurements to fCO_2 *in situ* data, we used polynomials given by Weiss and Price (1980) for vapour pressure and by Copin-Montégut (1988, 1989) for temperature (temperature in the equilibrium cell was on average 0.73 °C warmer than SST during OISO-11 and 0.097 °C warmer during CLIM-EPARSES). The oceanic fCO_2 for both cruises are available in SOCAT data product (version v2020, Bakker et al., 2016, 2020) and at NCEI/OCADS (Metzl, 2018; Lo Monaco et al., 2020a). Note that when added to SOCAT, original fCO_2 data are recomputed (Pfeil et al., 2013) using temperature correction from Takahashi et al (1993). Given the small difference between SST and equilibrium temperature, the fCO_2 data from our cruises are identical (within 1 µatm) in SOCAT and NCEI/OCADS. For coherence with other cruises we therefore used fCO_2 values as provided by SOCAT.

Atmospheric xCO_2 measured on-board was on average 377.02 (± 0.73) ppm in January 2004 and 410.90 (± 1.40) ppm in April 2019 in the Mozambique Channel (Supp. Figure 1). This corresponds to an increase of +33.9 ppm in 15 years, coherent with global atmospheric xCO_2 values. Our measurements on board in this specific region (10°S-26°S) are almost identical to the global averaged marine surface monthly mean xCO_2 of 377.04 ppm for January 2004 and 411.06 ppm for April 2019 (Dlugokencky and Tans, 2020). The relatively large standard-deviation of atmospheric xCO_2 encountered in the Mozambique Channel (up to ± 1.4 ppm in 2019) compared to other OISO cruises in the Southern Indian Ocean (Metzl, 2009) is likely linked to the terrestrial signal from Africa and/or Madagascar depending on the season and wind fields. However given the increase of atmospheric xCO_2 over 15 years, the observed regional atmospheric xCO_2 variability during each cruise had no significant impact on the air-sea CO_2 disequilibrium that we explored in this study. We thus used the mean xCO_2 values for each cruise (377 and 411 ppm) and converted xCO_2 to fCO_2 at 100% humidity following Weiss and Price (1980) for air-sea disequilibrium estimates.

2.2 Other observations and data

In order to investigate the long-term variability of fCO_2 and pH we used all fCO_2 data available in the Mozambique Channel from the SOCAT data product (version v2020, Bakker et al., 2016, 2020): our observations for 2004 and 2019 and the only other cruise conducted in the Channel in May 1963 (Keeling and Waterman, 1968). These three cruises offer a first view of fCO_2 variations over several decades in the Mozambique Channel, between 14°S and 25°S. However, because they are representative of different seasons (January, April and May) we included fCO_2 data collected in the southern part of the Channel at around 25°S to confirm the fCO_2 and pH trends over decades deduced in the band 14°S-25°S. All the cruises used in this study are shown in Figure 1 (listed in Table 1) from which we select only recommended fCO_2 data (with WOCE Flag 2 in SOCAT). In addition, in order to separate the natural and anthropogenic CO_2 signals, we used water-column data from June 1995 and December 2003 along 25°S (Sabine et al, 1999; Murata et al., 2010) quality controlled in GLODAPv2.2019 (Olsen et al., 2019). Our estimates of anthropogenic CO_2 (hereafter C_{ant}) in this region will be compared to a recent evaluation of C_{ant} inventory changes in the global ocean between 1994 and 2007 (Gruber et al, 2019 a, b). To discuss the seasonality of the carbonate system and air-sea CO_2 fluxes in this region we will also compare our observations with the climatology produced by Takahashi et al (2009, 2014). Finally, we will compare our results with reconstructed pCO_2 and pH monthly fields for the period 1985-2019 derived from a neural network model (named CMEMS-LSCE-FFNN, Denvil-Sommer et al., 2019; Chau et al 2020).

2.3 Calculations of carbonate system properties and anthropogenic carbon

Based on the carbonate properties available for each cruise (fCO_2, A_T and C_T) other carbonate system properties (like pH, $[H^+]$ or the carbonate saturation state Ω) are calculated using the CO2sys program (version CO2sys_v2.5, Orr et al., 2018) developed by Lewis and Wallace (1998) and adapted by Pierrot et al. (2006) with K1 and K2 dissociation constants from Lueker et al. (2000) and KSO_4 constant from Dickson (1990). The total boron concentration is calculated according to Uppström (1974). We have tested different K1, K2 constants (Merbach et al, 1973; Hansson, 1973; Dickson and Millero, 1987) and compared measured fCO_2 with fCO_2 calculated from A_T/C_T pairs collocated in space and time (Supp. Figure S2a,b). Given the uncertainties associated to the measurements of temperature (0.005°C), salinity (0.01), A_T and C_T (2.5 µmol.kg^{-1}), the error on calculated fCO_2 is ±13 µatm. This error is generally larger than the mean differences observed between measured and calculated fCO_2 (Supp. Figure S2b). For example, the average differences between measured and calculated fCO_2 when using K1, K2 constants from Lueker et al (2000) were -5.3 (std ±4.9) µatm for 154 co-located samples in January 2004, and +4.5 (std ±5.2) µatm for 268 co-located samples in April 2019. In line with previous recommendations (Dickson et al, 2007; Orr et al, 2015) we used constants from Lueker et al (2000) for all calculations. To account for the effect of salinity on A_T and C_T concentrations these properties are also normalized at constant salinity (35) following N-A_T = A_T * 35/SSS and N-C_T = C_T * 35/SSS. In this study we are interested in evaluating fCO_2 variations over several decades. As fCO_2 is highly dependent on SST, fCO_2 will be also normalized at constant temperature (29°C) following the relation established by Takahashi et al (1993).

$$fCO2_{29} = fCO2_{SST} * EXP\ (0.0423*(29-SST)) \quad (1)$$

For anthropogenic CO_2 calculations in the water column (C_{ant}) we used the TrOCA method (Touratier et al 2007) that was previously applied and compared to other methods in the Southern Indian Ocean along the 32°S section (Álvarez et al, 2009). In short, given A_T, C_T, Oxygen (O_2) and potential temperature (θ) observations at each depth level, the C_{ant} concentrations is derived from the evolution of the quasi-conservative tracer TrOCA compared to its pre-industrial value (see Touratier et al 2007 for a full description). The final expression used to calculate C_{ant} is:

$$C_{ant} = \frac{O_2 + 1{,}279\left(C_T - \frac{1}{2}A_T\right) - e^{\left[7{,}511 - \left(1{,}087.10^{-2}\right).\theta - \frac{7{,}81.10^{5}}{A_T^{2}}\right]}}{1{,}279} \qquad (2)$$

To compare with the observed C_T long-term trend in surface waters and given the uncertainty on C_{ant} of ±6.25 µmol.kg^{-1} using the TrOCA method (Touratier et al., 2007) our interpretations in the Mozambique Channel region will be limited to the upper layers (150-200m). In the Southern Indian subtropical region C_{ant} concentrations are generally less than 10 µmol.kg^{-1} below 1000m (Sabine et al, 1999; Álvarez et al 2009) and C_{ant} accumulation between 1994 and 2007 less than 10 µmol.kg^{-1} below 500 m (Murata et al., 2010; Gruber et al., 2019a).

2.4 Neural network reconstruction of the surface ocean carbonate system.

Surface ocean partial pressure of carbon dioxide (pCO_2) is obtained from an ensemble-based feed-forward neural network (FFNN) model described in Denvil-Sommer et al. (2019). For this study, we used results of the latest version of the model (Chau et al, 2020) which was developed as part of the Copernicus Marine Environment Monitoring Service (CMEMS). The mean pCO_2 of a 100 member ensemble is used for comparison and trend analysis throughout this study. Surface ocean pH is computed from reconstructed pCO_2 and alkalinity with the speciation software CO2sys-MATLAB_V2.05 (Van Heuven et al, 2011; Orr et al 2018). The multivariate linear regression model LIAR (Carter et al., 2016; 2018) is used to derive time and space varying surface ocean alkalinity fields as a function of sea surface temperature and salinity, as well as climatological monthly mean nitrate and dissolved silica concentrations from the World Ocean Atlas 2013 version 2 (Garcia et al, 2014; www.nodc.noaa.gov/OC5/woa13/). Global surface ocean pCO_2 and pH reconstructions at 1°x1° resolution start in 1985 and are updated annually in phase with yearly releases of SOCAT data. Here we used the SOCAT version v2020 (Bakker et al, 2020) and the model fields calculated for the period 1985-2019. For a full description, access to the data and a statistical evaluation of pCO_2 and pH reconstructions please refer to Chau et al (2020).

3 Results

3.1 Surface properties observed in January 2004 and April 2019 in the Mozambique Channel

3.1.1 Distributions along the Mozambique Channel

Here we first present the description of sea surface observations obtained in January 2004 and April 2019 in the Mozambique Channel. Underway measurements of SST, SSS and fCO_2 are shown in Figure 2 while A_T and C_T observations are presented in Figure 3. Averaged values in the band 14-25°S are listed in Table 2.

During both cruises SST presents a gradual increase from south to north (Figure 2a). SST was generally higher in January 2004 than in April 2019 except in the South (26°S) and in the North (14°S) of the Channel. In January 2004, SST reached the maximum value of 30°C at 22°S and was quite homogeneous in the band 14°S-22°S, whereas in April 2019, SST increased more gradually to reach 30.5°C north of Madagascar. We observed large SST and SSS variability in the central part of the Channel (18°S-22°S) probably linked to eddies occurring regularly in this region (Halo et al 2014; Hancke et al 2014; Ternon et al 2014). This was well identified from one drifting buoy migrating southwards with an anticyclonic eddy in March-April 2019 (Supp. Figure S3). The SST and SSS variability in the central part of the Channel is also recognized in A_T and C_T distributions (Figure 3) but not in fCO_2 (Figure 2c) because the effects of A_T and C_T on fCO_2 offset each other.

During each cruise, we observed a sharp front of salinity in the central part of the Mozambique Channel that was not associated to a change in SST: in January 2004 the front was located around 17°S (near Juan de Nova Island) whereas it was found at 22.5°S in April 2019 (south of Europa Island). Although the salinity was about the same in 2004 and 2019 in the South and the North of the channel, it was very different in the central region (17°S-23°S, Figure 2b). The low salinity (SSS < 35) observed in April 2019 was linked to an excess of precipitations that occurred in March during the dramatic tropical cyclone event called “Idai” (monthly anomaly of precipitation up to 150 mm in the band 18°S-22°S, Supp. Fig S4). This signal was confirmed by an Argo float (Platform Code 2902142) that recorded salinity as low as 34 in the surface layer in this region in late March 2019 (Supp Fig S5).

Precipitations caused by the cyclone Idai directly impacted the concentrations of A_T and C_T which were thus much lower in April 2019 in the central part of the channel (Figure 3a, b), although one would expect an increase in C_T over 15 years due to the accumulation of anthropogenic CO_2. The salinity fronts at 17°S or 22.5°S (depending on the cruise) were also well identified in A_T and C_T (Figure 3). The salinity normalized A_T (N-A_T) and C_T (N-C_T) distributions present much less spatial variability than A_T and C_T and are remarkably homogeneous in the Mozambique Channel south of 14°S during each cruise (Figure 4).

3.1.2 Differences in A_T and C_T between 2004 and 2019

The largest difference in N-C_T between 2004 and 2019 is observed in the southern part of the channel (21°S-25°S) where N-C_T concentrations were 10 to 20 µmol.kg^{-1} higher in April 2019 compared to January 2004 whereas N-A_T values were almost identical for both periods (Figure 4, Table 2). Given that C_T (and N-C_T) climatological annual cycles present higher concentrations in January than in April in the subtropical southern Indian Ocean including the Mozambique Channel (Bates et al 2006; Takahashi et al 2014, Supp Figure S6), the N-C_T average increase of +11.8 µmol.kg^{-1} observed between 2004 and 2019 (mean trend of 0.8 µmol.kg^{-1}.yr^{-1}) likely underestimates the anthropogenic signal. Taking into account the seasonality (based on the C_T climatology computed by Takahashi et al 2014, Supp Figure S6), C_T would be 16.9 µmol.kg^{-1} lower in April 2004 than in January 2004 (N-C_T in April 2004 would be 1952.2 µmol.kg^{-1} on average) and the annual increase from April 2004 to April 2019 would be +1.04 (± 0.79) µmol.kg^{-1}.yr^{-1} (Table 2). This number is in the range of the theoretical C_T trend of +1.2 µmol.kg^{-1}.yr^{-1} calculated by assuming that surface ocean fCO_2 follows the atmospheric growth rate observed over 2004-2019 (+2.2 ppm.yr^{-1}). This suggests that most of the increase in N-C_T is due to the accumulation of anthropogenic CO_2, which could also explain part of the changes in fCO_2 and pH observed between 2004 and 2019, as well as the long-term trends investigated back to the sixties in section 3.2.

3.1.3 fCO_2 variability, seasonality and biological processes.

Although the C_T and A_T distributions along the Mozambique Channel present large gradients associated with the salinity fronts at 22.5°S or 17°S (Figure 3), their impact on fCO_2 cancel each other and the fronts are not recognized in fCO_2 measurements (Figure 2c). In April 2019, fCO_2 increased progressively northward like SST, leading to a positive fCO_2/SST relationship, except for measurements conducted in the vicinity of Juan de Nova near 17°S (Supp. Figure S7). In January 2004, the fCO_2 distribution presented a larger spatial variation leading to a poor relation between fCO_2 and SST (Supp. Figure S7), notably due to the low fCO_2 values (below 390 µatm) and high SST observed north of 15°S and around 22°S where we also measured minima in C_T (Figure 3b) and in N-C_T (Figure 4b). These signals were linked to locally enhanced biological activity revealed in both surface Chl-a *in-situ* measurements around 15°S and 22°S in January 2004 (Supp. Fig S8) and at regional scale in the monthly Chl-a distribution derived from MODIS (Supp. Fig S8). In April 2019, *in-situ* Chl-a concentrations were in the same range as in January 2004 with few local maxima also detected around 15°S and 22°S (Supp. Fig S8) and also associated with minima in C_T and N-C_T (Figures 3b, 4b). In the vicinity of the islands (Europa at 22°S and Juan de Nova at 17°S) the Chl-a concentrations in April 2019 present some variability but in the range of observations in the open ocean (0-0.25 $mg.m^{-3}$). High *in-situ* Chl-a concentrations are thus only identified at small-scale during both cruises and these local events do not impact the overall trend of the fCO_2 and C_T changes in the Channel between 2004 and 2019. Instead, satellite derived Chl-a products suggest a rather homogeneous Chl-a distribution and slightly higher values in April 2019 compared to January 2004, notably in the central region (Supp Figure S8a). This is reflected in the mean seasonal cycle of Chl-a in this region, suggesting a slight gradual increase of Chl-a from December to July (Supp Figure S9). Over the region 15°S-26°S, the average Chl-a concentration derived from MODIS was 0.11 $mg.m^{-3}$ in January 2004 and 0.17 $mg.m^{-3}$ in April 2019, a mean difference of only 0.06 $mg.m^{-3}$ not captured in our *in-situ* localized data (Supp Figure S8). In April 2019, the MODIS Chl-a concentrations of 0.17 $mg.m^{-3}$ were the same as the mean climatological value for April (0.17 $mg.m^{-3}$ ±0.02 on average for years 2003-2019, Supp. Figure S9). Thus, although one would expect the cyclone "Idai" that occurred in March 2019 to have impacted primary production (e.g. through input of nutrients either from the subsurface or from terrigenous material through atmospheric transport), we conclude that, except for salinity, observations in April 2019 were close to climatological conditions.

As noted above, climatological C_T concentrations in the channel are on average lower in April than in January (Takahashi et al, 2014) and the fCO_2 decrease from January to April cannot be explained by temperature alone. The seasonal C_T change between winter and summer (up to 30 $\mu mol.kg^{-1}$) is likely driven by biological activity but not directly recognized by Chl-a observations (Supp. Figure S9). This seasonal drawdown of C_T is potentially associated to biological N_2-fixation similarly to observations in the south-western tropical Pacific where a similar C_T seasonality has been reported (Moutin et al., 2018).

In the Western Indian Ocean and the Mozambique Channel *Trichodesmium* blooms (N_2-fixers) have been detected from satellite data (Westberry and Siegel, 2006). However, the occurrence of blooms from remote sensing data only remains qualitative and obviously limited to large surface aggregations of cells (McKinna, 2015). The hypothesis that diazotrophy may play a significant role in C_T and fCO_2 seasonality is further supported by the observation of high abundances of *Trichodesmium* spp in the Mozambique Channel in April 2011 (Dupuy et al, 2016) but we have no *in-situ* data to document this process during the 2004 and 2019 cruises.

3.1.4 Difference in fCO_2 between 2004 and 2019

Although atmospheric fCO_2 was much higher in 2019 than in 2004, the oceanic fCO_2 range was similar (between 380 and 420 µatm for both periods, Figure 2c) as well as the mean fCO_2 in the band 14°S-25°S (Table 2). In January 2004, the ocean fCO_2 was much higher than in the atmosphere (a CO_2 source) with ΔfCO_2 ($\Delta fCO_2 = fCO_{2oc}-fCO_{2atm}$) ranging from 20 to 50 µatm, with a mean value of +36.8 (± 8.9) µatm. In April 2019, the mean ΔfCO_2 value was much lower (+2.5 ± 7.9) µatm: the ocean was a CO_2 source north of 18°S (maximum ΔfCO_2 of +20 µatm), near-equilibrium with the atmosphere in the central channel (22°S-18°S) and a CO_2 sink south of 25°S (minimum ΔfCO_2 of -20 µatm). Not taking into account the increase in oceanic fCO_2 from 2004 to 2019 due to anthropogenic CO_2 uptake, our mean results showing a CO_2 source in January and near-equilibrium in April, are coherent with monthly climatological ΔfCO_2 values in this region, i.e. +19.95 (± 3.3) µatm for January and +1.2 (± 5.3) µatm for April (Takahashi et al. 2009). Since very few observations in the Mozambique Channel were used to construct the pCO_2 climatology (Takahashi et al., 2009) our results validate the pCO_2 extrapolation in this region that has been later used to create C_T and pH climatologies (Takahashi et al 2014).

In the ocean the seasonal variation of fCO_2 is controlled by a complex interplay of thermodynamic, biological, chemical and mixing processes (Takahashi et al. 2002). In the subtropics, including the South Indian Ocean sector, the effect of temperature is generally found to be the dominant process at seasonal (Louanchi et al., 1996; Metzl et al., 1995; Takahashi et al. 2002) and inter-annual scales (Metzl et al., 1998). In order to take into account the thermal effect, observed fCO_2 in January 2004 and April 2019 were normalized to a constant temperature of 29°C (fCO_2-29C) close to the average SST observed in January and April. The fCO_2-29C distributions are shown in Figure 4c. For both periods, fCO_2-29C variations tend to follow the N-C_T distributions (Figure 4b). As opposed to fCO_2, but like for N-C_T, fCO_2-29C was on average slightly higher in April 2019 (403.4 ± 8.5 µatm) than in January 2004 (391.9 ± 10.9 µatm). The difference of only +11.5 µatm is much lower than the atmospheric increase of +33.9 ppm between 2004 and 2019. The temperature drives only part of the fCO_2 monthly variations and it is thus important to correct for other seasonal contributions to evaluate long-term trends in fCO_2. If we adjust the fCO_2 observed in January 2004 to April 2004 based on the climatology (Takahashi et al., 2014, Supp Fig S6b), fCO_2 data for January are reduced by 28.1 µatm and we obtain a mean value of 370.8 µatm for April 2004 (Table 2). The fCO_2 increase from April 2004 to April 2019 would lead to a rate of

1.75 (± 0.81) µatm.yr^{-1} over the last 15 years, slower than +2.2 ppm.yr^{-1} in the atmosphere over the same period. At constant A_T the observed increase in fCO_2 would translate into a trend of +1.01 (± 0.45) µmol.kg^{-1}.yr^{-1} in C_T, the same rate deduced from C_T measurements described above (+1.04 ± 0.79 µmol.kg^{-1}.yr^{-1} for C_T also adjusted to April, Table 2). This simple calculation based on 2 cruises conducted 15 years apart indicates that on average CO_2 concentrations increased in the Mozambique Channel at a rate of around 1.0 µmol.kg^{-1}.yr^{-1} and that seasonal signals of fCO_2 and C_T have to be taken into account to properly evaluate the fCO_2 and C_T trends. The same is true when one uses fCO_2 data and A_T/SSS relationship to calculate pH and to evaluate the long-term signal of ocean acidification (e.g. Lauvset et al., 2015).

3.1.5 Selecting the regional A_T/SSS relationship

Similar to what is commonly observed in the global ocean (Millero et al., 1998) there is a strong relationship between A_T and salinity for both cruises (Figure 5), except in the vicinity of Mayotte Island in January 2004 (north of 14°S). The A_T/SSS relationships are almost the same for January 2004 and April 2019 and close to A_T/SSS relationships derived at large scale in the subtropics or in the Indian Ocean (Millero et al., 1998; Lee et al., 2006). This suggests that these empirical A_T/SSS relationships could be used to reconstruct spatial and temporal distribution of A_T from salinity. In turn, pH can be calculated from reconstructed A_T and fCO_2 data (when only fCO_2 data are available as it is the case for SOCAT, Bakker et al., 2016). In order to select the best A_T/SSS relationship for the Mozambique Channel, we first compared several relations with A_T measurements obtained in January 2004 and April 2019 (Supp. Figure S10). All relationships, including that of Millero et al. (1998) or Lee et al. (2006), lead to the same residuals with no statistical differences. Therefore, in the following we used the A_T/SSS relationship derived from our observations in 2004 and 2019 (black line in Figure 5): A_T (µmol.kg^{-1}) = 73.841 (± 1.15) * SSS – 291.02 (± 40.4) (n= 548, r^2= 0.88).

3.1.6 Detecting recent pH changes in the Mozambique Channel

The A_T/SSS relationship described above enables to calculate pH from fCO_2 and SSS underway measurements. Here we are first interested in detecting the change in pH between 2004 and 2019. As we had A_T, C_T and fCO_2 observations for both cruises, we compared pH calculated with A_T and C_T pairs or with fCO_2 and A_T based on the A_T/SSS relationship. Average calculated pH values in the band 14°S-25°S are listed in Table 3. Both results are presented in Figure 6 for pH at 29°C (pH-29C). Although calculated pH is subject to uncertainties due to the error in each property (SST, SSS, A_T, C_T or fCO_2) the overall pH-29C distributions are the same either based on A_T-C_T pairs or on underway fCO_2 data. Except in the vicinity of the islands pH-29C values ranged between 8.02 and 8.06. Although pH values at in-situ temperature were almost the same (Table 3), pH-29C values were clearly lower in April 2019 compared to January 2004 (Figure 6, Table 3). On average pH-29C in April 2019 was lower by -0.0116 or -0.0218 depending on the calculation. The pH difference between the 2 cruises reflects both the seasonality and probably the pH decrease due to the accumulation of anthropogenic CO_2 over 15 years. To take into account the seasonality, we adjusted the mean fCO_2 and C_T observation in January 2004 to April 2004 based on the climatology (Takahashi et al., 2014) and recalculate pH adjusted to April 2004 (Table 3). The pH difference between 2019 and 2004 was -0.0238 (± 0.0018) (using average fCO_2 data and associated errors) or -0.0244 (±0.0050) (using average A_T-C_T data). Over 15 years, both results lead to a trend of between -0.0154.decade^{-1} and -0.016.decade^{-1} (Table 3). Given all uncertainties attached to pH calculations, our estimates either based on fCO_2 (and reconstructed A_T) or A_T-C_T observations show that acidification occurred in the Mozambique Channel at a rate similar to that reported for the northern subtropics (-0.017.decade^{-1}, e.g. Bates et al., 2014; Ono et al, 2019). This is, however, much lower than previous estimates of pH trends derived from fCO_2 data at large scale in the Indian Ocean. Lauvset et al (2015) report rates between -0.024.decade^{-1} for the period 1981-2011 and -0.027.decade^{-1} for 1991-2011 which suggests a faster pH decrease in the Indian Ocean compared to other regions. The pH trend of -0.00160.yr^{-1} (± 0.00149) derived in our observations in the Mozambique Channel between 2004 and 2019 is also close to the average trend of -0.00165.yr^{-1} (± 0.00038) computed over 2004-2019 in the same region from reconstructed monthly pH fields using a neural-network method (Denvil-Sommer et al., 2019; Chau et al 2020).

The carbonate system parameters (A_T, C_T, fCO_2) measured in January 2004 and April 2019 described in this section, along with pH estimates using different inputs (A_T and C_T or fCO_2), show that (i) N-A_T concentrations are stable, (ii) there is a well characterized A_T/SSS relationship, (iii) the changes in C_T, fCO_2 and pH over 15 years are significant and (iv) when seasonality is taken into account the observed trends of C_T, fCO_2 and pH likely reflect the uptake of anthropogenic CO_2. In the following section, we explore these signals over a longer time period extending back to the sixties.

3.2 Detecting the long-term trends of fCO_2 and pH in the Mozambique Channel

3.2.1 Comparison with historical observations collected in the Mozambique Channel in 1963

In order to explore the long-term change in fCO_2 and pH in the Mozambique Channel, we compared our fCO_2 observations obtained in 2004 and 2019 with the only other fCO_2 dataset obtained in this region along a latitudinal transect in May 1963 (Keeling and Waterman, 1968). To estimate pH changes, we used fCO_2, SST and SSS data for the 3 cruises and the A_T/SSS relation described above. We note that in May 1963, salinity was not measured and for this cruise we used the mean monthly salinity from the World Ocean Atlas, WOA (Antonov et al., 2006), as listed in the SOCAT data product (Bakker et al., 2016). The mean WOA salinity in the band 14°S-25°S in May is 34.88 close to those measured in January 2004 (35.15) and April 2019 (34.97). The use of WOA salinity has a negligible impact on pH calculations and derived trends. The comparison of observations obtained in 1963, 2004 and 2019 is presented in Figure 7 for the original data and in Figure 8 for fCO_2 and pH normalized at SST 29°C along with calculated N-C_T for these cruises.

The atmospheric xCO_2 value in May 1963 was around 315 ppm, 90 ppm lower than in 2019. Like in April 2019, oceanic fCO_2 in May 1963 was quite homogeneous in the Mozambique Channel increasing progressively northward with values ranging from 290 µatm at 25°S to 305 µatm at 16°S (Figure 7b). This region was a small CO_2 sink during this period. Average ΔfCO_2 was -9.3 (± 4.9) µatm in May 1963, very close to the climatological value for May (-5.3 ±7.4 µatm for a reference year 2000, Takahashi et al., 2009) and not very different from our recent observations in April 2019 (near equilibrium with average ΔfCO_2 of +2.5 ±7.9 µatm). The most remarkable change is, like for atmospheric CO_2, the much lower ocean fCO_2 observed in May 1963 (Figure 7b, Table 2). Consequently this leads to higher pH in 1963 compared to 2004 or 2019 (Figure 7c, Table 3). Based on these data, oceanic fCO_2 increased by + 101 (± 5) µatm from 1963 to 2019 and pH decreased by -0.104 (± 0.006). This change in pH is similar to the reduction estimated for the global ocean between preindustrial and modern times of -0.11 (Jiang et al., 2019). These differences are a snapshot between two cruises conducted 56 years apart and modulated by SST variations that should be taken into account to better interpret the long-term trends of fCO_2 and pH.

3.2.2 Seasonal temperature and the impact of long-term warming on the fCO_2 trend

The observed SST seasonal variation is significant with the ocean being much colder in May 1963 compared to January 2004 or April 2019 (Figure 7a). The measurements in 1963 present also a sharp front in SST at 20°S which is not seen in fCO_2 records (Figure 7b). This is probably because both A_T and C_T concentrations in May 1963 (not measured in 1963) drive fCO_2 the same way as observed in April 2019 (see description above, Figure 2). In 1963, the increase in SST from 24°C in the south to 27°C in the north would lead to a fCO_2 increase of about +45 µatm but measurements show only a difference of + 15 µatm from south to north. This suggests a competitive balance between the thermal, physical and biological processes, all leading to rather homogeneous fCO_2 and pH distributions in 1963 (Figures 7b,c).

In addition, the Indian Ocean, including the Mozambique Channel, experienced a significant long-term warming in recent decades that would drive part of the fCO_2 and pH trends. Based on monthly SST products (Reynolds et al., 2002) extracted at 15°S-20°S in the Mozambique Channel from 1981 to 2019 we estimated an annual long-term warming of +0.011 (± 0.007) °C.yr^{-1} (Supp. Figure S11). Such a pronounced warming has also been identified in the Indian Ocean subtropics (> 0.1°C.decade^{-1}) dating back to the sixties (Alory et al, 2007; Roxy et al, 2014). It could be due to a fast response to recent climate change or to natural multi-decadal variability (Zinke et al 2014). Relying on corals sampled in the reefs off Southwestern Madagascar at 43°E-23°S, Zinke et al (2014) reconstructed a warming rate of +0.13 °C.decade^{-1} between the years 1720 and 1800 and between 1900 to present.

A long-term warming around +0.1°C.decade $^{-1}$ is also consistent with the observed SST in May 1963 in the band 14°S-20°S (26.82 ± 0.25 °C) being 0.7°C lower than the mean climatological SST in May computed in recent years (27.52 ± 0.39°C for the period 2000-2018). This long-term warming would increase sea surface fCO_2 by about +7.5 µatm and would decrease pH by -0.009 units, a signal not directly linked to the oceanic CO_2 uptake. This corresponds to about 7% of the net fCO_2 increase of +101 µatm observed between 1963 and 2019.

3.2.3 Changes in fCO_2, pH and C_T in the Mozambique Channel over 56 years

To separate the effect of temperature and anthropogenic CO_2, fCO_2 and pH were normalized at SST 29°C (Figure 8a, b). We also compared N-C_T calculated with fCO_2 and reconstructed A_T for the 3 cruises (Figure 8c, Table 2). To validate the pH and N-C_T calculations based on fCO_2 data for 1963, we first compared the N-C_T calculated with fCO_2 (N-C_{Tcal}) and reconstructed A_T with N-C_T derived from the measurements (N-C_{Tmes}) described in Section 3.1 for 2004 and 2019. On average and taking into account the uncertainty of the measurements and calculations, the N-C_{Tcal} and N-C_{Tmes} values were of the same order for each cruise (Table 2). In 2019 both N-C_{Tcal} and N-C_{Tmes} were higher than in 2004 (respectively +7 and +12 µmol.kg^{-1}) and adjusted values for April lead to the same N-C_T trend for 2004-2019 (Table 2). We have thus confidence in N-C_T and pH values calculated with fCO_2 and the A_T/SSS for 1963.

For all three cruises, fCO_2-29C and N-C_T decreased northward and the opposite for pH-29C (Figure 8). In May 1963 the decrease occurred more sharply at the SST front near 20°S (Figure 7a). Consequently, the changes in fCO_2, pH and N-C_T between 1963 and 2004/2019 are slightly more pronounced in the North. The same contrast is observed for aragonite (Ω_{Ar}) and calcite (Ω_{Ca}) saturation states calculated with fCO_2 and A_T/SSS for each cruise (Supp. Figure S12).

On average fCO_2 and N-C_T in 1963 were much lower than in 2004 and 2019, and pH-29C much higher (Figure 8, Table 2, 3). To estimate the long-term trend, fCO_2 observations in May 1963 were adjusted to April 1963 (+11.9 µatm based on the climatology) and compared with April 2004 and 2019 to calculate the trends (Tables 2, 3). From 1963 to 2004, the fCO_2, N-C_T and pH trends were respectively +1.5 (± 0.3) µatm.yr^{-1}, +1.0 (± 0.4) µmol.kg^{-1}.yr^{-1} and -0.0015.yr^{-1} (± 0.0004). From 1963 to 2019 results are almost the same, +1.6 (± 0.2) µatm.yr^{-1}, +1.0 (± 0.3) µmol.kg^{-1}.yr^{-1} and -0.0015.yr^{-1} (±0.0003).

These results, although based on only three cruises, are remarkably close to the atmospheric xCO_2 trend of +1.6 ppm.yr^{-1} over 1963-2019 and to theoretical trends of +1.04 µmol.kg^{-1}.yr^{-1} for C_T and -0.00165.yr^{-1} for pH assuming that the ocean followed the atmospheric CO_2 increase and constant alkalinity. Subtracting the effect of the long-term warming in this region (+0.011°C.yr^{-1}) on the fCO_2 trend (+0.13 µatm.yr^{-1}), leads to a trend of fCO_2 of 1.39 µatm.yr^{-1} (1963-2004) or 1.44 µatm.yr^{-1} (1963-2019) that would reflect the anthropogenic CO_2 uptake. Our results also suggest that observed trends in the Mozambique Channel were slightly more pronounced in the recent decades (Tables 2, 3), but this is deduced from only three cruises. For a better evaluation of the decadal variability and long-term trends we now focus on the southern region of the Mozambique Channel where more fCO_2 data are available for different seasons and years (Table 1).

3.3 Long-term trends in the southern region of the Mozambique Channel

To confirm the changes observed in the Mozambique Channel from the three cruises in 1963, 2004 and 2019, we explored the fCO_2 and pH variations based on all data available in SOCAT-v2020 around 25°S. Here we selected the data in the region 23.5°S-26.5°S/38°E-42°E (identified with a green circle in Figure 1). This added 3 cruises conducted in June 1995, December 2003 and July 2014 (Table 1). In 1995 and 2003 C_T and A_T were also measured at fixed stations (Sabine et al., 1999; Murata et al., 2010) and we used these surface data (3-10m) to compare with N-C_T calculated from fCO_2 and A_T.

Sea surface temperature, fCO_2 and pH (calculated) for the six cruises are shown in Figure 9 and the averages of observed and calculated properties around 25°S for each cruise are listed in Table 4. For each period SST, fCO_2 and pH are fairly homogeneous in this region (Figure 9) and this translates into a low standard-deviations around the mean (Table 4). The ocean was colder in May, June and July than in December, January and April (Figure 9a). For the cold season as expected, the fCO_2 was the lowest in May 1963 (< 300 µatm) compared to June 1995 (>300 µatm) and July 2014 (>350 µatm) and pH was higher in 1963 (> 8.15) compared to 2014 (< 8.09). During the warm season (December-April), fCO_2 was always higher than 370 µatm (Figure 9b). As described above, the same fCO_2 values (near 390 µatm) were observed in January 2004 and April 2019, i.e. 15 years apart. The lowest pH (range 8.033 < pH < 8.066) was always observed during the warm season (Figure 9c).

The two cruises conducted one month apart in December 2003 and January 2004 on different ships recorded surprisingly the same range of fCO_2, around 385-390 µatm (Table 4). At 40°E, however, despite SST being the same (Figure 9a), fCO_2 was higher in December 2003 than in January 2004 by +12 µatm on average (Figure 9b). This is opposed to the climatology according to which December fCO_2 is generally lower by -20 µatm than January in this region (Supp. Figure S6). An inspection of the Quality Control information available on-line in SOCAT (www.socat.info) indicated that for the December 2003 cruise (Expocode 49NZ20031209) there was no equilibrator temperature and pressure recorded. We are thus less confident with the accuracy of fCO_2 data for this cruise (Lauvset et al, 2019). Like for our cruises in 2004 and 2019, the C_T concentrations measured in 1995 and 2003 were close to the C_T calculated from fCO_2 and our A_T/SSS relationship (last two columns in Table 4) confirming the pH values calculated the same way for different years and seasons. For the trend analysis we thus use pH and C_T calculated using fCO_2 data for all cruises (except December 2003).

The temporal evolutions of fCO_2, pH and N-C_T averaged at 25°S are shown in Figure 10 and the trends evaluated on different periods listed in Table 5 and illustrated in Figure 11. The trends were estimated after adjusting fCO_2 data to June each year (grey diamonds in Figure 10). We also compared the observational results with the pCO_2 and pH values reconstructed by Chau et al (2020). Here we extracted the CMEMS-LSCE-NN model gridded results at the location 25°S-40°E. The trends from the model are evaluated for June to compare with observations (Figure 12) or using the annual values (Table 5). Given the errors in the trends estimated for each property based on both measurements uncertainty, spatial variability and pH or N-C_T calculations, trends for short periods, e.g. 1995-2004 (Figure 11) have large errors and thus the interpretation of observed changes is mainly limited to multi-decadal variations (1963-1995 versus 1995-2019).

We first noted that the long-term trends estimated with all data at 25°S are almost identical to those derived when using only 1963 and 2019 observations in the Mozambique Channel for the band 14°S-25°S as described above. This suggests that the results at 25°S reflect the trends in a larger domain. However, these additional data allowed us to identify a shift in the trends before and after 1995, as expected from the recent faster increase of atmospheric CO_2 concentrations. At 25°S, the trends evaluated over the period 1995-2019 were almost twice as large as those evaluated over 1963-1995 (Table 5, Figure 11). For fCO_2 we estimated an annual rate that changed from +1.14 (± 0.23) µatm.yr^{-1} in 1963-1995 to +2.20 (± 0.26) µatm.yr^{-1} in 1995-2019 (Figures 10a and 11). For pH the trends varied from -0.00129 (± 0.00042) to -0.00227 (± 0.00048) unit yr^{-1} for the same periods (Figures 10b and 11). To confirm these results we also evaluated the temporal change of pH based on $[H^+]$ concentrations calculated for each cruise (Supp. Figure S13) and using Equation (3) (Kwiatkowski and Orr, 2018).

$$\Delta pH = -1\ \Delta[H^+]/2.303\ [H^+] \qquad (3)$$

where ΔpH and $\Delta[H^+]$ are the temporal differences between each period (1995 versus 1963 or 2019 versus 1995) and $[H^+]$ the concentration at the beginning of each period (1963 or 1995). The derived pH trends using Equation (3) are -0.00137 yr^{-1} for 1963-1995 and -0.00232 yr^{-1} for 1995-2019 (Table 5). Like for the trends deduced from the mean pH values at 25°S (Figure 10b), the pH trend based on $[H^+]$ concentrations is about twice faster in 1995-2019. For the recent period the observed fCO_2 and pH trends are remarkably close to those derived from the CMEMS-LSCE-NN model (Figure 10a,b, Figure 12, Table 5). For C_T, we estimated a trend of +0.82 (± 0.41) µmol.kg^{-1}.yr^{1} for 1963-1995 and +1.37 (± 0.42) µmol.kg^{-1}.yr^{1} for 1995-2019 in the same range as the trends deduced when comparing data collected in 2004 and 2019 in the whole Channel (section 3.1, Table 2) and indicative of the accumulation of anthropogenic CO_2.

3.4 Anthropogenic CO_2 in the southern region of the Mozambique Channel

In order to separate the contributions of natural or climate change induced variations (e.g. warming) and the accumulation of anthropogenic CO_2 to the fCO_2 and pH trends described above, we evaluated the anthropogenic fraction of C_T (hereafter noted C_{ant}) in the southern Mozambique Channel region based on water-column observations. Data from two cruises at 25°S in June 1995 and December 2003 are available in the GLODAPv2.2019 data product (Olsen et al., 2019). Murata et al (2010) used these observations to evaluate the changes of anthropogenic CO_2 concentrations in the interior of the South Indian Ocean. They estimated a mean increase of C_{ant} of +7.9 (± 1.1) µmol.kg^{-1} from June 1995 to December 2003 in the upper layer of the subtropical water in the Central Indian Ocean. Over 8.5 years this corresponds to a trend of +0.93 (± 0.13) µmol.kg^{-1}.yr^{-1}, in the range of our estimate based on surface observations (Figure 10c, Table 5). Specifically for the period 1995-2004, we evaluated an increase in N-C_T of +10.5 µmol.kg^{-1} in surface waters but over only 9 years the trend is uncertain, +1.15 (± 1.25) µmol.kg^{-1}.yr^{-1} (Table 5).

To further explore C_T and C_{ant} variations across the Mozambique Channel, we revisited the data used by Murata et al (2010) focusing on the stations within the same region as selected for surface data described in the previous section (25°S/38°E-42°E). To calculate C_{ant} we used the TrOCA method developed by Touratier et al. (2007) (see Section 2.3). Because indirect methods like TrOCA are not suitable to evaluate C_{ant} concentrations in surface waters (due to biological activity and gas exchange) we calculated C_{ant} in the layer 150-200m below the nitracline. The averages of observed and calculated properties in this layer are listed in Table 6 as well as the differences between the cruises. From 1995 to 2003 C_T and N-C_T increased by about 10 µmol.kg^{-1} and no significant change was observed for A_T. Our C_{ant} estimate in this region increased from 35.1 (± 1.2) µmol.kg^{-1} in 1995 to 42.3 (± 3.2) µmol.kg^{-1} in 2003. The C_{ant} increase of +7.3 (± 3.4) µmol.kg^{-1} reported here around 25°S is very close to the average value of +7.9 (± 1.1) µmol.kg^{-1} derived by Murata et al (2010) in the subtropical Indian Ocean subsurface waters. The C_{ant} increase explains 70 % of the C_T increase of +10.5 µmol.kg^{-1} over this period (1995-2003). The remaining 30% is probably linked to natural C_T variations associated to internal processes such as eddy activity around 24°S (Swart et al., 2010) and/or remineralization as revealed by the decrease in oxygen concentration (Table 6).

Our estimate of C_{ant} variations at regional scale can be also compared to the results by Gruber et al (2019a) who evaluated the changes in C_{ant} in the global ocean between 1994 and 2007. We extracted the C_{ant} data for the Mozambique Channel made available by Gruber et al (2019b) and estimated the mean C_{ant} changes at 25°S in different layers (Table 7). The accumulation of C_{ant} between 1994 and 2007 is rather homogeneous in the Mozambique Channel (Supp. Figure S14). In the top layer (0-200m) the mean C_{ant} increase between 1994 and 2007 is +14.03 (± 0.78) µmol.kg^{-1} in the Channel (15°S-27°S). At 25°S, the accumulation in the layer 150-200m is +12.94 (± 0.56) µmol.kg^{-1}, i.e. a rate of +1.00 (± 0.04) µmol.kg^{-1}.yr^{-1} which is slightly higher than our C_{ant} estimate of +0.86 (± 0.4) µmol.kg^{-1}.yr^{-1} based on TrOCA and for the period June 1995 to December 2003.

Although the C_{ant} estimates described above were obtained for different periods and using different methods (Murata et al., 2010; Gruber et al, 2019a; this study), all results lead to the same conclusion: there was a gradual increase in C_T concentrations in the upper waters of the southern Mozambique Channel from +0.82 (± 0.41) µmol.kg^{-1}.yr^{-1} in 1963-1995 to +1.37 (± 0.42) µmol.kg^{-1}.yr^{-1} in 1995-2019 (Table 5, Figure 11). It is mainly driven by the accumulation of anthropogenic CO_2 (Table 6, 7). This also explains the observed long-term trends of fCO_2 and the progressive pH decline in this region (Figure 10). The warming of +0.11°C.decade^{-1} would translate into a pH decrease of -0.0017.decade^{-1}, i.e. about 10% of the observed long-term trend for 1963-2019 of -0.0167 (±0.002) .decade^{-1}. Most of the observed pH change in the Mozambique Channel is thus likely due to anthropogenic CO_2. This could impact not only the biological processes in the open ocean but also coral reef ecosystems in this region.

3.5 A Paleo-acidification perspective

Like in other regions, coral reefs in the Mozambique Channel are subject to multiple stressors due to warming, sea level rise and acidification, combined or not to local anthropization (e.g. in Mayotte). Historical SST and pH can be reconstructed from aragonite skeletal cores collected from massive scleractinian coral species like *Porites* sp. from geochemical proxies such as trace element ratios (e.g. Li/Mg, Sr/Ca), oxygen ($\delta^{18}O$) or boron ($\delta^{11}B$) isotopic ratio (e.g. Montagna et al, 2014; Tierney et al, 2015; Liu et al; 2014; Wu et al, 2018; D'Olivo et al, 2019; Cuny-Guirriec et al, 2019). Above we have estimated the change in pH since 1963. If we assume that the trends derived from observations between the sixties and 2019 are representative of the trend over the historical period (i.e. fCO_2 tracks atmospheric CO_2) historical changes in sea surface fCO_2, pH and N-C_T can be evaluated back to the pre-industrial period (Figures 13a,b). We used historical atmospheric xCO_2 data for the southern hemisphere reconstructed by Meinshausen et al (2017) for the period 1800-2014 along with recent atmospheric xCO_2 recorded over 2015-2019 (Dlugokencky and Tans, 2020). C_T and pH were calculated assuming constant salinity (35) and alkalinity (2300 µmol.kg^{-1}, the mean of all A_T observations in January 2004 and April 2019 was 2297.6 ±14.7 µmol.kg^{-1}, Figure 3a). We also assume that the oceanic fCO_2 is either in equilibrium with the atmosphere (orange line in Figures 13a,b) or that fCO_2 seasonality is constant over time (grey lines in Figures 13a,b).

The results of the reconstruction for the recent decades (Figures 13a) show a good agreement with observations for fCO_2 and pH when available. For the period 1985-2019 the reconstructed fCO_2 and pH are also close to the monthly values from the neural network model (Chau et al 2020, purple lines in Figures 13a). Reconstructed N-C_T concentrations are also in the range of N-C_T measured or calculated between 1963 and 2019. In the year 1800, values of fCO_2, pH and N-C_T were respectively around 270 (± 10) µatm, 8.18 (± 0.014) and 1915 (± 10) µmol.kg^{-1}. This gives a reference for pH reconstructions based on 2 m-long coral cores recently collected at different locations along the Mozambique Channel during the CLIM-EPARSES cruise (work in progress, Tribollet, 2019, 2020).

Since 1800, the mean annual pH decreased progressively from 8.180 to 8.136 in 1963 (the first direct observation) and then decreased sharply to reach 8.05 in 2019. The pH decline of -0.13 between 1800 and 2019, evaluated here at local scale, is slightly larger than the -0.11 pH units estimated for the global ocean (Jiang et al., 2019). Based on our reconstruction, we evaluated a pH trend of -0.0027.decade^{-1} during 1800-1963, -0.0138.decade^{-1} during 1963-1995 and -0.0187.decade^{-1} during 1995-2019. Recalling our results based on observations (Table 5), it is clear that the rate of acidification has increased over the past recent decades, and it is likely that this process will continue in the next decade given the rapid increase of atmospheric CO_2 concentrations that reached a new record of +2.6 ppm.yr^{-1} in 2019 for a non ENSO year (Dlugokencky and Tans, 2020). If future atmospheric CO_2 levels keep increasing at the same rate, a further decrease of pH by -0.1 is likely to occur by 2040 (pH < 8) while aragonite saturation state (Ω_{Ar}) would reach the value of 3 (Supp. Fig S14) which is below the critical threshold of Ω_{Ar} = 3.25 that seems to limit the distribution of tropical coral reefs in the contemporary ocean (e.g. Hoegh-Guldberg et al., 2007).

Such a rapid reduction of pH and Ω_{Ar} in the Mozambique Channel in response to anthropogenic CO_2 emissions could have severe negative impacts on coral reefs because of a simultaneous reduction of calcification of the main reef framebuilders (corals and crustose coralline algae; Pandolfi et al. 2011) and a stimulation of carbonate dissolution processes (Schönberg et al. 2017; Eyre et al. 2018; Tribollet et al. 2019). Impacts on coral reefs of combined effects of ocean warming and acidification, together with local disturbances (e.g. eutrophication), need to be further investigated as the interaction of stressors might be synergistic or antagonistic (Chauvin et al. 2011; Trnovsky et al. 2016; Schönberg et al. 2017; Boyd et al 2018). Future studies need to address impacts of multiple drivers on coral reefs at the regional scale, f.i. along thermal, pH and pollution gradients, to better apprehend and predict the fate of those ecosystems.

4. Summary and Concluding remarks

This study presents new observations of the carbonate system in the Mozambique Channel for January 2004 and April 2019. Remarkable differences are observed between these cruises conducted 15 years apart and at different seasons. The region was a large CO_2 source in January due to high temperature (30°C) and near equilibrium in April. In 2019 this region was hit by the strong cyclone "Idai" leading to low salinity and low C_T and A_T concentrations. However, when normalized to salinity, N-C_T concentrations were higher in 2019 compared to 2004 by about 12 (± 7) µmol.kg^{-1}, which reflects in part the uptake of anthropogenic CO_2 over 15 years. Surprisingly the fCO_2 (and pH) data at in-situ SST were almost identical in 2004 and 2019, although atmospheric xCO_2 observed onboard increased by +34 ppm. However, when the thermal effect is taken into account, we estimate a small increase in fCO_2 (+11.5 ± 9.8 µatm) and decrease in pH (-0.012 ± 0.008) driven by N-C_T changes. N-A_T concentrations are the same in 2004 and 2019 and do not impact fCO_2 and pH variations. The relatively small difference of fCO_2 between the two cruises is due to seasonal variability that has to be taken into account to detect long-term trends. The decrease in C_T and fCO_2 from January to April is in part due to biological processes. Diazotrophy provides a likely explanation as *Trichodesmium* spp has been observed in abundance in the Mozambique Channel (Dupuy et al, 2016). When the seasonality is taken into account, our observations in 2004 and 2019 reveal an increase in fCO_2 of +1.75 (± 0.81) µatm.yr^{-1}, in C_T of +1.04 (± 0.79) µmol.kg^{-1}.yr^{-1} and a decrease of pH of -0.0016.yr^{-1} (± 0.0015).

The data from these two cruises lead to a robust A_T/SSS relationship in this region that can be used to calculate pH from fCO_2 data from other cruises. We attempted a comparison of our recent observations with sea surface data collected in 1963 in the Mozambique Channel (Keeling and Waterman, 1968). As expected, the fCO_2 was much higher in 2004/2019 than in 1963 (by about 100 µatm) reflecting an atmospheric CO_2 increase by +90 ppm between 1963 and 2019. In addition to anthropogenic CO_2 uptake, long-term ocean warming in this region (+0.11°C.decade^{-1}) contributes to fCO_2 increase from 1963 to 2019 (by approximately about +10 µatm). For pH, we observed a large decrease in all sectors of the Mozambique Channel, including near coral reef areas in the Eparses Islands (Europa, Juan de Nova). We estimated a mean decrease of -0.104 (± 0.006) pH unit between 1963 and 2019, typical of the preindustrial versus modern change in the global ocean (Jiang et al., 2019).

Results from the three cruises (1963, 2004 and 2019) covering a large region (14°S-25°S) are corroborated by three additional observations collected in the southern part of the Mozambique Channel (25°S). Based on those 6 cruises from 1963 to 2019, we evaluated a long-term trend for fCO_2 of +1.55 (± 0.11) µatm.yr^{-1} almost identical to the atmospheric trend. For pH the trend over 1963-2019 is -0.00167.yr^{-1} (± 0.0002), and for C_T we estimated an increase of +1.04 (± 0.21) µmol.kg^{-1}.yr^{-1}. This is close to the trend of anthropogenic CO_2 evaluated in the upper ocean layers ranging between +0.93 (± 0.13) and +1.00 (±0.04) µmol.kg^{-1}.yr^{-1} depending on the method and data used (Murata et al., 2010, Gruber et al., 2019a, this study). It is worth noting that the fCO_2, pH and C_T trends appear to be more pronounced in the recent decades although this is derived from few cruises only (Table 5). For pH we estimated a trend of -0.0129.decade^{-1} (± 0.0042) over 1963-1995 and -0.0227.decade^{-1} (± 0.0048) for 1995-2019 suggesting an acceleration of acidification. Our different estimates based either on fCO_2 or A_T/C_T measurements in the Mozambique Channel agree with trends in this region derived from global scale reconstructions of pCO2 and pH (Denvil-Sommer et al., 2019; Chau et al, 2020). We also note that the pH trend in the Mozambique Channel appears lower than previous estimates at basin scale in the Indian Ocean which range between -0.024.decade^{-1} for the period 1981-2011 and -0.027.decade^{-1} for 1991-2011 (Lauvset et al, 2015).

The results presented in this analysis aimed at evaluating the change of the carbonate system in the Mozambique Channel at regional scale and we conclude that the anthropogenic CO_2 emissions are responsible for a significant acidification in surface waters supported here by various sea surface observations and independent anthropogenic CO_2 concentration estimates in the water column. Given the results based on observations since the sixties, we reconstructed the pH change back to the pre-industrial period. In the year 1800, we estimated that pH in the Mozambique Channel was about 8.18 (±0.014), i.e. 0.13 higher than in 2019. Concentration of C_T in the year 1800 was likely around 1915 (±10) µmol.kg^{-1}. These values could serve as a reference for reconstructing pH from coral core samples collected during the CLIM-EPARSES cruise in April 2019 (Tribollet, 2019, 2020).

Our analysis reflects only the change in the open ocean and the "remote" anthropogenic impact through CO_2 emissions. To further evaluate impacts of global environmental change and ocean acidification on coral reefs, a continuous *in situ* sampling program will be needed at higher temporal and spatial scale. It should include the sea level changes either due to global warming or linked to marine heat waves or climate fluctuations such as the Indian Ocean Dipole (IOD) and ENSO in the Pacific (Ampou et al., 2017), the frequency of cyclone events or local anthropization (especially in Mayotte). In the present analysis, pH was calculated from carbonate system properties, i.e. not from direct pH measurements. In the future and similarly to what is done in other coral reefs areas (Tilbrook et al., 2019), pH should be monitored at high frequency. Detailed analysis of the observations obtained during CLIM-EPARSES cruise near the Islands and in coral reefs (Juan de Nova, Europa, Mayotte and Glorieuses) will be investigated in further studies.

Authors contribution: AT is PI of the ongoing CLIM-EPARSES project. NM was PI of the OISO-11 cruise in 2004. fCO_2, A_T and C_T data for OISO-11 were measured and qualified by NM and CLM. fCO_2, A_T and C_T data for CLIM-EPARSES were measured and qualified by CLM, JF, CM and NM. PC provided the Chl-a data for CLIM-EPARSES. MG and TC provided the neural network model results. NM wrote the draft of this manuscript and prepared figures with contributions from all authors.

Acknowledgments: The OISO program was supported by the French institutes INSU (Institut National des Sciences de l'Univers) and IPEV (Institut Polaire Paul-Emile Victor), the French program SOERE/Great-Gases, and the European programs CARBOOCEAN (grant 511176) and CARBOCHANGE (grant 264879). The CLIM-EPARSES project is supported by TAAF (Terres Australes et Antarctic Françaises), IRD (Institut de Recherche pour le Développement), Fondation Prince Albert II de Monaco (www.fpa2.org), INSU (Institut National des Sciences de l'Univers), CNRS (Centre National de Recherche Scientifique), Museum National d'Histoire Naturelle (MNHN), UMRs LOCEAN-IPSL, ENTROPIE and LSCE. We thank the captains and crew of *R.R.V. Marion Dufresne* and the staff at the French Polar Institute (IPEV). The development of the neural network model benefited from funding by the French INSU-GMMC project "PPR-Green-Grog (grant no 5-DS-PPR-GGREOG), the EU H2020 project AtlantOS (grant no 633211), as well as through the Copernicus Marine Environment Monitoring Service (project CMEMS-TAC-MOB). Anna Conchon contributed to the development and computation of pCO2 and pH reconstructions. The Surface Ocean CO_2 Atlas (SOCAT, www.socat.info) is an international effort, endorsed by the International Ocean Carbon Coordination Project (IOCCP), the Surface Ocean Lower Atmosphere Study (SOLAS) and the Integrated Marine Biogeochemistry and Ecosystem Research program (IMBER), to deliver a uniformly quality-controlled surface ocean CO2 database. We thank the two anonymous reviewers for making constructive suggestions, which resulted in improvements of this paper and Raleigh Hood, Editor of this IIOE-2 special issue.

References:

Alory, G., Wijffels, S., and Meyers, G., 2007. Observed temperature trends in the Indian Ocean over 1960–1999 and associated mechanisms, *Geophys. Res. Lett.*, 34, L02606, doi:10.1029/2006GL028044.

Álvarez, M., Lo Monaco, C., Tanhua, T., Yool, A., Oschlies, A., Bullister, J. L., Goyet, C., Metzl, N., Touratier, F., McDonagh, E., and Bryden, H. L., 2009. Estimating the storage of anthropogenic carbon in the subtropical Indian Ocean: a comparison of five different approaches, Biogeosciences, 6, 681–703, https://doi.org/10.5194/bg-6-681-2009.

Aminot, A., and R. Kérouel, 2004. *Hydrologie des écosystèmes marins: paramètres et analyses*. Ed. Ifremer, 336 p.

Ampou, E. E., Johan, O., Menkes, C. E., Niño, F., Birol, F., Ouillon, S., and Andréfouët, S., 2017. Coral mortality induced by the 2015–2016 El-Niño in Indonesia: the effect of rapid sea level fall, Biogeosciences, 14, 817–826, https://doi.org/10.5194/bg-14-817-2017.

Antonov, J. I., Locarnini, R. A., Boyer, T. P., Mishonov, A. V., and Garcia, H. E, 2006. World Ocean Atlas 2005, in: Volume 2: Salinity, edited by Levitus, S., NOAA Atlas NESDIS 62, US Government Printing Office, Washington, DC, 182 pp.

Bakker, D. C. E., Pfeil, B., Smith, K., Hankin, S., Olsen, A., Alin, S. R., Cosca, C., Harasawa, S., Kozyr, A., Nojiri, Y., O'Brien, K. M., Schuster, U., Telszewski, M., Tilbrook, B., Wada, C., Akl, J., Barbero, L., Bates, N. R., Boutin, J., Bozec, Y., Cai, W.-J., Castle, R. D., Chavez, F. P., Chen, L., Chierici, M., Currie, K., de Baar, H. J. W., Evans, W., Feely, R. A., Fransson, A., Gao, Z., Hales, B., Hardman-Mountford, N. J., Hoppema, M., Huang, W.-J., Hunt, C. W., Huss, B., Ichikawa, T., Johannessen, T., Jones, E. M., Jones, S. D., Jutterström, S., Kitidis, V., Körtzinger, A., Landschützer, P., Lauvset, S. K., Lefèvre, N., Manke, A. B., Mathis, J. T., Merlivat, L., Metzl, N., Murata, A., Newberger, T., Omar, A. M., Ono, T., Park, G.-H., Paterson, K., Pierrot, D., Ríos, A. F., Sabine, C. L., Saito, S., Salisbury, J., Sarma, V. V. S. S., Schlitzer, R., Sieger, R., Skjelvan, I., Steinhoff, T., Sullivan, K. F., Sun, H., Sutton, A. J., Suzuki, T., Sweeney, C., Takahashi, T., Tjiputra, J., Tsurushima, N., van Heuven, S. M. A. C., Vandemark, D., Vlahos, P., Wallace, D. W. R., Wanninkhof, R., and Watson, A. J., 2014. An update to the Surface Ocean CO2 Atlas (SOCAT version 2), Earth Syst. Sci. Data, 6, 69–90, doi:10.5194/essd-6-69-2014.

Bakker, D. C. E., Pfeil, B., Landa, C. S., Metzl, N., O'Brien, K. M., Olsen, A., Smith, K., Cosca, C., Harasawa, S., Jones, S. D., Nakaoka, S.-I., Nojiri, Y., Schuster, U., Steinhoff, T., Sweeney, C., Takahashi, T., Tilbrook, B., Wada, C., Wanninkhof, R., Alin, S. R., Balestrini, C. F., Barbero, L., Bates, N. R., Bianchi, A. A., Bonou, F., Boutin, J., Bozec, Y., Burger, E. F., Cai, W.-J., Castle, R. D., Chen, L., Chierici, M., Currie, K., Evans, W., Featherstone, C., Feely, R. A., Fransson, A., Goyet, C., Greenwood, N., Gregor, L., Hankin, S., Hardman-Mountford, N. J., Harlay, J., Hauck, J., Hoppema, M., Humphreys, M. P., Hunt, C. W., Huss, B., Ibánhez, J. S. P., Johannessen, T., Keeling, R., Kitidis, V., Körtzinger, A., Kozyr, A., Krasakopoulou, E., Kuwata, A., Landschützer, P., Lauvset, S. K., Lefèvre, N., Lo Monaco, C., Manke, A., Mathis, J. T., Merlivat, L., Millero, F. J., Monteiro, P. M. S., Munro, D. R., Murata, A., Newberger, T., Omar, A. M., Ono, T., Paterson, K., Pearce, D., Pierrot, D., Robbins, L. L., Saito, S., Salisbury, J., Schlitzer, R., Schneider, B., Schweitzer, R., Sieger, R., Skjelvan, I., Sullivan, K. F., Sutherland, S. C., Sutton, A. J., Tadokoro, K., Telszewski, M., Tuma, M., Van Heuven, S. M. A. C., Vandemark, D., Ward, B., Watson, A. J., and Xu, S., 2016. A multi-decade record of high-quality fCO_2 data in version 3 of the Surface Ocean CO_2 Atlas (SOCAT), Earth Syst. Sci. Data, 8, 383-413, doi:10.5194/essd-8-383-2016.

Bakker, D. C. E. et al. , 2020. Surface Ocean CO2 Atlas Database Version 2020 (SOCATv2020) (NCEI Accession 0210711). NOAA National Centers for Environmental Information. Dataset. https://doi.org/10.25921/4xkx-ss49. Last Access 15/6/2020.

Bates, N. R., A. C. Pequignet, and C. L. Sabine, 2006. Ocean carbon cycling in the Indian Ocean: 1. Spatiotemporal variability of inorganic carbon and air-sea CO2 gas exchange, Global Biogeochem. Cycles, 20, GB3020, doi:10.1029/2005GB002491.

Bates, N., Astor, Y., Church, M., Currie, K., Dore, J., Gonaález-Dávila, M., Lorenzoni, L., Muller-Karger, F., Olafsson, J. and Santa-Casiano, M., 2014. A Time-Series View of Changing Ocean Chemistry

Due to Ocean Uptake of Anthropogenic CO2 and Ocean Acidification, Oceanography, 27(1), 126–141, doi:10.5670/oceanog.2014.16.

Beaufort, L., I. Probert, T. de Garidel-Thoron, E.M. Bendif, D. Ruiz-Pino, N. Metzl, C. Goyet, N. Buchet, P. Coupel, M. Grelaud, B. Rost, R.E.M. Rickaby and C. de Vargas, 2011. Sensitivity of coccolithophores to carbonate chemistry and ocean acidification. *Nature*, doi:10.1038/nature10295.

Boyd, P.W., S. Collins, S. Dupont, K. Fabricius, J.-P. Gattuso, J. Havenhand, D. A. Hutchins, U. Riebesell, M. S. Rintoul, M. Vichi, H. Biswas, A. Ciotti, K. Gao, M. Gehlen, C. L. Hurd, H. Kurihara, C. M. McGraw, J. M. Navarro, G. E. Nilsson, U. Passow, H.-O. Pörtner, 2018. Experimental strategies to assess the biological ramifications of multiple drivers of global ocean change—A review. *Glob Change Biol*. 2018; 24: 2239–2261. doi:10.1111/gcb.14102.

Carter, B. R., N. L. Williams, A. R. Gray, and R. A. Feely. 2016. Locally interpolated alkalinity regression for global alkalinity estimation. Limnol. Oceanogr.: Methods 14: 268–277. doi:10.1002/lom3.10087.

Carter, B. R., R. A. Feely, N. L. Williams, A. G. Dickson, M. B. Fong and Y. Takeshita, 2018. Updated methods for global locally interpolated estimation of alkalinity, pH, and nitrate. Limnology and Oceanography: Methods, 16: 119-131. doi: 10.1002/lom3.10232

Chau, T. T., Gehlen, M., and Chevallier, F., 2020: Global Ocean Surface Carbon Product MULTIOBS_GLO_BIO_CARBON_SURFACE_REP_015_008, E.U. Copernicus Marine Service Information. "https://resources.marine.copernicus.eu/documents/QUID/CMEMS-MOB-QUID-015-008.pdf".

Chauvin, A., V. Denis, and P. Cuet, 2011. Is the response of coral calcification to seawater acidification related to nutrient loading?. *Coral Reefs* **30,** 911. DOI:10.1007/s00338-011-0786-7

Copin-Montégut, C., 1988. A new formula for the effect of temperature on the partial pressure of CO_2 in seawater. *Marine Chemistry*, 25, 29-37. https://doi.org/10.1016/0304-4203(88)90012-6

Copin-Montégut, C., 1989. A new formula for the effect of temperature on the partial pressure of CO_2 in seawater. Corrigendum. *Marine Chemistry*, 27, 143-144. https://doi.org/10.1016/0304-4203(89)90034-0.

Cuny-Guirriec K., E. Douville, S. Reynaud, D. Allemand, L. Bordier, M. Canesi, C. Mazzoli, M. Taviani, S. Canese, M. McCulloch, J. Trotter, S. D. Rico-Esenaro, J.A. Sanchez-Cabeza, A.C.Ruiz-Fernández, J.P Carricart-Ganivet, P. Scott, A. Sadekov and P. Montagna, 2019. Coral Li/Mg thermometry: Caveats and constraints. *Chemical Geology*, 523, 162-178. https://doi.org/10.1016/j.chemgeo.2019.03.038.

Cyronak, T., Schulz, K. G., Santos, I. R. and Eyre, B. D., 2014. Enhanced acidification of global coral reefs driven by regional biogeochemical feedbacks, *Geophys. Res. Lett.*, 2014GL060849, doi:10.1002/2014GL060849.

Cyronak, T., Takeshita, Y., Courtney, T.A., DeCarlo, E.H., Eyre, B.D., Kline, D.I., Martz, T., Page, H., Price, N.N., Smith, J., Stoltenberg, L., Tresguerres, M. and Andersson, A.J., 2020. Diel temperature and pH variability scale with depth across diverse coral reef habitats. Limnol Oceanogr, 5: 193-203. doi:10.1002/lol2.10129.

de Moel, H., Ganssen, G. M., Peeters, F. J. C., Jung, S. J. A., Kroon, D., Brummer, G. J. A., and Zeebe, R. E., 2009. Planktic foraminiferal shell thinning in the Arabian Sea due to anthropogenic ocean acidification? Biogeosciences, 6, 1917–1925, https://doi.org/10.5194/bg-6-1917-2009.

Denvil-Sommer, A., Gehlen, M., Vrac, M. and Mejia, C., 2019. LSCE-FFNN-v1: a two-step neural network model for the reconstruction of surface ocean pCO_2 over the global ocean, Geosci. Model Dev., 12, 2091-2105, https://doi.org/10.5194/gmd-12-2091-2019.

Dickson, A. G. 1990. Standard potential of the reaction: AgCl(s) + ½H2(g) = Ag(s) + HCl(aq), and the standard acidity constant of the ion HSO4– in synthetic sea water from 273.15 to 318.15 K. *J. Chem. Thermodyn.* **22**: 113–127. doi:10.1016/0021-9614(90)90074-Z

Dickson, A. G. and Millero, F. J. 1987. A comparison of the equilibrium constants for the dissociation of carbonic acid in seawater media. *Deep Sea Res.* **34**(10), 1733–1743. Doi:10.1016/0198-0149(87)90021-5.

Dickson, A.G., Sabine, C.L. and Christian, J.R. (Eds.) 2007. Guide to Best Practices for Ocean CO2 Measurements. *PICES Special Publication* 3, 191 pp.

Dlugokencky, E. and Tans, P., 2020. Trends in atmospheric carbon dioxide, National Oceanic & Atmospheric Administration, Earth System Research Laboratory (NOAA/ESRL), available at: http:// www.esrl.noaa.gov/gmd/ccgg/trends/global.html, (last access: 22 February 2020).

D'Olivo J. P., G. Ellwood, T. M. DeCarlo and M. T. McCulloch, 2019. Deconvolving the long-term impacts of ocean acidification and warming on coral biomineralisation. *Earth and Planetary Science Letters*, Volume 526, 115785, https://doi.org/10.1016/j.epsl.2019.115785.

Doney, S. C., Fabry, V. J., Feely, R. A., and Kleypas, J. A., 2009. Ocean acidification: The other CO2 problem. *Annual Review of Marine Science*, 1(1), 169–192. 10.1146/annurev.marine.010908.163834

Dupuy, C., M. Pagano, P. Got, I. Domaizon, A. Chappuis, G. Marchessaux, M. Bouvy, 2016. Trophic relationships between metazooplankton communities and their plankton food sources in the Iles Eparses (Western Indian Ocean). *Marine Environmental Research*, 116, 18-31, doi.org/10.1016/j.marenvres.2016.02.011.

Edmond, J. M., 1970. High precision determination of titration alkalinity and total carbon dioxide content of sea water by potentiometric titration, *Deep-Sea Res*., 17, 737–750, https://doi.org/10.1016/0011-7471(70)90038-0.

Eyre B.D., Cyronak T., Drupp P., De Carlo E.H., Sachs J.P., Andersson A.J., 2018. Coral reefs will transition to net dissolving before end of century. *Science* 359, 6378, 908–911, DOI:10.1126/science.aao1118.

Fabry, V. J., Seibel, B. A., Feely, R. A. and Orr, J. C, 2008. Impacts of ocean acidification on marine fauna and ecosystem processes. *ICES J. Mar. Sci.* 65, 414–432. https://doi.org/10.1093/icesjms/fsn048

Feely, R. A., Doney, S. C., and Cooley, S. R., 2009. Ocean acidification: Present conditions and future changes in a high-CO2 world. Oceanography, 22(4), 36–47. 10.5670/oceanog.2009.95

Friedlingstein, P., Jones, M. W., O'Sullivan, M., Andrew, R. M., Hauck, J., Peters, G. P., Peters, W., Pongratz, J., Sitch, S., Le Quéré, C., Bakker, D. C. E., Canadell, J. G., Ciais, P., Jackson, R. B., Anthoni, P., Barbero, L., Bastos, A., Bastrikov, V., Becker, M., Bopp, L., Buitenhuis, E., Chandra, N., Chevallier, F., Chini, L. P., Currie, K. I., Feely, R. A., Gehlen, M., Gilfillan, D., Gkritzalis, T., Goll, D. S., Gruber, N., Gutekunst, S., Harris, I., Haverd, V., Houghton, R. A., Hurtt, G., Ilyina, T., Jain, A. K., Joetzjer, E., Kaplan, J. O., Kato, E., Klein Goldewijk, K., Korsbakken, J. I., Landschützer, P., Lauvset, S. K., Lefèvre, N., Lenton, A., Lienert, S., Lombardozzi, D., Marland, G., McGuire, P. C., Melton, J. R., Metzl, N., Munro, D. R., Nabel, J. E. M. S., Nakaoka, S.-I., Neill, C., Omar, A. M., Ono, T., Peregon, A., Pierrot, D., Poulter, B., Rehder, G., Resplandy, L., Robertson, E., Rödenbeck, C., Séférian, R., Schwinger, J., Smith, N., Tans, P. P., Tian, H., Tilbrook, B., Tubiello, F. N., van der Werf, G. R., Wiltshire, A. J., and Zaehle, S., 2019. Global Carbon Budget 2019, *Earth Syst. Sci. Data*, 11, 1783–1838, https://doi.org/10.5194/essd-11-1783-2019.

Garcia, H. E., R. A. Locarnini, T. P. Boyer, J. I. Antonov, O.K. Baranova, M.M. Zweng, J.R. Reagan, D.R. Johnson, 2014. World Ocean Atlas 2013, Volume 4: Dissolved Inorganic Nutrients (phosphate, nitrate, silicate). S. Levitus, Ed., A. Mishonov Technical Ed.; NOAA Atlas NESDIS 76, 25 pp.

Gattuso J.-P., Magnan A., Billé R., Cheung W. W. L., Howes E. L., Joos F., Allemand D., Bopp L., Cooley S., Eakin M., Hoegh-Guldberg O., Kelly R. P., Pörtner H.-O., Rogers A. D., Baxter J. M., Laffoley D., Osborn D., Rankovic A., Rochette J., Sumaila U. R., Treyer S. and Turley C., 2015. Contrasting futures for ocean and society from different anthropogenic CO_2 emissions scenarios. *Science* 349:aac4722.doi: 10.1126/science.aac4722

Gruber, N., D. Clement, B. R. Carter, R. A. Feely, S. van Heuven, M. Hoppema, M. Ishii, R. M. Key, A. Kozyr, S. K. Lauvset, C. Lo Monaco, J. T. Mathis, A. Murata, A. Olsen, F. F. Perez, C. L. Sabine, T. Tanhua, and R. Wanninkhof, 2019a. The oceanic sink for anthropogenic CO_2 from 1994 to 2007, *Science* vol. 363 (issue 6432), pp. 1193-1199. DOI: 10.1126/science.aau5153

Gruber, N., Clement, D., Carter, B. R., Feely, R. A., Heuven, S. van, Hoppema, M., Ishii, M., Key, R. M., Kozyr, A., Lauvset, S. K., Lo Monaco, C., Mathis, J. T., Murata, A., Olsen, A., Perez, F. F., Sabine, C. L., Tanhua, T. and Wanninkhof, R., 2019b: The oceanic sink for anthropogenic CO2 from 1994 to 2007 - the data (NCEI Accession 0186034). NOAA National Centers for Environmental Information. Dataset. https://doi.org/10.25921/wdn2-pt10. [last acces 17/02/2020].

Halo, I., B. Backeberg, P. Penven, I. Ansorge, C. Reason, and J.E. Ullgren, 2014. Eddy properties in the Mozambique Channel: A comparison between observations and two numerical ocean circulation models. *Deep Sea Research Part II: Topical Studies in Oceanography*, 100, 38-53, https://doi.org/10.1016/j.dsr2.2013.10.015.

Hancke, L., M.J. Roberts, and J.F. Ternon, 2014. Surface drifter trajectories highlight flow pathways in the Mozambique Channel. *Deep Sea Research Part II: Topical Studies in Oceanography*, 100, 27-37, doi:/10.1016/j.dsr2.2013.10.014.

Hansson, I. 1973. The determination of dissociation constants of carbonic acid in synthetic sea water in the salinity range of 20 – 40‰ and temperature range of 5 – 30°C. *Acta Chem. Scand.* **27**, 931–944. Doi: 10.3891/acta.chem.scand.27-0931.

Hoegh-Guldberg, O., P. J. Mumby, A. J. Hooten, R. S. Steneck, P. Greenfield, E. Gomez, C. D. Harvell, P. F. Sale, A. J. Edwards, K. Caldeira, N. Knowlton, C. M. Eakin, R. Iglesias-Prieto, N. Muthiga, R. H. Bradbury, A. Dubi and M. E. Hatziolos, 2007. Coral Reefs Under Rapid Climate Change and Ocean Acidification. *Science,* 14, 1737-1742, doi:10.1126/science.1152509

Hofmann GE, Smith JE, Johnson KS, Send U, Levin LA, et al., 2011. High-Frequency Dynamics of Ocean pH: A Multi-Ecosystem Comparison. PLoSONE 6(12): e28983. doi:10.1371/journal.pone.0028983.

Iida, Y., Takatani, Y., Kojima, A. and Ishii, M., 2020. Global trends of ocean CO_2 sink and ocean acidification: an observation-based reconstruction of surface ocean inorganic carbon variables. *J Oceanogr*. doi:10.1007/s10872-020-00571-5

IPCC, 2019: IPCC Special Report on the Ocean and Cryosphere in a Changing Climate [H.-O. Pörtner, D.C. Roberts, V. Masson-Delmotte, P. Zhai, M. Tignor, E. Poloczanska, K. Mintenbeck, M. Nicolai, A. Okem, J. Petzold, B. Rama, N. Weyer (eds.)]. In press.

Ishii, M., N. Kosugi, D. Sasano, S. Saito, T. Midorikawa, and H. Y. Inoue, 2011, Ocean acidification off the south coast of Japan: A result from time series observations of CO2 parameters from 1994 to 2008, *J. Geophys. Res.*, 116, C06022, doi:10.1029/2010JC006831.

Jabaud-Jan, A., Metzl, N., Brunet, C., Poisson, A. and Schauer, B., 2004: Interannual variability of the carbon dioxide system in the southern Indian Ocean (20°S–60°S): The impact of a warm anomaly in austral summer 1998, *Global Biogeochemical Cycles*, 18(1), doi:10.1029/2002GB002017.

Jiang, L.-Q., Carter, B. R., Feely, R. A., Lauvset, S. K. and Olsen, A., 2019: Surface ocean pH and buffer capacity: past, present and future, *Sci Rep*, 9(1), 1–11, doi:10.1038/s41598-019-55039-4.

Kapsenberg, L., Alliouane, S., Gazeau, F., Mousseau, L., and Gattuso, J.-P., 2017. Coastal ocean acidification and increasing total alkalinity in the northwestern Mediterranean Sea. *Ocean Sci.*, 13, 411-426, doi:10.5194/os-13-411-2017.

Keeling, C. D., and Waterman, L. S., 1968. Carbon dioxide in surface ocean waters: 3. Measurements on Lusiad Expedition 1962–1963, *J. Geophys. Res.*, 73(14), 4529– 4541, doi:10.1029/JB073i014p04529.

Key, R., Olsen, A., Van Heuven, S., Lauvset, S., Velo, A., Lin, X., Schirnick, C., Kozyr, A., Tanhua, T., Hoppema, M., Jutterstrom, S., Steinfeldt, R., Jeansson, E., Ishii, M., Perez, F., and Suzuki, T., 2015. Global Ocean Data Analysis Project, Version 2 (GLODAPv2), ORNL/CDIAC-162, ND-P093, dataset, https://doi.org/10.3334/CDIAC/OTG.NDP093_GLODAPv2.

Kleypas, J. A., R. W. Buddemeier, D. Archer, J.-P. Gattuso, C. Langdon, and B. N. Opdyke, 1999. Geochemical consequences of increased atmospheric carbon dioxide on coral reefs. *Science*, 284(5411), 118–120, doi:10.1126/science.284.5411.118.

Kwiatkowski L. and J. C. Orr, 2018. Diverging seasonal extremes for ocean acidification during the twenty-first century, Nature Climate Change, doi:10.1038/s41558-017-0054-0

Lauvset, S. K., Gruber, N., Landschützer, P., Olsen, A., and Tjiputra, J., 2015. Trends and drivers in global surface ocean pH over the past 3 decades. *Biogeosciences*, 12, 1285–1298, doi:10.5194/bg-12-1285-2015.

Lauvset S., K. Currie, N. Metzl, S. Nakaoka, D. Bakker, K. Sullivan, A. Sutton, K. O'Brien and A. Olsen, 2019. SOCAT Quality Control Cookbook for SOCAT version 7. Int. Report. Available at www.socat.info.

Lee, K., Tong, L.T., Millero, F.J., Sabine, C.L., Dickson, A.G., Goyet, C., Park, G.H., Wanninkhof, R., Feely, R.A., and Key, R.M., 2006. Global relationships of total alkalinity with salinity and temperature in surface waters of the world's oceans. *Geophys. Res. Lett.* 33, L19605. doi10.1029/2006GL027207.

Lewis E., and D. W. R. Wallace, 1998. Program developed for CO2 system calculations. ORNL/CDIAC-105. Carbon Dioxide Information Analysis Center, Oak Ridge National Laboratory, US. Dept. of Energy, Oak Ridge, TN.

Liu, Y., Z. Peng, R. Zhou, S. Song, W. Liu, C.-F. You, Y.-P. Lin, K. Yu, C.-C. Wu, G. Wei, L. Xie, G. S. Burr and C.-C. Shen, 2014. Acceleration of modern acidification in the South China Sea driven by anthropogenic CO2. *Sci. Rep*. 4, 5148. DOI: 10.1038/srep05148.

Lo Monaco, C., Álvarez, M., Key, R. M., Lin, X., Tanhua, T., Tilbrook, B., Bakker, D. C. E., van Heuven, S., Hoppema, M., Metzl, N., Ríos, A. F., Sabine, C. L., and Velo, A., 2010: Assessing the internal consistency of the CARINA database in the Indian sector of the Southern Ocean, *Earth Syst. Sci. Data*, 2, 51–70, https://doi.org/10.5194/essd-2-51-2010.

Lo Monaco, C., Metzl, N., and Tribollet, A., 2020a. Sea surface measurements of fugacity of CO2 (fCO2), temperature and salinity during the cruise Clim-EPARSES (EXPOCODE 35MV20190405) onboard R/V Marion-Dufresne in the Indian Ocean and Mozambique Channel from 2019-04-04 to 2019-04-30 (NCEI Accession 0208809). NOAA National Centers for Environmental Information. Dataset. https://accession.nodc.noaa.gov/0208809.

Lo Monaco C., N. Metzl, J. Fin and A. Tribollet, 2020b. Sea surface measurements of dissolved inorganic carbon (DIC) and total alkalinity (TALK), temperature and salinity during the R/V Marion-Dufresne cruise CLIM-EPARSES (EXPOCODE 35MV20190405) in the Indian Ocean and Mozambique Channel from 2019-04-04 to 2019-04-30. (NCEI Accession 0212218). [indicate subset used]. NOAA National Centers for Environmental Information. Dataset. https://accession.nodc.noaa.gov/0212218.

Louanchi, F., N. Metzl, A. Poisson, 1996. Modelling the monthly sea surface fCO2 fields in the Indian Ocean. *Marine Chemistry*, 55, 265-279. https://doi.org/10.1016/S0304-4203(96)00066-7.

Lueker, T.J., Dickson, A.G., Keeling, C.D., 2000. Ocean pCO(2) calculated from dissolved inorganic carbon, alkalinity, and equations for K-1 and K-2: validation based on laboratory measurements of CO2 in gas and seawater at equilibrium. *Marine Chemistry* 70, 105-119. https://doi.org/10.1016/S0304-4203(00)00022-0.

McKinna, L.I.W., 2015. Three decades of ocean-color remote-sensing Trichodesmium spp. in the World's oceans: A review. *Progress in Oceanography*, 131, 177-199 https://doi.org/10.1016/j.pocean.2014.12.013.

Meinshausen, M., Vogel, E., Nauels, A., Lorbacher, K., Meinshausen, N., Etheridge, D. M., Fraser, P. J., Montzka, S. A., Rayner, P. J., Trudinger, C. M., Krummel, P. B., Beyerle, U., Canadell, J. G., Daniel, J. S., Enting, I. G., Law, R. M., Lunder, C. R., O'Doherty, S., Prinn, R. G., Reimann, S., Rubino, M., Velders, G. J. M., Vollmer, M. K., Wang, R. H. J., and Weiss, R, 2017. Historical greenhouse gas concentrations for climate modelling (CMIP6), *Geosci. Model Dev.*, 10, 2057–2116, https://doi.org/10.5194/gmd-10-2057-2017.

Mehrbach, C., Culberson, C. H., Hawley, J. E. and Pytkowicz, R. M. 1973. Measurement of the apparent dissociation constants of carbonic acid in seawater at atmospheric pressure. *Limnol. Oceanogr.* **18**, 897–907. doi:10.4319/lo.1973.18.6.0897.

Metzl, N., A. Poisson, F. Louanchi, C. Brunet, B. Schauer & B. Bres, 1995. Spatio-temporal distributions of air-sea fluxes of CO_2 in the Indian and Antarctic oceans, *Tellus B: Chemical and Physical Meteorology*, 47:1-2, 56-69, DOI:10.3402/tellusb.v47i1-2.16006

Metzl, N., F. Louanchi, and A. Poisson, 1998. Seasonal and interannual variations of sea surface carbon dioxide in the subtropical indian ocean. *Marine Chemistry*, 60, 131-146. https://doi.org/10.1016/S0304-4203(98)00083-8.

Metzl, N., C. Brunet, A. Jabaud-Jan, A. Poisson and B. Schauer, 2006. Summer and winter air-sea CO2 fluxes in the Southern Ocean *Deep Sea Res I*, 53, 1548-1563, doi:10.1016/j.dsr.2006.07.006

Metzl, N., 2009. Decadal increase of oceanic carbon dioxide in the Southern Indian Ocean surface waters (1991-2007). *Deep Sea Research Part II: Topical Studies in Oceanography*, 56, 8–10, 607-619. https://doi.org/10.1016/j.dsr2.2008.12.007.

Metzl, N., 2018. Carbon dioxide, temperature, salinity, and other variables collected via surface underway survey from Volunteer Observing Ship Marion Dufresne in the Indian Ocean and Southern Oceans (> 60 degrees South) from 2004-01-06 to 2004-02-08 (NCEI Accession 0080996). NOAA National Centers for Environmental Information. Dataset. https://doi.org/10.3334/cdiac/otg.vos_oiso_11.

Metzl, N., and Lo Monaco, C., 2018. Sea surface measurements of dissolved inorganic carbon (DIC), total alkalinity (TALK), temperature and salinity during the R/V Marion-Dufresne Ocean Indien Service d'Observations - 11 (OISO-11) cruise (EXPOCODE 35MV20040106) in the Indian Ocean from 2004-01-06 to 2004-02-08 (NCEI Accession 0173515). Version 1.1. NOAA National Centers for Environmental Information. Dataset. doi:10.7289/V52805Z3.

Millero, F. J., Lee, K. and Roche, M. 1998. Distribution of alkalinity in the surface waters of the major oceans. *Mar. Chem.* **60**, 111–130. https://doi.org/10.1016/S0304-4203(97)00084-4.

Mollica N. R., W. Guo, A. L. Cohen, K. –F. Huang, G. L. Foster, H. K. Donald and A. R. Solow, 2018. Ocean acidification affects coral growth by reducing skeletal density. Proceedings of the National Academy of Sciences, 115 (8) 1754-1759; DOI: 10.1073/pnas.1712806115

Montagna, P., M. McCulloch, E. Douville, M. López Correa, J. Trotter, R. Rodolfo-Metalpa, D. Dissard, C. Ferrier-Pagès, N. Frank, A. Freiwald, S. Goldstein, C. Mazzoli, S. Reynaud, A. Rüggeberg, S. Russo, M. Taviani, 2014. Li/Mg systematics in scleractinian corals: Calibration of the thermometer, *Geochimica et Cosmochimica Acta*, 132, 288-310, https://doi.org/10.1016/j.gca.2014.02.005.

Moutin, T., Wagener, T., Caffin, M., Fumenia, A., Gimenez, A., Baklouti, M., Bouruet-Aubertot, P., Pujo-Pay, M., Leblanc, K., Lefevre, D., Helias Nunige, S., Leblond, N., Grosso, O., and de Verneil, A., 2018. Nutrient availability and the ultimate control of the biological carbon pump in the western tropical South Pacific Ocean, *Biogeosciences*, 15, 2961-2989, https://doi.org/10.5194/bg-15-2961-2018.

Murata, A., Kumamoto, Y., Sasaki, K., Watanabe, S., & Fukasawa, M., 2010. Decadal increases in anthropogenic CO2 along 20°S in the South Indian Ocean. *Journal of Geophysical Research*, *115*, C12055. https://doi.org/10.1029/2010JC006250

Olsen, A., R. M. Key, S. van Heuven, S. K. Lauvset, A. Velo, X. Lin, C. Schirnick, A. Kozyr, T. Tanhua, M. Hoppema, S. Jutterström, R. Steinfeldt, E. Jeansson, M. Ishii, F. F. Pérez & T. Suzuki, 2016. An internally consistent data product for the world ocean: the Global Ocean Data Analysis Project, version 2 (GLODAPv2), Earth Syst. Sci. Data, 8, 297-323, doi:10.5194/essd-8-297-2016.

Olsen, A., Lange, N., Key, R. M., Tanhua, T., Álvarez, M., Becker, S., Bittig, H. C., Carter, B. R., Cotrim da Cunha, L., Feely, R. A., Heuven, S. van, Hoppema, M., Ishii, M., Jeansson, E., Jones, S. D., Jutterström, S., Karlsen, M. K., Kozyr, A., Lauvset, S. K., Monaco, C. L., Murata, A., Pérez, F. F., Pfeil, B., Schirnick, C., Steinfeldt, R., Suzuki, T., Telszewski, M., Tilbrook, B., Velo, A. and Wanninkhof, R., 2019. GLODAPv2.2019 – an update of GLODAPv2, Earth System Science Data, 11(3), 1437–1461, doi:https://doi.org/10.5194/essd-11-1437-2019.

Ono H, Kosugi N, Toyama K, Tsujino H, Kojima A, Enyo K, Iida Y, Nakano T, Ishii M, 2019. Acceleration of ocean acidification in the Western North Pacific. Geophys Res Lett.doi:10.1029/2019G L0851 21

Orr, J. C., Fabry, V. J., Aumont, O., Bopp, L., Doney, S. C., Feely, R. A., Gnanadesikan, A., Gruber, N., Ishida, A., Joos, F., Key, R. M., Lindsay, K., Maier-Reimer, E., Matear, R., Monfray, P., Mouchet, A., Najjar, R. G., Plattner, G.-K., Rodgers, K. B., Sabine, C. L., Sarmiento, J. L., Schlitzer, R., Slater, R. D., Totterdell, I. J., Weirig, M.-F., Yamanaka, Y. and Yool, A., 2005. Anthropogenic ocean acidification over the twenty-first century and its impact on calcifying organisms, *Nature*, 437(7059), 681–686, doi:10.1038/nature04095.

Orr, J. C., J.-M. Epitalon, and J.-P. Gattuso, 2015. Comparison of ten packages that compute ocean carbonate chemistry, *Biogeosciences*, 12(5), 1483–1510, doi:10.5194/bg-12-1483-2015.

Orr, J. C., J.-M. Epitalon, A. G. Dickson and J.–P. Gattuso, 2018. Routine uncertainty propagation for the marine carbon dioxide system, *Marine Chemistry*, Vol. 207, 84-107, doi:10.1016/j.marchem.2018.10.006.

Pandolfi, J.M., S. R. Connolly, D. J. Marshall and A. L. Cohen, 2011. Projecting Coral Reef Futures Under Global Warming and Ocean Acidification. *Science*, 333, 418-422. Doi:10.1126/science.1204794

Pfeil, B., Olsen, A., Bakker, D. C. E., Hankin, S., Koyuk, H., Kozyr, A., Malczyk, J., Manke, A., Metzl, N., Sabine, C. L., Akl, J., Alin, S. R., Bates, N., Bellerby, R. G. J., Borges, A., Boutin,J., Brown, P. J., Cai, W.-J., Chavez, F. P., Chen, A., Cosca, C., Fassbender, A. J., Feely, R. A., González-Dávila, M., Goyet, C., Hales, B., Hardman-Mountford, N., Heinze, C., Hood, M., Hoppema, M., Hunt, C. W., Hydes, D., Ishii, M., Johannessen, T., Jones, S. D., Key, R. M., Körtzinger, A., Landschützer, P., Lauvset, S. K., Lefèvre, N., Lenton, A., Lourantou, A., Merlivat, L., Midorikawa, T., Mintrop, L., Miyazaki, C., Murata, A., Nakadate, A., Nakano, Y., Nakaoka, S., Nojiri, Y., Omar, A. M., Padin, X. A., Park, G.-H., Paterson, K., Perez, F. F., Pierrot, D., Poisson, A., Ríos, A. F., Santana-Casiano, J. M., Salisbury, J., Sarma, V. V. S. S., Schlitzer, R., Schneider, B., Schuster, U., Sieger, R., Skjelvan, I., Steinhoff, T., Suzuki, T., Takahashi, T., Tedesco, K., Telszewski, M., Thomas, H., Tilbrook, B., Tjiputra, J., Vandemark, D., Veness, T., Wanninkhof, R., Watson, A. J., Weiss, R., Wong, C. S., and Yoshikawa-Inoue, H., 2013. A uniform, quality controlled Surface Ocean CO2 Atlas (SOCAT), Earth Syst. Sci. Data, 5, 125-143, doi:10.5194/essd-5-125-2013.

Pierrot, D., E. Lewis, and D. W. R. Wallace, 2006. MS Excel Program Developed for CO2 System Calculations ORNL/CDIAC-105, Carbon Dioxide Inf. Anal. Cent., Oak Ridge Natl. Lab., U. S. Dept. of Energy, Oak Ridge, Tenn.

Poisson, A., Metzl, N., Brunet, C., Schauer, B., Bres, B., Ruiz-Pino, D., and Louanchi, F., 1993. Variability of sources and sinks of CO_2 in the western Indian and southern oceans during the year 1991, *J. Geophys. Res.*, 98(C12), 22759– 22778, doi:10.1029/93JC02501.

Reynolds, R. W., N. A. Rayner, T. M. Smith, D. C. Stokes, and W. Wang, 2002: An Improved In Situ and Satellite SST Analysis for Climate. *J. Climate*, **15**, 1609–1625, https://doi.org/10.1175/1520-0442(2002)015<1609:AIISAS>2.0.CO;2.

Riebesell U., Zondervan I., Rost B., Tortell P.D., Zeebe R.E. and Morel F.M.M., 2000. Reduced calcification of marine plankton in response to increased atmospheric CO_2. Nature. 407(6802): 364–7. doi:10.1038/35030078.

Roxy, M. K., K. Ritika, P. Terray and S. Masson, 2014. The Curious Case of Indian Ocean Warming. *Journal of Climate*, American Meteorological Society, 27 (22), pp.8501-8509. 10.1175/JCLI-D-14-00471.1.

Sabine, C. L., Key, R. M., Johnson, K. M., Millero, F. J., Poisson, A., Sarmiento, J. L., Wallace, D. W. R. and Winn, C. D., 1999. Anthropogenic CO2 inventory of the Indian Ocean. *Global Biogeochemical Cycles*, 13(1), 179–198, doi:10.1029/1998GB900022.

Sabine, C. L., R. Wanninkhof, R. M. Key, C. Goyet, and F. J. Millero, 2000. Seasonal CO2 fluxes in the tropical and subtropical Indian Ocean, *Mar. Chem.*, 72, 33–53. https://doi.org/10.1016/S0304-4203(00)00064-5.

Schlitzer, R, 2013. Ocean Data View, http:/odv.awi.de.

Schönberg C.H.L., Fang J.K.H., Carreiro-Silva M., Tribollet A. and Wisshak M., 2017. Bioerosion: the other ocean acidification problem *ICES Journal of Marine Science* fsw254. DOI:10.1093/icesjms/fsm254

Swart, N. C., Lutjeharms, J. R. E., Ridderinkhof, H., and de Ruijter, W. P. M., 2010. Observed characteristics of Mozambique Channel eddies, *J. Geophys. Res.*, 115, C09006, doi:10.1029/2009JC005875.

Takahashi, T., Olafsson, J., Goddard, J. G., Chipman, D. W., and Sutherland, S. C., 1993. Seasonal variation of CO_2 and nutrients in the high-latitude surface oceans: A comparative study, *Global Biogeochem. Cycles*, 7(4), 843– 878, doi:10.1029/93GB02263.

Takahashi, T., Sutherland, S. C., Sweeney, C., Poisson, A., Metzl, N., Tilbrook, B., Bates, N., Wanninkhof, R., Feely, R. A., Sabine, C., Olafsson, J., and Nojiri, Y., 2002. Global Sea-Air CO_2 Flux Based on Climatological Surface Ocean pCO_2, and Seasonal Biological and Temperature Effect. *Deep-Sea Res. II*, 49, 9-10, 1601-1622, https://doi.org/10.1016/S0967-0645(02)00003-6.

Takahashi, T., Sutherland, S. C., Wanninkhof, R., Sweeney, C., Feely, R. A., Chipman, D. W., Hales, B., Friederich, G., Chavez, F., Sabine, C., Watson, A. J., Bakker, D. C., Schuster, U., Metzl, N., Yoshikawa-Inoue, H., Ishii, M., Midorikawa, T., Nojiri, Y., Körtzinger, A., Steinhoff, T., Hoppema, M., Olafsson, J., Arnarson, T. S., Tilbrook, B., Johannessen, T., Olsen, A., Bellerby, R., Wong, C., Delille, B., Bates, N., and de Baar, H. J., 2009. Climatological mean and decadal change in surface ocean pCO_2, and net sea air CO_2 flux over the global oceans. *Deep-Sea Res. II*,56(8-10), 554–577, http://dx.doi.org/10.1016/j.dsr2.2008.12.009.

Takahashi, T., Sutherland, S. C., Chipman, D. W., Goddard, J. G., Ho, C., Newberger, T., Sweeney, C. and Munro, D. R., 2014. Climatological distributions of pH, pCO_2, total CO_2, alkalinity, and $CaCO_3$ saturation in the global surface ocean, and temporal changes at selected locations. *Marine Chemistry*, 164, 95–125, doi:10.1016/j.marchem.2014.06.004.

Tan, K. and H. Zheng, 2020. Ocean acidification and adaptive bivalve farming. Science of The Total Environment, Volume 701, 134794,https://doi.org/10.1016/j.scitotenv.2019.134794.

Ternon, J.F., M.J. Roberts, T. Morris, L. Hancke, and B. Backeberg, 2014. In situ measured current structures of the eddy field in the Mozambique Channel. *Deep Sea Research Part II: Topical Studies in Oceanography*,100,10-26,https://doi.org/10.1016/j.dsr2.2013.10.013.

Tierney, J. E., N. J. Abram, K. J. Anchukaitis, M. N. Evans, C. Giry, K. H. Kilbourne, C. P. Saenger, H. C. Wu, and J. Zinke, 2015. Tropical sea surface temperatures for the past four centuries reconstructed from coral archives, *Paleoceanography*, *30*, 226–252, doi:10.1002/2014PA002717.

Tilbrook, B., Jewett, E. B., DeGrandpre, M. D., Hernandez-Ayon, J. M., Feely, R. A., Gledhill, D. K., Hansson, L., Isensee, K., Kurz, M. L., Newton, J. A., Siedlecki, S. A., Chai, F., Dupont, S., Graco, M., Calvo, E., Greeley, D., Kapsenberg, L., Lebrec, M., Pelejero, C., Schoo, K. L. and Telszewski, M., 2019. An Enhanced Ocean Acidification Observing Network: From People to Technology to Data Synthesis and Information Exchange, *Front. Mar. Sci.*, 6, doi:10.3389/fmars.2019.00337.

Touratier, F., Azouzi, L. and Goyet, C., 2007. CFC-11, Δ14C and 3H tracers as a means to assess anthropogenic CO_2 concentrations in the ocean. *Tellus B*, 59(2), 318–325, doi:10.1111/j.1600-0889.2006.00247.x.

Tréguer, P., and P. Le Corre, 1975. Manuel d'analyse des sels nutritifs dans l'eau de mer (utilisation de l'autoanalyseur II Technicon), 2nd ed., 110 pp., L.O.C.U.B.O., Brest, 1975.

Tribollet, A., 2019. Rapport de campagne, Rotation du Marion Dufresne dans les Iles Eparses du 4 au 30 avril 2019, CONSORTIUM DE RECHERCHE TAAF « ILES EPARSES 2017-2020 », Rapport Interne LOCEAN, 15 pp.

Tribollet, A., 2020. Rapport d'activité intermédiaire 2019 : Projet CLIM-EPARSES. CONSORTIUM DE RECHERCHE TAAF "Iles Eparses 2017-2020". 8 pp.

Tribollet A., A. Chauvin and P. Cuet, 2019. Carbonate dissolution by reef microbial borers: a biogeological process producing alkalinity under different pCO2 conditions. *FACIES*, 65, 2, DOI:10.1007/s10347-018-0548-x

Trnovsky, D., L. Stoltenberg, T. Cyronak and B.D. Eyre, 2016. Antagonistic Effects of Ocean Acidification and Rising Sea Surface Temperature on the Dissolution of Coral Reef Carbonate Sediments. *Frontiers in Mar. Sci.* doi: 10.3389/fmars.2016.00211

Uppström, L. R., 1974. The boron/chlorinity ratio of deep-sea water from the Pacific Ocean, Deep Sea Research and Oceanographic Abstracts, 21, 161–162, https://doi.org/10.1016/0011-7471(74)90074-6.

Van Heuven, S., Pierrot, D., Rae, J.W.B., Lewis, E., Wallace, D.W.R., 2011. MATLAB Program Developed for CO2 System Calculations. ORNL/CDIAC-105b. Oak Ridge, TN: Carbon Dioxide Information Analysis Center, Oak Ridge National Laboratory, U.S. Department of Energy. DOI:10.3334/CDIAC/otg.CO2SYS_MATLAB_v1.1.

Waldbusser, G. G., Hales, B., Langdon, C. J., Haley, B. A., Schrader, P., Brunner, E. L., Gray, M. W., Miller, C. A., and Gimenez, I., 2015. Saturation-state sensitivity of marine bivalve larvae to ocean acidification. *Nature Clim. Change*, 5(3), 273-280. Doi:10.1038/NCLIMATE2479.

Weiss, R. F. and Price, B. A., 1980. Nitrous oxide solubility in water and seawater. *Marine Chemistry*, 8(4), 347–359, doi:10.1016/0304-4203(80)90024-9.

Westberry, T. K., and D. A. Siegel, 2006. Spatial and temporal distribution of Trichodesmium blooms in the world’s oceans, *Global Biogeochem. Cycles*, 20, GB4016, doi:10.1029/2005GB002673.

Wu H., Dissard D., Douville E., Blamart D., Bordier L., Tribollet A., Le Cornec F., Pons-Branchu E., Dapoigny A. and Lazareth C.E., 2018. Surface ocean pH variations since 1689 CE and recent ocean acidification in the tropical south Pacific. *Nature Comm.,* 9:2543, DOI:10.1038/s41467-018-04922-1

Zinke, J., Loveday, B., Reason, C., Dullo, W.-C., & Kroon, D., 2014. Madagascar corals track sea surface temperature variability in the Agulhas Current core region over the past 334 years. *Scientific Reports*, *4*, 4393. https://doi.org/10.1038/srep04393

Figures Captions

Figure 1: Cruises in the Mozambique Channel included to the SOCAT data product (version v2020, www.socat.info, Bakker et al., 2016, 2020). Color code is for Year. In the Mozambique Channel, cruises for May 1963 (in blue), January 2004 (OISO-11, in orange), April 2019 (CLIM-EPARSES, in brown). Water-column data from GLODAP at 25°S were collected in Jun-1995 (yellow) and Dec-2003 (orange). All cruises used in this study are listed in Table 1. Figure produced with ODV (Schlitzer, 2013).

Figure 2: Sea surface temperature (a), salinity (b) and fCO_2 (c) in the Mozambique Channel observed in January 2004 (orange) and April 2019 (blue). In (c) the dashed lines correspond to atmospheric fCO_2. All underway data, including near Islands are shown.

Figure 3: (a) Sea surface A_T (µmol.kg^{-1}) and (b) sea surface C_T (µmol.kg^{-1}) in the Mozambique Channel observed in January 2004 (orange) and April 2019 (blue). All underway data, including near Islands are shown.

Figure 4: Same as Figure 3 for (a) Salinity normalized A_T (N-A_T, µmol.kg^{-1}) and (b) Salinity normalized C_T (N-C_T, µmol.kg^{-1}) in the Mozambique Channel observed in January 2004 (orange) and April 2019 (blue). Also presented in (c) the fCO_2 normalized at SST 29°C (fCO_2-29C, µatm). All underway data, including near Islands are shown.

Figure 5: Total Alkalinity (A_T, µmol.kg^{-1}) versus salinity in surface water in the Mozambique Channel (14-25°S) observed in January 2004 (orange circles) and April 2019 (blue triangle). Linear relation for each period are also shown (orange and blue dashed-lines). In January 2004 data north of 14°S near Mayotte are identified with filled orange circles and not used for the A_T/SSS relationship. Also shown are the A_T/SSS relationships from Millero et al. (1998) for the Indian Ocean (Purple dashed) and from Lee et al. (2006) for the subtropical oceans (Grey dashed). The A_T/SSS relationship based on Jan-2004 and Apr-2019 data in the Mozambique Channel (noted AT-MOZ, black line) is the final relationship used in this analysis: A_T= 73.841* S – 291.02.

Figure 6: Surface water pH (at SST 29°C) distribution in the Mozambique Channel observed in January 2004 (orange) and April 2019 (blue). (a) pH at 29°C calculated with A_T and C_T pairs. (b) pH at 29°C calculated with fCO_2 and A_T reconstructed from salinity. Data very close to Islands filtered (e.g. Juan de Nova at 17°S).

Figure 7: Surface water temperature (a), fCO_2 (b) and calculated pH (c) in the Mozambique Channel observed in May 1963 (grey), January 2004 (orange) and April 2019 (blue). In (b) atmospheric fCO_2 also shown for each year (same color, dashed line).

Figure 8: Surface water fCO_2 at SST=29°C (a) and calculated pH at SST=29°C (b) in the Mozambique Channel observed in May 1963 (grey), January 2004 (orange) and April 2019 (blue). In (c) also shown N-C_T distribution calculated with fCO_2 and A_T reconstructed.

Figure 9: Sea surface water temperature (a), fCO_2 (b) and calculated pH (c) around 25°S in the Mozambique Channel observed in May 1963, June 1995, December 2003, January 2004, July 2014 and April 2019. Cruises are listed in Table 1 and tracks identified in Figure 1. The mean observations for each cruise are listed in Table 4.

Figure 10: Temporal evolution of fCO_2 (a), pH (b) and N-C_T (c) around 25°S in the Mozambique Channel based on data shown in Figure 9. Measured fCO_2 and N-C_T are indicated by orange dots. pH and N-C_T calculated with fCO_2 and A_T are indicated by open circles. In all panels, values adjusted to the month of June indicated by grey diamond and used for trend estimates (dashed grey lines). In (a) and (b) results from monthly reconstructed pCO_2 and pH (at 25°S-40°E) shown in purple line for June 1985-2019 (CMEMS-LSCE-NN, Chau et al 2020). In (a) also shown the atmospheric fCO_2 (orange dotted line). The mean observations for each cruise are listed in Table 4 and trends listed in Table 5. Standard-deviations for observations and calculated pH or N-C_T are indicated by vertical bars (generally about the size of symbols).

Figure 11: Annual trends (see Table 5) estimated for different periods in the southern Mozambique Channel (25°S) based on observations for fCO_2 (grey, $\mu atm.yr^{-1}$), pH (orange, $unit.yr^{-1}$) and N-C_T (blue, $\mu mol.kg^{-1}.yr^{-1}$). For pH, the annual trend is multiplied by -1000 (a pH trend of 1.5 in the figure is -0.0015.yr^{-1}). For short periods such as 1995-2004 the errors are large and thus the interpretation is limited. For longer periods, fCO_2 and pH trends are higher in 2004-2019 compared to 1963-1995 and mainly linked to anthropogenic CO_2 as suggested by N-C_T changes.

Figure 12: Annual trends (see Table 5) for fCO_2 (grey, $\mu atm.yr^{-1}$) and pH (orange, $unit.yr^{-1}$) estimated for different periods in the southern Mozambique Channel (25°S) based on observations (filled bars) and the CMEMS-LSCE-FFNN model (hatched bars). For pH, the trend is multiplied by -1000 (a pH trend of 1.5 in the figure is -0.0015.yr^{-1}). Given the errors associated to these estimates, the trends are the same either based on observations or the CMEMS-LSCE-FFNN model.

Figure 13a: Reconstructed (black lines) sea surface fCO_2 (a), pH (b) and N-C_T (c) for the periods 1960-2019 based on atmospheric xCO_2 historical data. Also shown the mean results at 25°S based on observations (orange circles for fCO_2 and N-C_T) or calculated from fCO_2 and A_T/SSS (blue triangles) as described in Figure 10 and listed in Table 4. The monthly pCO_2 and pH (at 25°S-40°E) for 1985-2019 from the CMEMS-LSCE-NN model (Chau et al 2020) is shown in purple line in (a) and (b). In all figures the orange curves are the reconstructed values assuming ocean fCO_2 in equilibrium with the atmosphere.

Figure 13b: Same as figure 11a for the period 1800-2019. For clarity results from the CMEMS-LSCE-NN model for 1985-2019 not shown here.

Tables

Table 1: List of cruises in the Mozambique Channel (10°S-25°S) used in this study for surface fCO_2 data (SOCAT, version v2020, Bakker et al., 2016, 2020) and for A_T/C_T water column at 25°S (GLODAPv2.2019, Olsen et al, 2019).

Data-Base	Expocode	Period Month-Year	Region (Lat. Band)	PI or Reference
		Surface Underway fCO_2		
SOCAT-v2020	31AR19630216	May-1963	10°S-27°S	Keeling and Waterman (1968)
SOCAT-v2020	316N19950611	Jun-1995	at 25°S	Key R.
SOCAT-v2020	49NZ20031209	Dec-2003	at 25°S	Murata A.
SOCAT-v2020	35MV20040106	Jan-2004	10°S-27°S	Metzl (2009) and this study[(a)]
SOCAT-v2020	06BE20140710	Jul-2014	at 25°S	Steinhoff, T., Koertzinger, A
SOCAT-v2020	35MV20190405	Apr-2019	10°S-27°S	This Study[a]
		Hydrocast stations (with C_T and A_T in water column)		
GLODAPv2-2019	316N19950611	Jun-1995	at 25°S	Sabine et al (1999)
GLODAPv2-2019	49NZ20031209	Dec-2003	at 25°S	Murata et al (2010)

(a) In January 2004 and April 2019 A_T and C_T were also measured underway

Table 2: Mean measured, calculated and trends of surface properties in the band 14°S-25°S based on observations in May 1963, January 2004 and April 2019 in the Mozambique Channel. Nb is the number of data (ND= No Data). Standard deviations are indicated in bracket. Average N-C_T and N-A_T measured only in 2004 and 2019 are also listed to compare with N-C_T and N-A_T calculated with fCO_2 and A_T/SSS relationship. Adjusted values for April 2004 and April 1963 as specified were used to estimate the trends of fCO_2 and N-C_T for different periods. Errors for the trends (in bracket) are based on fCO_2, A_T and C_T measurements uncertainty for each cruise as documented in the main text and Table S1 in Supplementary Material. Last line is the fCO_2 trend without the long-term warming of +0.011 °C.yr^{-1}.

Period	Nb	SST °C	fCO_2 µatm	N-C_{Tcal} µmol/kg	N-A_{Tcal} µmol/kg	Nb	N-C_{Tmes} µmol/kg	N-A_{Tmes} µmol/kg
April-2019	1677	28.61 (0.83)	397.2 (7.9)	1964.9 (4.4)	2293.1 (1.3)	376	1967.5 (6.9)	2292.8 (4.8)
January-2004	480	29.45 (0.73)	398.9 (8.9)	1958.0 (5.8)	2294.7 (1.3)	142	1955.8 (8.6)	2296.3 (5.8)
May-1963	59	25.77 (1.45)	296.2 (4.9)	1925.7 (10.0)	2292.4 (1.0)	ND	ND	ND
April-2004 (adjusted)			370.8	1949.9			1952.2	
April-1963 (adjusted)			308.1	1908.4			ND	
Trend			fCO_2 µatm.yr^{-1}	N-C_{Tcal} µmol.kg^{-1}.yr^{-1}			N-C_{Tmes} µmol.kg^{-1}.yr^{-1}	
2004-2019			+1.75 (0.81)	+1.00 (0.81)			+1.04 (0.79)	
1963-2004			+1.53 (0.28)	+1.00 (0.39)			ND	
1963-2019			+1.58 (0.18)	+1.00 (0.29)			ND	
1963-2019 (without warming)			+1.44 (0.18)					

Table 3: Mean sea surface and trends of pH in the band 14°S-25°S in May 1963, January 2004 and April 2019 in the Mozambique Channel. Nb is the number of data (ND= No Data). Standard deviations for mean values and errors for trends are indicated in bracket. Errors for trends are based on fCO_2, A_T and C_T measurements uncertainty for each cruise as documented in the main text and Table S1 in Supplementary Material. pH is calculated with fCO_2 data and A_T/SSS relationship or with measured C_T and A_T (for 2004 and 2019). Averaged pH at SST-29°C is also listed. Adjusted values for April 2004 and April 1963 as specified were used to estimate the trends of pH for different periods. Last line is the pH trend without the long-term warming of +0.011 °C.yr^{-1}.

Period	Nb (fCO_2)	pH TS	pH-29C TS	Nb (A_T-C_T)	pH TS	pH-29C TS
April-2019	1677	8.040 (0.008)	8.034 (0.007)	376	8.035 (0.008)	8.029 (0.008)
January-2004	480	8.039 (0.008)	8.045 (0.009)	142	8.044 (0.010)	8.051 (0.010)
May-1963	59 (0.008)	8.143 (0.015)	8.094	ND	ND	ND
April-2004 (adjusted)		8.063			8.059	
Avril-1963 (adjusted)		8.126			ND	

Trend	pH (fCO_2) TS.yr^{-1}	pH (A_T-C_T) TS.yr^{-1}
2004-2019	-0.00154 (0.00100)	-0.00160 (0.00149)
1963-2004	-0.00154 (0.00039)	
1963-2019	-0.00154 (0.00028)	
1963-2019 (without warming)	-0.00137 (0.00028)	

Table 4: Mean sea surface measured or calculated properties around 25°S for 6 cruises in the south part of Mozambique Channel. Nb = number of data from surface underway sampling used to calculate $[H^+]$, pH and N-C_T. Standard deviations are in bracket. N-C_T stands for salinity normalized C_T concentrations either calculated with fCO_2 and A_T (N-C_{Tcal}) or measured (N-C_{Tmes}) when available. ND= No Data

Period	Nb	SST °C	fCO_2 µatm	$[H^+]$ nmol.kg^{-1}	pH TS	N-C_{Tcal} µmol.kg^{-1}	N-C_{Tmes} µmol.kg^{-1}
May-1963	15	23.70	288.6	6.965	8.157	1937.8	ND
		(0.59)	(2.6)	(0.055)	(0.003)	(5.6)	
June-1995	717	22.66	314.6	7.381	8.132	1964.7	1961.3
		(0.39)	(1.9)	(0,044)	(0.003)	(2.6)	(4.8) n9
Dec-2003	180	27.58	389.3	8.901	8.051	1968.4	1967.4
		(0.53)	(8.1)	(0.146)	(0.007)	(3.9)	(5.3) n5
Jan-2004	111	27.61	384.6	8.813	8.055	1965.6	1960.5
		(0.53)	(4.5)	(0.101)	(0.005)	(3.3)	(4.5) n24
Jul-2014	820	23.57	359.7	8.268	8.083	1985.9	ND
		(0.67)	(3.9)	(0.080)	(0.004)	(5.0)	
Apr-2019	156	27.31	387.8	8.864	8.052	1969.9	1972.6
		(0.16)	(3.8)	(0.080)	(0.004)	(1.4)	(2.0) n17

Table 5: Trends observed around 25°S in the Mozambique Channel evaluated from observations between 1963 and 2019 adjusted to June (as shown in Figure 10 and Supp. Figure S13 for $[H^+]$). Standard errors of slope are in bracket. Trends for pH are also calculated from $[H^+]$ concentrations following Equation 3 (see text, noted pH_{H+}). Also indicated are the trends for atmospheric xCO_2 for different periods and from the monthly reconstructed pCO_2 and pH values based on a neural network model (CMEMS-LSCE-NN, Denvil-Sommer et al 2019; Chau et al 2020). For CMEMS-LSCE-NN the trends are for June or using all months in 1985-2019. For comparison the trends in June for period 1995-2004, 2004-2019 and 1995-2019 are underlined. ND = No Data. Detail for errors on the trends is documented in the Methods and Table S2 in the Supplementary Material.

Period	Atm xCO_2 ppm.yr^{-1}	fCO_2 µatm.yr^{-1}	$[H^+]$ nmol.kg^{-1}.yr^{-1}	pH_{H+} TS.yr^{-1}	pH TS.yr^{-1}	N-C_{Tcal} µmol.kg^{-1}.yr^{-1}
1963-2019	+1.60	+1.55	0.0290	-0.00188	-0.00167	+1.04
	(0.02)	(0.11)	(0.0036)		(0.0002)	(0.21)
1963-1995	+1.35	+1.14	0.0213	-0.00137	-0.00129	+0.82
	(0.02)	(0.23)	(0.0069)		(0.00042)	(0.41)
1995-2004	+1.82	+1.70	0.0318	-0.00190	-0.00185	+1.15
	(0.04)	(0.81)	(0.0242)		(0.00144)	(1.25)
2004-2019	+2.13	+2.41	0.0452	-0.00247	-0.00243	+1.46
	(0.04)	(0.43)	(0.0145)		(0.00079)	(0.69)
1995-2019	+2.04	+2.20	0.0412	-0.00232	-0.00227	+1.37
	(0.03)	(0.26)	(0.0085)		(0.00048)	(0.42)

CMEMS-LSCE-NN	fCO_2 µatm.yr^{-1}	pH TS.yr^{-1}
1995-2004 June	+1.70	-0.00186
	(0.95)	(0.00163)
2004-2019 June	+2.45	-0.00247
	(0.51)	(0.00078)
1995-2019 June	+2.28	-0.00234
	(0.23)	(0.00039)
1985-2019 June	+1.89	-0.00196
	(0.14)	(0.00024)
1995-2004 Annual	+2.02	-0.00203
	(0.48)	(0.00071)
1995-2019 Annual	+1.88	-0.00180
	(0.14)	(0.00019)
2004-2019 Annual	+1.80	-0.00165
	(0.30)	(0.00038)
1985-2019 Annual	+1.80	-0.00177
	(0.09)	(0.00012)

Table 6: Mean observed or calculated properties and their temporal differences in the layer 150-200m in the region 25°S/38-42°E. Data are from GLODAPv2.2019 (Olsen et al., 2019). All units in µmol.kg^{-1}. Standard-deviations are in bracket. Nb is number of samples in the 150-200m layer.

Month-Year	Expocode	C_T	N-C_T	A_T	N-A_T	O_2	C_{ant}	Nb
Jun-1995	316N19950611	2070.8 (5.9)	2039.0 (5.2)	2329.8 (2.6)	2293.8 (1.9)	194.8 (11.8)	35.1 (1.2)	9
Dec-2003	49NZ20031209	2081.3 (14.2)	2048.0 (15.6)	2332.8 (5.6)	2295.5 (3.1)	184.4 (14.7)	42.3 (3.2)	8
Difference 2003-1995		+10.5 (15.4)	+9.0 (16.4)	+3 (6.7)	+1.6 (3.7)	-10.4 (18.9)	+7.3 (3.4)	

Table 7: Mean C_{ant} accumulation and trends between 1994 and 2007 in the region 25°S/42°E in different layers (data from Gruber et al, 2019b). Standard-deviations are in bracket.

Layer	Delta-C_{ant} µmol.kg^{-1}	Trend (1994 to 2007) µmol.kg^{-1}.yr^{-1}
0-30m	14.44 (0.05)	1.11 (0.004)
50-100m	14.04 (0.19)	1.08 (0.015)
100-150m	13.64 (0.15)	1.05 (0.012)
150-200m	12.94 (0.56)	1.00 (0.043)

Figures

Figure 1

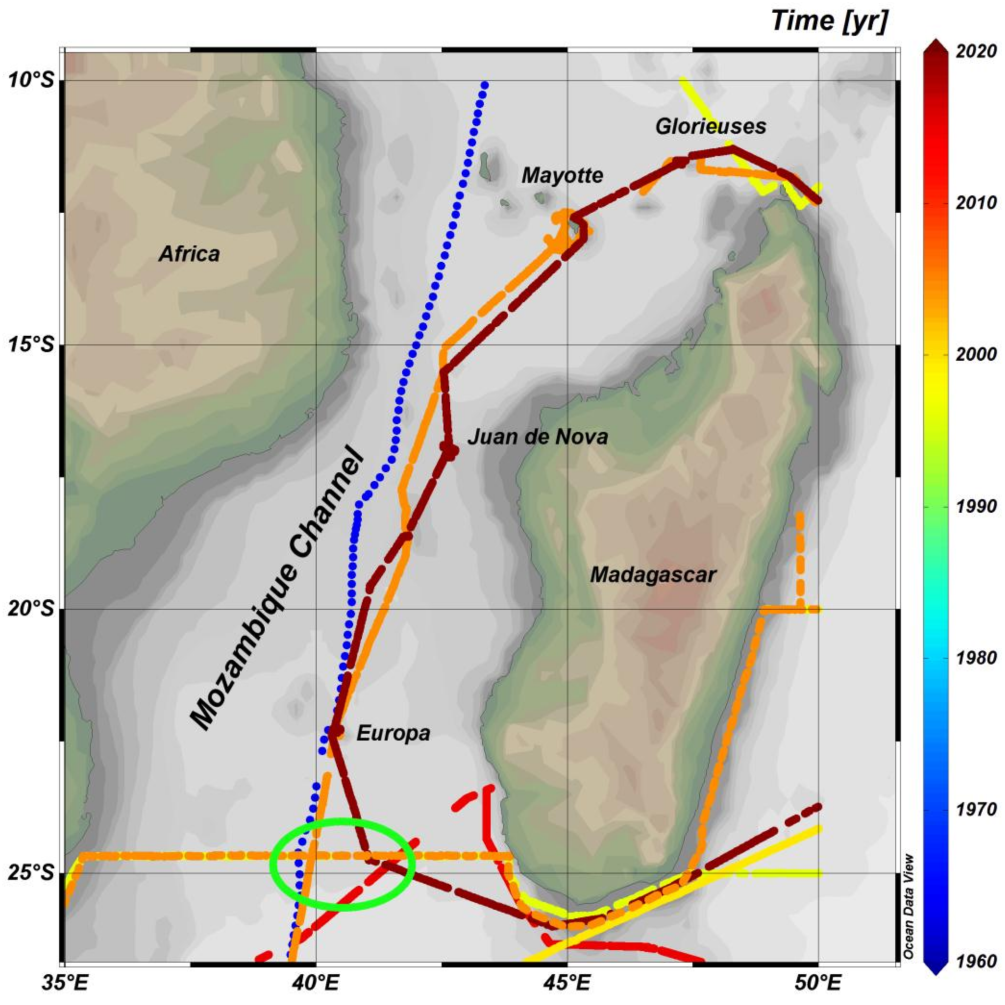

Figure 2

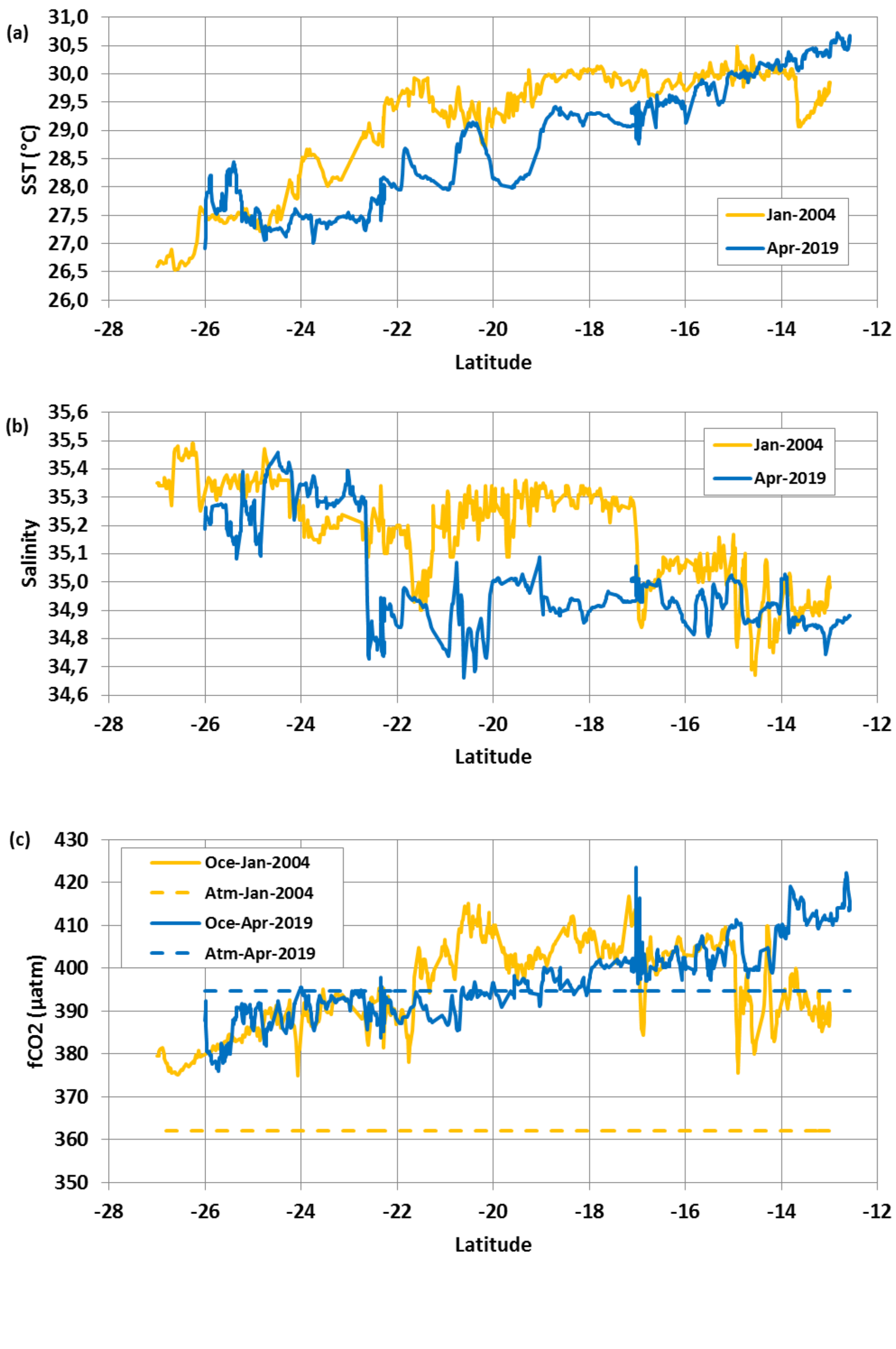

(a)
SST (°C)
Latitude
Jan-2004
Apr-2019
(b)
Salinity
Latitude
Jan-2004
Apr-2019
(c)
fCO2 (µatm)
Latitude
Oce-Jan-2004
Atm-Jan-2004
Oce-Apr-2019
Atm-Apr-2019

Figure 3

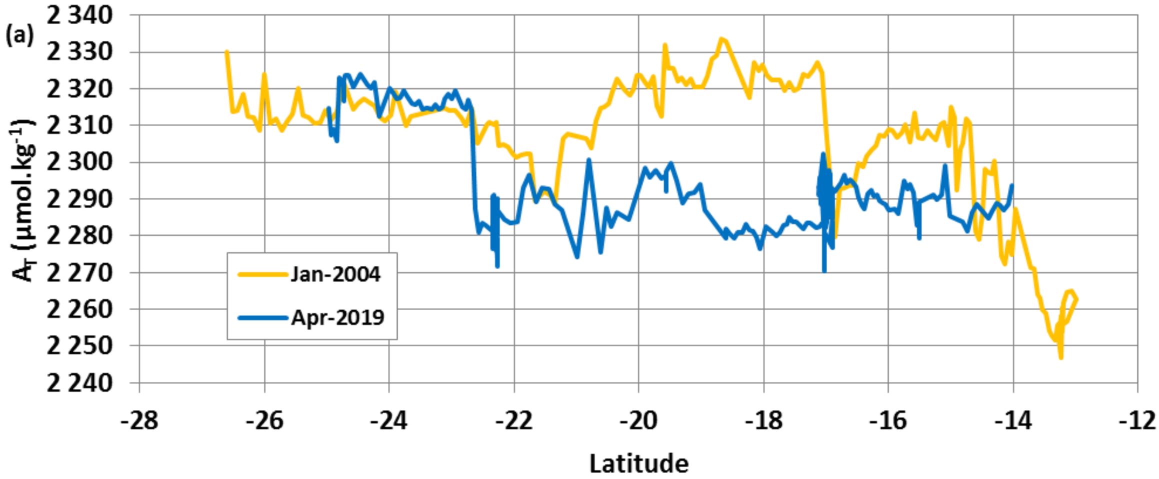

(a)
2 340
2 330
2 320
2 310
2 300
2 290
2 280
2 270
2 260
2 250
2 240
A_T (µmol.kg^{-1})
Jan-2004
Apr-2019
-28
-26
-24
-22
-20
-18
-16
-14
-12
Latitude

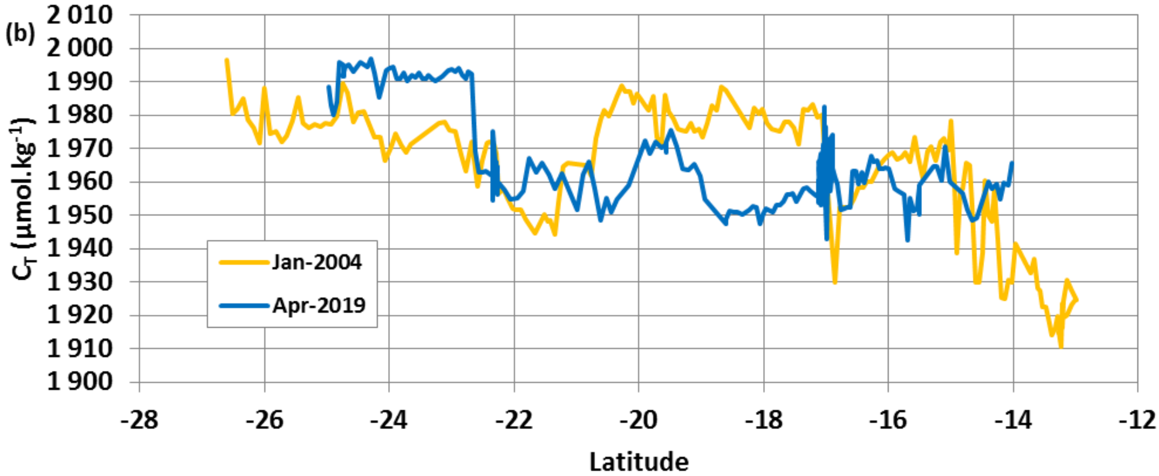

(b)
2 010
2 000
1 990
1 980
1 970
1 960
1 950
1 940
1 930
1 920
1 910
1 900
C_T (µmol.kg^{-1})
Jan-2004
Apr-2019
-28
-26
-24
-22
-20
-18
-16
-14
-12
Latitude

Figure 4

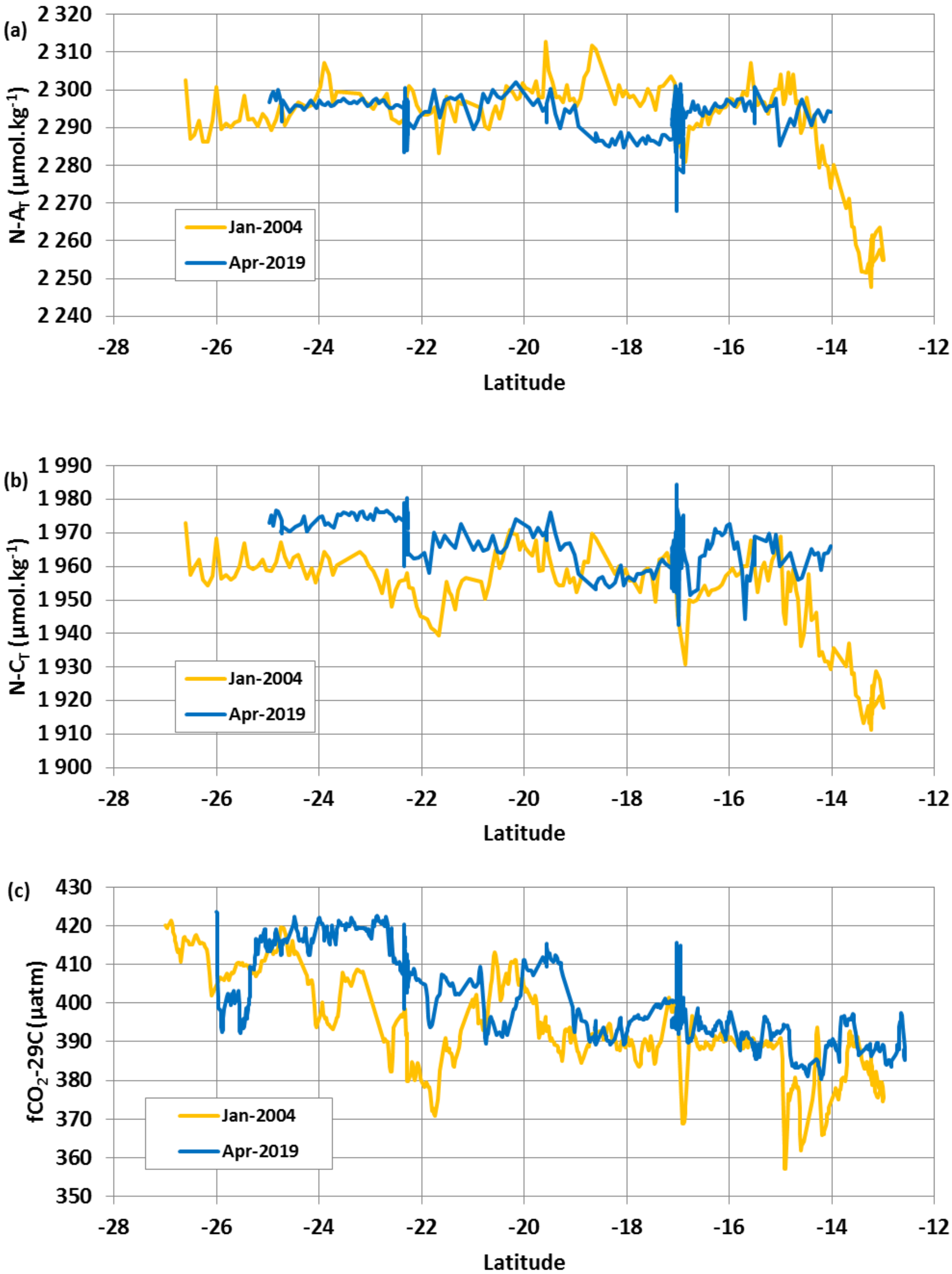

(a)
2 320
2 310
2 300
2 290
2 280
2 270
2 260
2 250
2 240
N-A$_T$ (µmol.kg^{-1})
Jan-2004
Apr-2019
-28
-26
-24
-22
-20
-18
-16
-14
-12
Latitude
(b)
1 990
1 980
1 970
1 960
1 950
1 940
1 930
1 920
1 910
1 900
N-C$_T$ (µmol.kg^{-1})
Jan-2004
Apr-2019
-28
-26
-24
-22
-20
-18
-16
-14
-12
Latitude
(c)
430
420
410
400
390
380
370
360
350
fCO$_2$-29C (µatm)
Jan-2004
Apr-2019
-28
-26
-24
-22
-20
-18
-16
-14
-12
Latitude

Figure 5

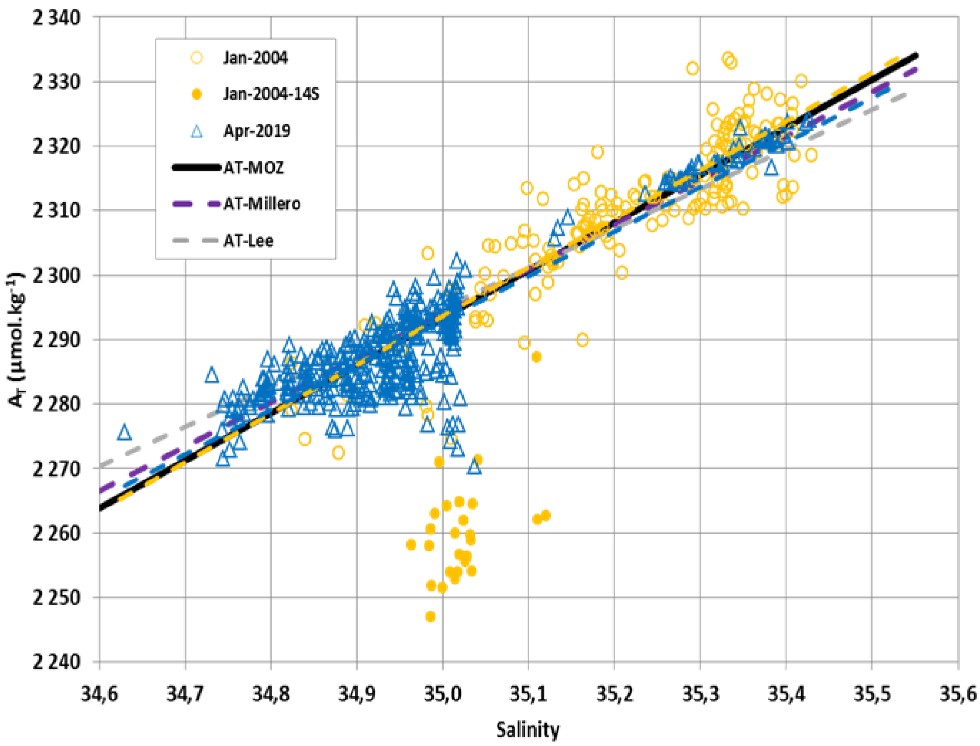

Jan-2004
Jan-2004-14S
Apr-2019
AT-MOZ
AT-Millero
AT-Lee
2 340
2 330
2 320
2 310
2 300
2 290
2 280
2 270
2 260
2 250
2 240
A_T (µmol.kg^{-1})
34,6
34,7
34,8
34,9
35,0
35,1
35,2
35,3
35,4
35,5
35,6
Salinity

Figure 6

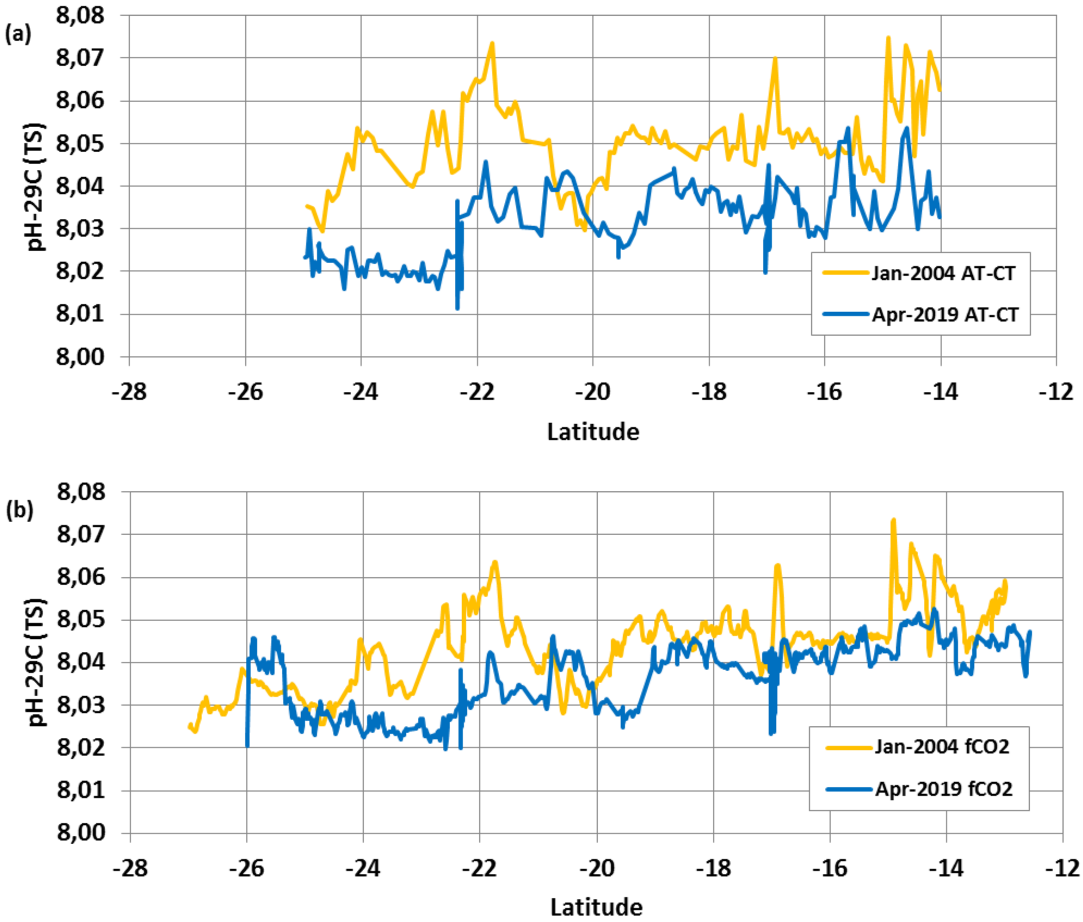

(a)
8,08
8,07
8,06
8,05
8,04
8,03
8,02
8,01
8,00
pH-29C (TS)
-28
-26
-24
-22
-20
-18
-16
-14
-12
Latitude
Jan-2004 AT-CT
Apr-2019 AT-CT
(b)
8,08
8,07
8,06
8,05
8,04
8,03
8,02
8,01
8,00
pH-29C (TS)
-28
-26
-24
-22
-20
-18
-16
-14
-12
Latitude
Jan-2004 fCO2
Apr-2019 fCO2

Figure 7

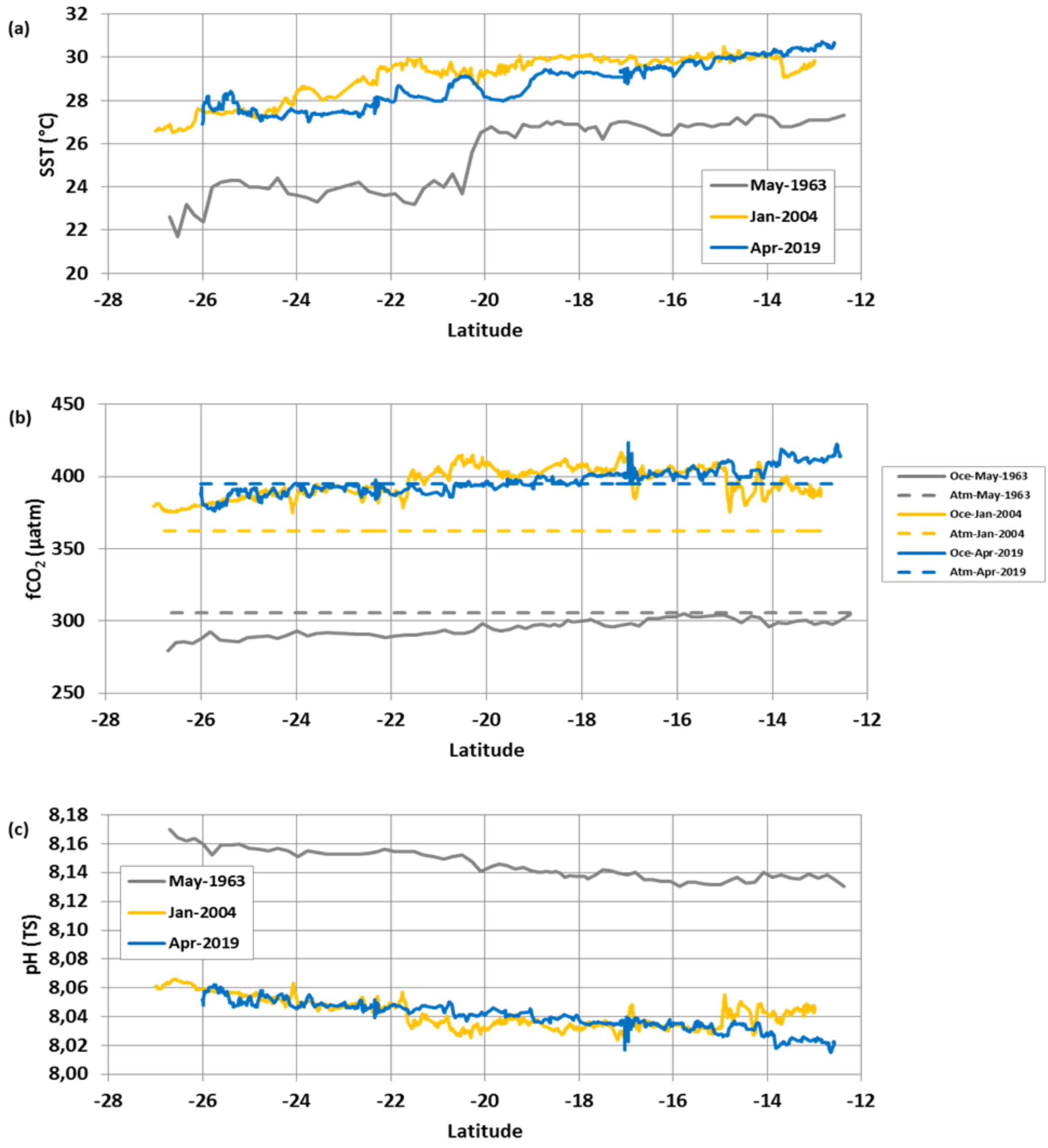

(a)
SST (°C)
32
30
28
26
24
22
20
-28
-26
-24
-22
-20
-18
-16
-14
-12
Latitude
May-1963
Jan-2004
Apr-2019
(b)
fCO2 (µatm)
450
400
350
300
250
-28
-26
-24
-22
-20
-18
-16
-14
-12
Latitude
Oce-May-1963
Atm-May-1963
Oce-Jan-2004
Atm-Jan-2004
Oce-Apr-2019
Atm-Apr-2019
(c)
pH (TS)
8,18
8,16
8,14
8,12
8,10
8,08
8,06
8,04
8,02
8,00
-28
-26
-24
-22
-20
-18
-16
-14
-12
Latitude
May-1963
Jan-2004
Apr-2019

Figure 8

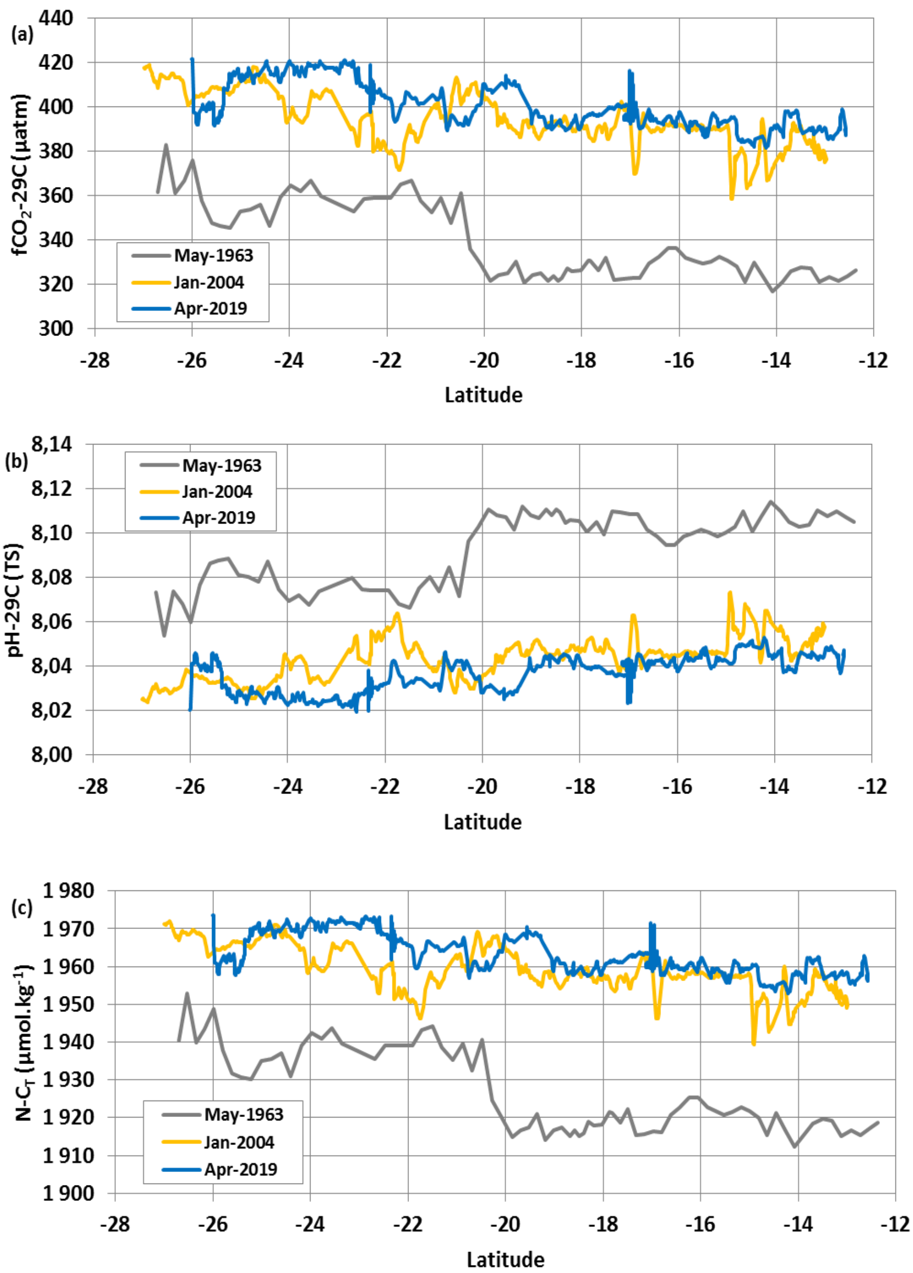
(a)
fCO$_2$-29C (µatm)
440
420
400
380
360
340
320
300
-28
-26
-24
-22
-20
-18
-16
-14
-12
Latitude
May-1963
Jan-2004
Apr-2019
(b)
pH-29C (TS)
8,14
8,12
8,10
8,08
8,06
8,04
8,02
8,00
-28
-26
-24
-22
-20
-18
-16
-14
-12
Latitude
May-1963
Jan-2004
Apr-2019
(c)
N-C$_T$ (µmol.kg^{-1})
1 980
1 970
1 960
1 950
1 940
1 930
1 920
1 910
1 900
-28
-26
-24
-22
-20
-18
-16
-14
-12
Latitude
May-1963
Jan-2004
Apr-2019

Figure 9

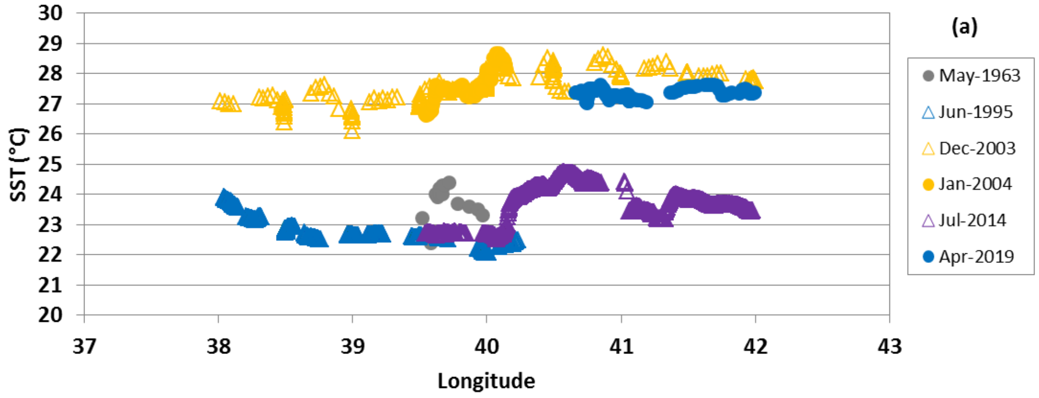

(a)
SST (°C)
Longitude
May-1963
Jun-1995
Dec-2003
Jan-2004
Jul-2014
Apr-2019

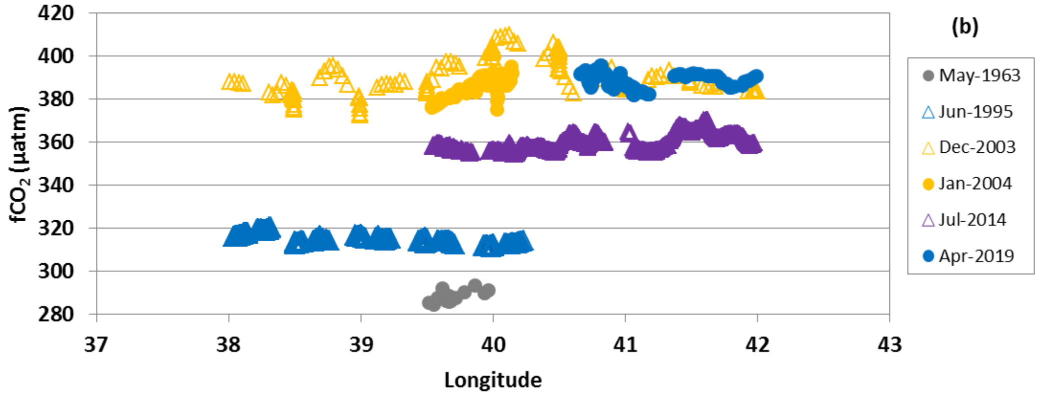

(b)
fCO2 (µatm)
Longitude
May-1963
Jun-1995
Dec-2003
Jan-2004
Jul-2014
Apr-2019

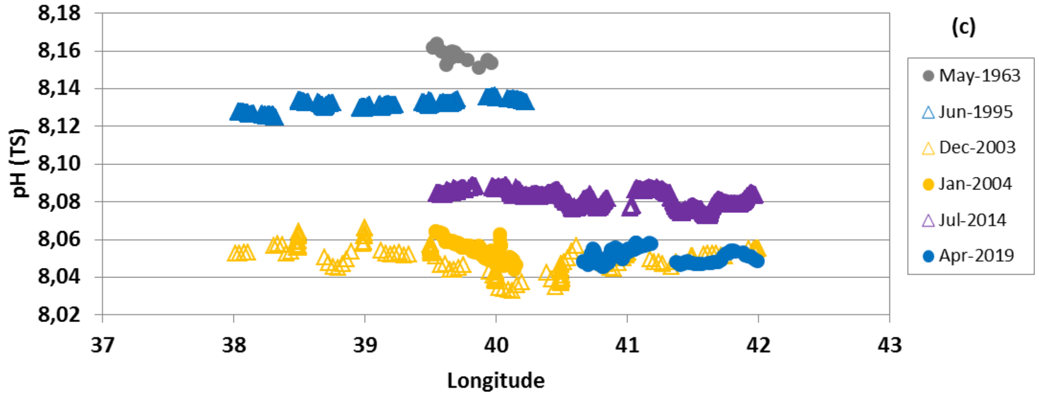

(c)
pH (TS)
Longitude
May-1963
Jun-1995
Dec-2003
Jan-2004
Jul-2014
Apr-2019

Figure 10

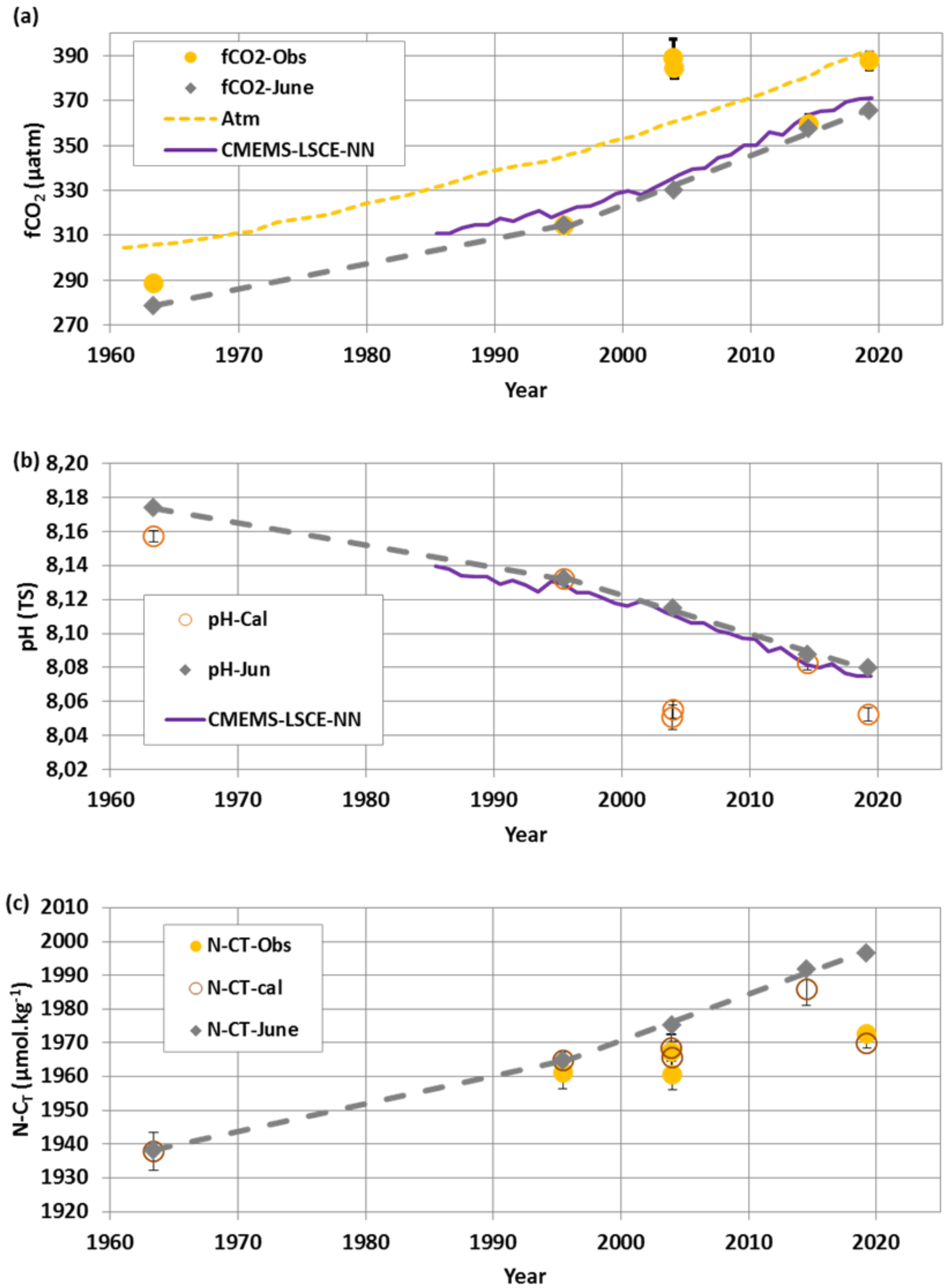

(a)
fCO2-Obs
fCO2-June
Atm
CMEMS-LSCE-NN
fCO_2 (µatm)
390
370
350
330
310
290
270
1960
1970
1980
1990
2000
2010
2020
Year
(b)
pH-Cal
pH-Jun
CMEMS-LSCE-NN
pH (TS)
8,20
8,18
8,16
8,14
8,12
8,10
8,08
8,06
8,04
8,02
1960
1970
1980
1990
2000
2010
2020
Year
(c)
N-CT-Obs
N-CT-cal
N-CT-June
N-C_T (µmol.kg^{-1})
2010
2000
1990
1980
1970
1960
1950
1940
1930
1920
1960
1970
1980
1990
2000
2010
2020
Year

Figure 11

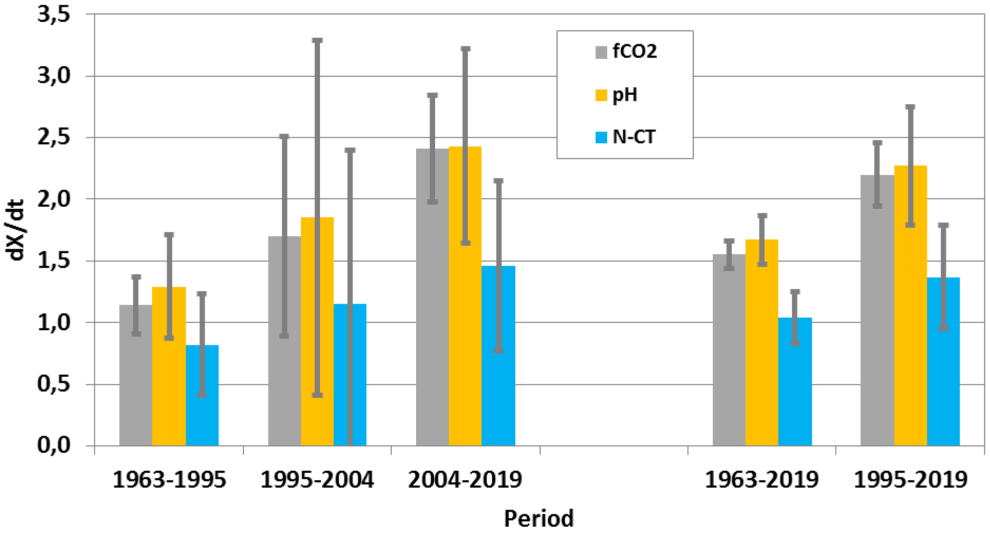

3,5
3,0
2,5
2,0
1,5
1,0
0,5
0,0
dX/dt
fCO2
pH
N-CT
1963-1995
1995-2004
2004-2019
1963-2019
1995-2019
Period

Figure 12

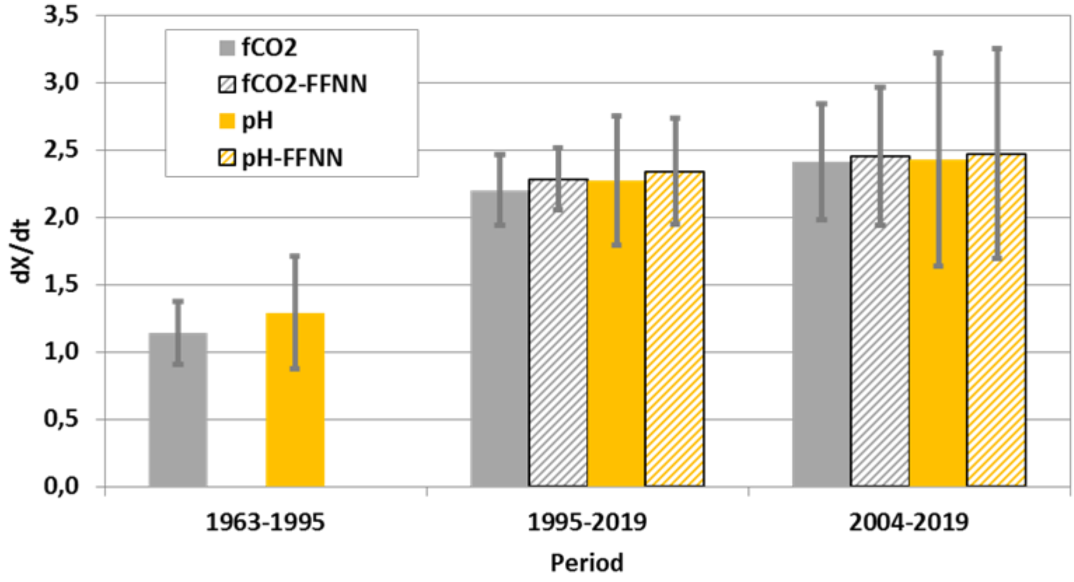

3,5
3,0
2,5
2,0
1,5
1,0
0,5
0,0
dX/dt
fCO2
fCO2-FFNN
pH
pH-FFNN
1963-1995
1995-2019
2004-2019
Period

Figure 13a

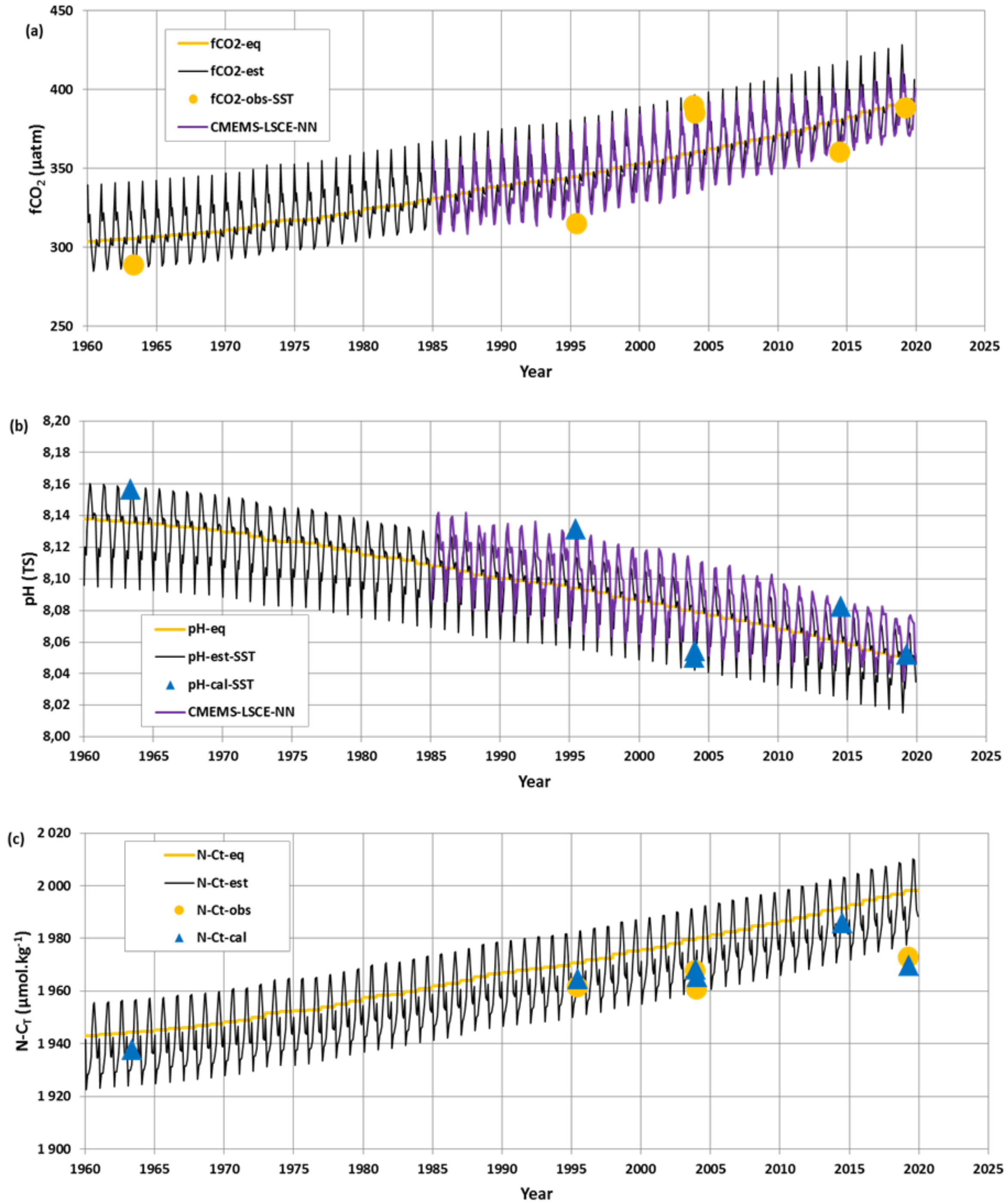

(a)
fCO2-eq
fCO2-est
fCO2-obs-SST
CMEMS-LSCE-NN
fCO2 (µatm)
450
400
350
300
250
1960
1965
1970
1975
1980
1985
1990
1995
2000
2005
2010
2015
2020
2025
Year
(b)
pH-eq
pH-est-SST
pH-cal-SST
CMEMS-LSCE-NN
pH (TS)
8,20
8,18
8,16
8,14
8,12
8,10
8,08
8,06
8,04
8,02
8,00
Year
(c)
N-Ct-eq
N-Ct-est
N-Ct-obs
N-Ct-cal
N-CT (µmol.kg-1)
2 020
2 000
1 980
1 960
1 940
1 920
1 900
Year

Figure 13b

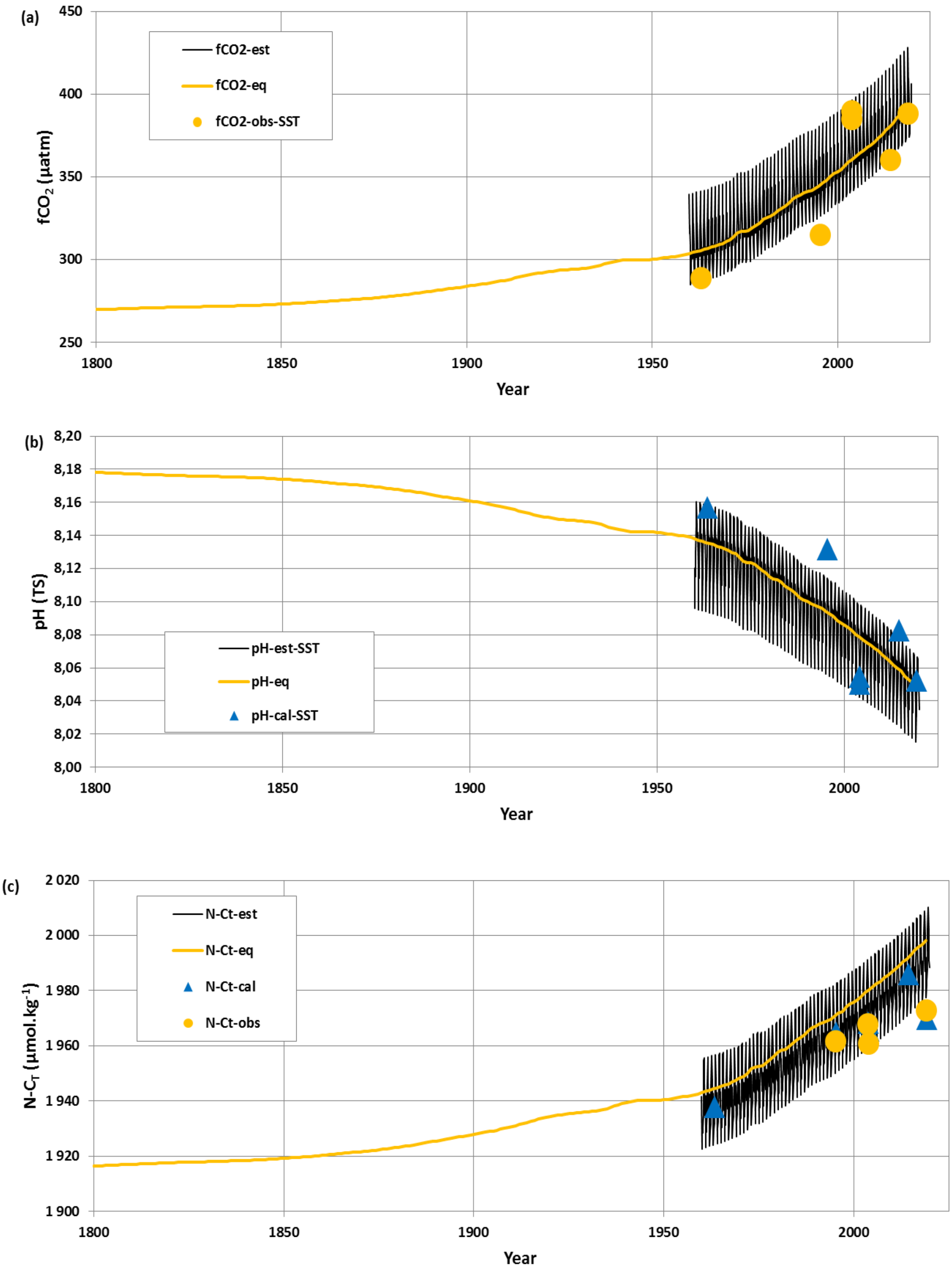

(a)
450
400
350
300
250
fCO2 (µatm)
fCO2-est
fCO2-eq
fCO2-obs-SST
1800
1850
1900
1950
2000
Year
(b)
8,20
8,18
8,16
8,14
8,12
8,10
8,08
8,06
8,04
8,02
8,00
pH (TS)
pH-est-SST
pH-eq
pH-cal-SST
1800
1850
1900
1950
2000
Year
(c)
2 020
2 000
1 980
1 960
1 940
1 920
1 900
N-CT (µmol.kg-1)
N-Ct-est
N-Ct-eq
N-Ct-cal
N-Ct-obs
1800
1850
1900
1950
2000
Year

Supplementary Material

Title: Distribution and long-term change of the sea surface carbonate system in the Mozambique Channel (1963-2019).

Claire Lo Monaco[1], Nicolas Metzl[1], Jonathan Fin[1], Claude Mignon[1], Pascale Cuet[2], Eric Douville[3], Marion Gehlen[3], Thi Tuyet Trang Chau[3], and Aline Tribollet[1]

[1] Laboratoire LOCEAN/IPSL, Sorbonne Université-CNRS-IRD-MNHN, Paris, 75005, Fr

[2] Laboratoire ENTROPIE and Laboratoire d'Excellence CORAIL, Université de La Réunion-IRD- CNRS-IFREMER-Université de la Nouvelle-Calédonie, Saint-Denis, La Réunion, 97744, Fr

[3] Laboratoire LSCE/IPSL, CEA-CNRS-UVSQ, Université Paris-Saclay Gif-sur-Yvette, 91191, Fr

Correspondence to: Nicolas Metzl (nicolas.metzl@locean.ipsl.fr)
Laboratoire LOCEAN – IPSL - UMR 7159 CNRS/IRD/SU/MNHN,
Sorbonne Université, Case 100 - 4 Place Jussieu 75252 Paris cedex 05, France

Revision, Submitted for Special Issue DSRII, "IIOE-2 Volume 4"
Second Revised version, April 1st, 2021

This document includes Figures S1 to S15, Methods for trends and uncertainties estimates, Tables S1, S2 and Figure S16 to S17.

Figure S1: Atmospheric xCO_2 (ppm) measured on-board during OISO-11 in January 2004 (Orange symbols) and Clim-EPARSES in April 2019 (Blue symbols) in the Mozambique Channel. Mean xCO_2 concentrations along these tracks were respectively 377.02 and 410.90 ppm.

Figure S2a: Comparison of measured fCO_2 and calculated fCO_2 from A_T/C_T pairs using K1, K2 constants from Lueker et al (2000). Results are presented for January 2004 (top, orange), April 2019 (middle, blue) and the difference fCO_2calc-fCO_2mes (bottom) for both cruises. Each point corresponds to co-localized values (within 5-10 minutes time). In January 2004, for 154 co-located samples the mean difference was -5.3 µatm (±4.9). In April 2019, for 268 co-located samples the mean difference was +4.5 µatm (±5.2).

Figure S2b: Comparison of measured fCO_2 and calculated fCO_2 from A_T/C_T pairs using K1, K2 constants from (i) Lueker et al (2000) as in figure S2a, (ii) Merbach et al (1973) refitted by Dickson and Millero (1987) (noted MDM) or (iii) from Hansson (1973) and Merbach et al (1973) refitted by Dickson and Millero (1987) (noted HMDM). Figures show the difference fCO_2calc-fCO_2mes for January 2004 (top) and April 2019 (middle). Each point corresponds to co-localized fCO2 and A_T/C_T data (within 5-10 minutes time). Differences of fCO_2 as a function of the ratio C_T/A_T are also shown for the two cruises (bottom). Mean differences for each cruise and different constants K1, K2 listed below.

Figure S3: Left: Trajectory of a drifting buoy (Platform code 1601545) for the period 1-Jan-2019 to 8-June-2019 in the Mozambique Channel, showing the Eddy-like trajectories in the central channel. Right: In mid-March 2019 around 20°S-40°E the buoy recorded low atmospheric pressure (< 990 hPa) due to the passage of the Cyclone "Idai" leading to high precipitation (Figure S4). This explains the SST and SSS records in April 2019. Source: http://www.coriolis.eu.org/Data-Products/Data-Delivery/Data-selection. (Last access, 03-Dec-2020). Figures produced with ODV (Schlitzer, 2013).

Figure S4: Precipitation anomaly in March 2019 in the western Indian Ocean. The maximum anomaly (150mm) in the Mozambique Channel was linked to the severe Cyclone event Idai.
Map from: *https://iridl.ldeo.columbia.edu/maproom/Global/Precipitation/Anomaly.html*
(last access, 28-Nov-2020).

Figure S5: ARGO float trajectory (Plate-form Code 2902142) in the Mozambique Channel. Left: The map shows the float trajectory from Aug-2014 to Feb-2020. Right: Salinity at surface recorded when the float enters the Mozambique Channel in January 2017 (note the minimum in March 2019). Bottom: Salinity section (0-50m) recorded by the float in Jan-May 2019 showing the salinity minimum in late March 2019 after the Cyclone Event Idai. All figures produced with Ocean Data View, ODV (Schlitzer, 2013). Float data obtained from http://www.coriolis.eu.org/Data-Products/Data-Delivery/Data-selection. (last access, 25-Feb-2020).

Figure S6: The annual cycle of SST (a), pCO2 (b) and C_T (c) in the Mozambique Channel (at 16°S, 20°S and 24°S) from the climatology (Takahashi et al 2014).

Figure S7: fCO_2 (µatm) versus SST (°C) for January 2004 (orange circles) and April 2019 (blue triangles) in the Mozambique Channel. The green ellipse identifies data in the vicinity of Juan de Nova Islands.

Figure S8: Top: Surface Chl-a (mg.m^{-3}) observations in the Mozambique Channel measured at several locations in January 2004 (orange) and April 2019 (blue). In 2004, the higher Chl-a values at 14-15°S and 22°S explain the low fCO_2 and departure from fCO_2/SST relation (fig S7). In 2019 a minimum in C_T

was observed at 15.5°S where Chl-a reached a maximum. Bottom: Map of monthly surface Chl-a ($mg.m^{-3}$) in the region for January 2004 and April 2019 derived from MODIS data, highlighting the maximum around 22°S in 2004 extended from the coastal zone of Madagascar. In April 2019, MODIS data show higher Chl-a over the central region. Map produced with ODV (Schlitzer, 2013) from data downloaded at http://marine.copernicus.eu/services-portfolio/access-to-products/ (OCEANCOLOUR_GLO_CHL_L4_REP_OBSERVATIONS_009_082), last access, 20-Oct-2020. In both figures the Chl-a scale is 0-0.5 $mg.m^{-3}$.

Figure S9: Top: Time-series of monthly sea surface Chl-a concentration ($mg.m^{-3}$) averaged in the Mozambique Channel (mean in bounding Box: 38E/26S-43E/15S). Data extracted from MODIS (Giovanni/NASA, last access 31/5/20). Bottom: Mean annual cycles of monthly Chl-a (from data in the top figure) and of N-C_T climatology at 20°S/42°E (open triangles, from Takahashi et al 2014). The N-C_T decrease from January to April is in part linked to biological activity.

Figure S10: Difference of A_T calculated with different A_T/SSS relationships and measured A_T (January 2004 and April 2019, total 505 data) versus salinity. Only A_T samples from open ocean waters are included (i.e. samples measured closed to Islands are not used). A_T/SSS relationships are from Millero et al. (1998) for the Indian Ocean (open squares), from Lee et al. (2006) for the subtropical oceans (open circles), from January 2004 data (orange circles), from April 2019 data (blue triangles) or using Jan-2004 + Apr-2019 data (noted AT-MOZ, black squares). All relationships lead to the same results with no clear statistical differences. Therefore, in this analysis, we use the relationship derived from January 2004 + April 2019 data: A_T= 73.841* S – 291.02 (as shown in Figure 5, see main text).

Figure S11: Monthly SST in the Mozambique Channel for the period 1981-2019 The dashed-line is the estimated annual SST trend of +0.011 (+/-0.007) $°C.yr^{-1}$. Data from Reynolds et al (2002). http://iridl.ldeo.columbia.edu/SOURCES/.NOAA/.NCEP/.EMC/.CMB/.GLOBAL/.Reyn_SmithOIv2/.monthly/ (last access 1/4/2020).

Figure S12: Sea surface distribution of (a) Ω_{Ca} and (b) Ω_{Ar} in the Mozambique Channel calculated from fCO_2 observations in May 1963 (grey), January 2004 (orange) and April 2019 (blue).

Figure S13: Top: Sea surface water [H+] concentrations around 25°S in the Mozambique Channel based on fCO_2 data in May 1963, June 1995, December 2003, January 2004, July 2014 and April 2019. Bottom: Temporal evolution of [H+] around 25°S in the Mozambique Channel based on data shown on top. [H+] concentrations calculated with fCO_2 and A_T are indicated by black circles (listed in Table 4). Values adjusted to the month of June indicated by grey diamond and used for trend estimates (dashed grey lines). Trends for 1963-1995 and 1995-2019 are respectively +0.0212 $nmol.kg.yr^{-1}$ and +0.0409 $nmol.kg.yr^{-1}$.

Figure S14: Distribution in the top 1000m of C_{ant} accumulated between 1994 and 2007 (Delta-C_{ant} in $\mu mol.kg^{-1}$) in the Mozambique Channel. Data are from Gruber et al., (2019b). Figure produced with Ocean Data View, ODV (Schlitzer, 2013).

Figure S15: Reconstructed Aragonite saturation state (Ω_{Ar}) based on atmospheric xCO_2 historical data for seasonal fCO_2 (grey line) or assuming equilibrium (orange line). Calculated values from fCO_2 and A_T/SSS observations in 1963 to 2019 are also shown (blue triangles). The Orange circle identifies Ω_{Ar} = 3 in 2040 if the observed trend in recent decade is projected.

Figure S16: Trend analysis on a Monte Carlo simulation of fCO_2 and pH observed around 25°S in the Mozambique Channel, and adjusted to June (blue stars: mean values of observations, light blue bars: mean ± total uncertainty, black points: pseudo samples, grey and light blue lines: linear functions fitted to the samples and mean observations).

Figure S17: Trend analysis on a Monte Carlo simulation of the CMEMS-LSCE-FFNN estimates for fCO_2 and pH around 25°S in the Mozambique Channel in June for 1985-2019 or 2004-2019 (blue stars: mean values of observations, light blue envelop: mean ± model uncertainty, black points: pseudo samples, grey and light blue lines: linear functions fitted to the samples and mean observations).

Figure S1: Atmospheric xCO_2 (ppm) measured on-board during OISO-11 in January 2004 (Orange symbols) and Clim-EPARSES in April 2019 (Blue symbols) in the Mozambique Channel. Mean xCO_2 concentrations along these tracks were respectively 377.02 and 410.90 ppm.

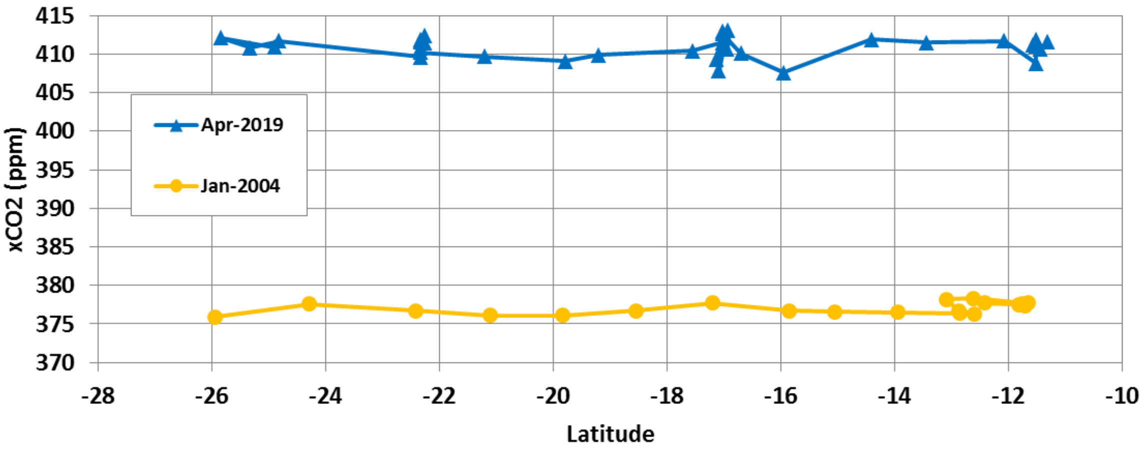

Figure S2a: Comparison of measured fCO_2 and calculated fCO_2 from A_T/C_T pairs using K1, K2 constants from Lueker et al (2000). Results are presented for January 2004 (top, orange), April 2019 (middle, blue) and the difference fCO_2calc-fCO_2mes (bottom) for both cruises. Each point corresponds to co-localized values (within 5-10 minutes time). In January 2004, for 154 co-located samples the mean difference was -5.3 µatm (±4.9). In April 2019, for 268 co-located samples the mean difference was +4.5 µatm (±5.2).

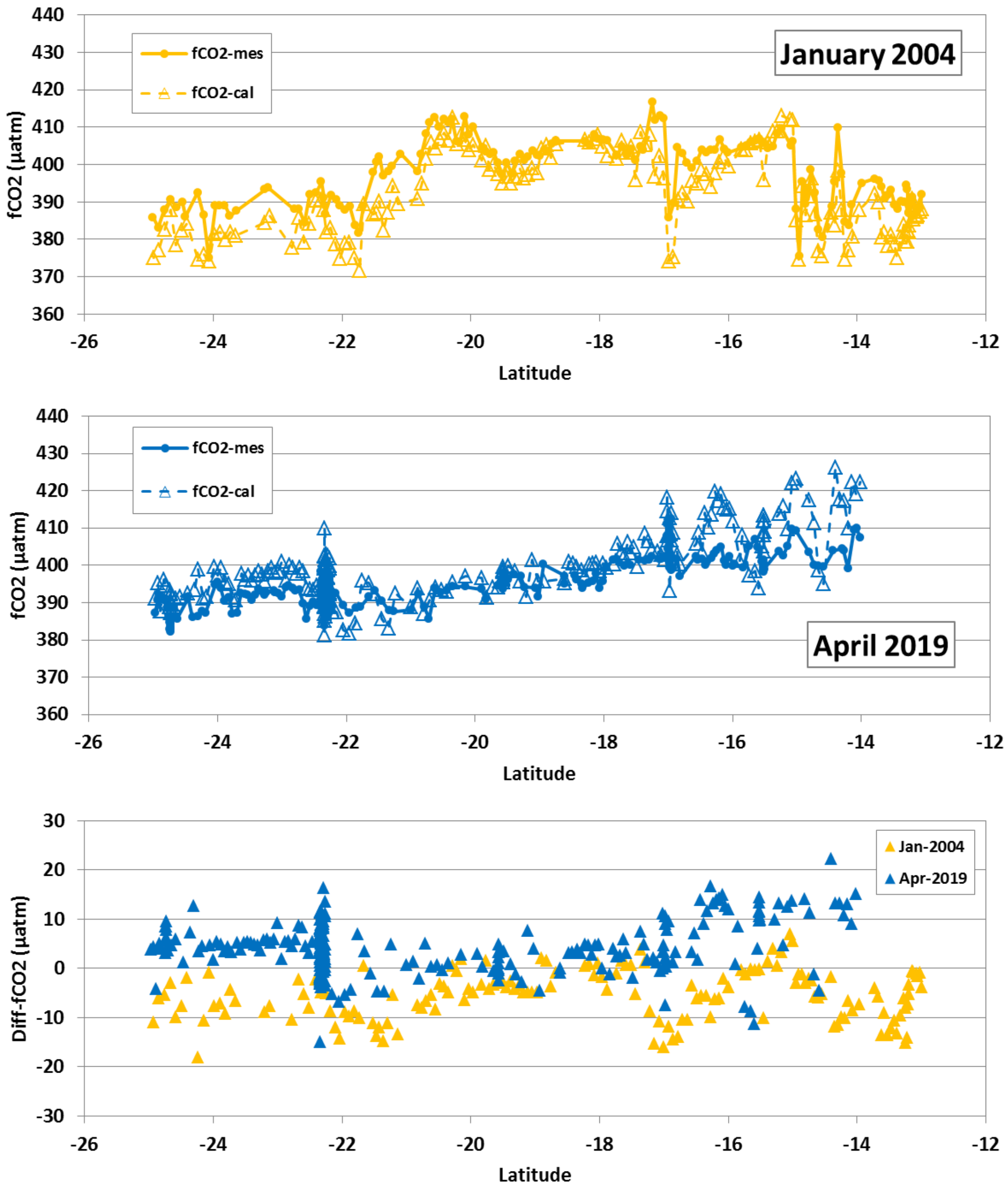

Figure S2b: Comparison of measured fCO_2 and calculated fCO_2 from A_T/C_T pairs using K1, K2 constants from (i) Lueker et al (2000) as in figure S2a, (ii) Merbach et al (1973) refitted by Dickson and Millero (1987) (noted MDM) or (iii) from Hansson (1973) and Merbach et al (1973) refitted by Dickson and Millero (1987) (noted HMDM). Figures show the difference fCO_2calc-fCO_2mes for January 2004 (top) and April 2019 (middle). Each point corresponds to co-localized fCO2 and A_T/C_T data (within 5-10 minutes time). Differences of fCO_2 as a function of the ratio C_T/A_T are also shown for the two cruises (bottom). Mean differences for each cruise and different constants K1, K2 listed below:

Mean difference: fCO_{2cal}-fCO_{2mes} (in µatm)

Cruise	Nb samples	K1,K2 Lueker	K1,K2 MDM	K1,K2 HMDM
OISO-11 Jan-2004	154	-5.4 (±4.9)	-5.9 (±4.9)	+1.8 (±4.9)
CLIM-EPARSES Apr-2019	268	+4.5 (±5.3)	+4.2 (±5.3)	+13.6 (±5.3)

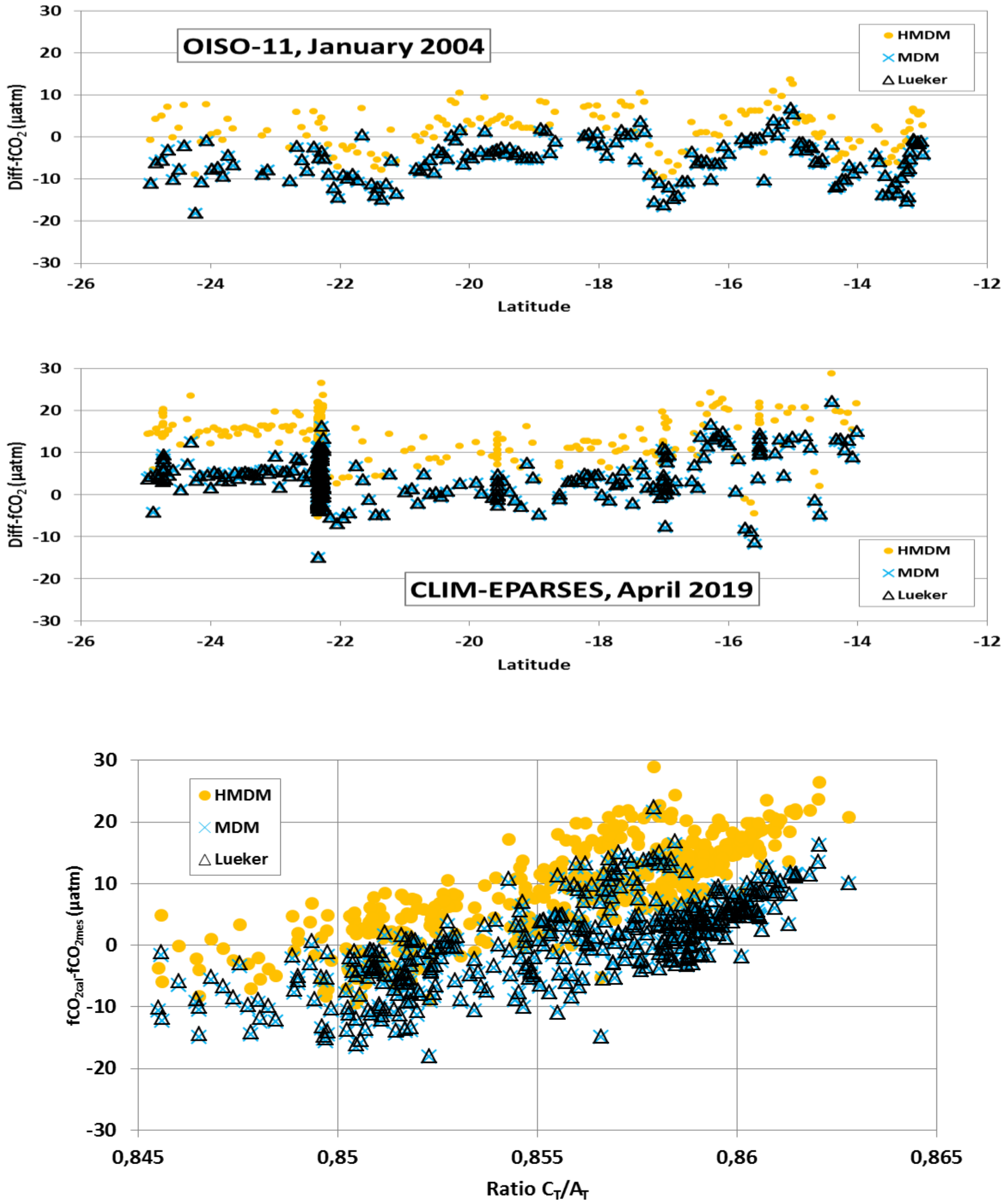

Figure S3: Left: Trajectory of a drifting buoy (Platform code 1601545) for the period 1-Jan-2019 to 8-June-2019 in the Mozambique Channel, showing the Eddy-like trajectories in the central channel. Right: In mid-March 2019 around 20°S-40°E the buoy recorded low atmospheric pressure (< 990 hPa) due to the passage of the Cyclone “Idai” leading to high precipitation (Figure S4). This explains the SST and SSS records in April 2019. Source: http://www.coriolis.eu.org/Data-Products/Data-Delivery/Data-selection. (Last access, 03-Dec-2020). Figures produced with ODV (Schlitzer, 2013).

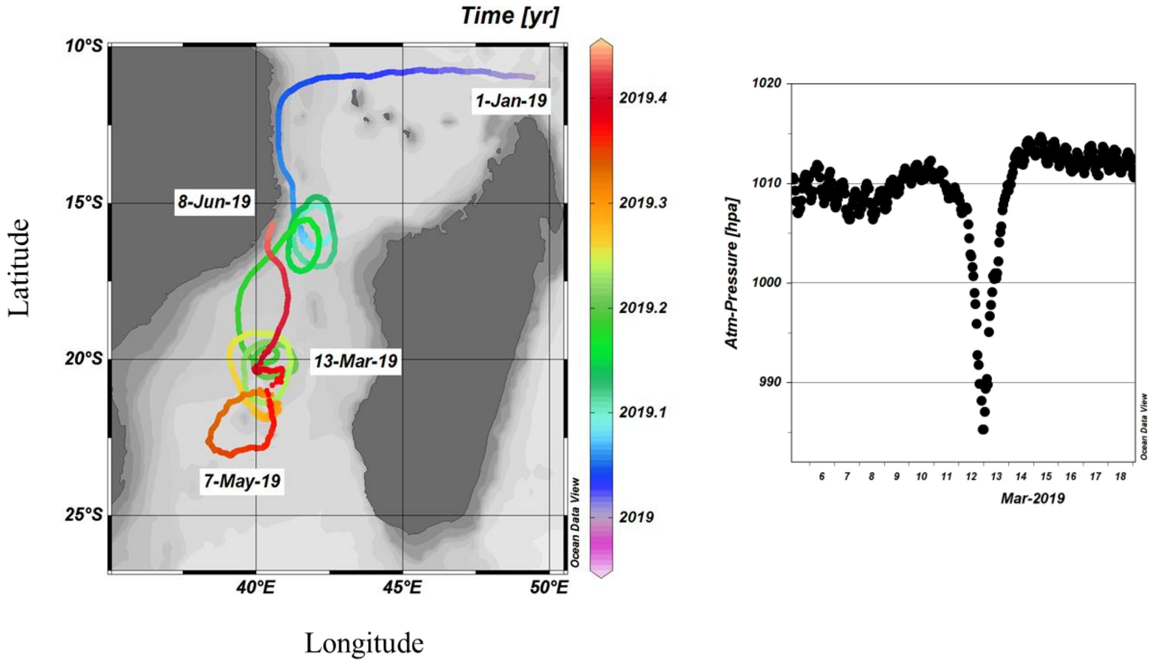

Figure S4: Precipitation anomaly in March 2019 in the western Indian Ocean. The maximum anomaly (150mm) in the Mozambique Channel was linked to the severe Cyclone event Idai.
Map from: *https://iridl.ldeo.columbia.edu/maproom/Global/Precipitation/Anomaly.html*
(Last access, 28-Nov-2020).

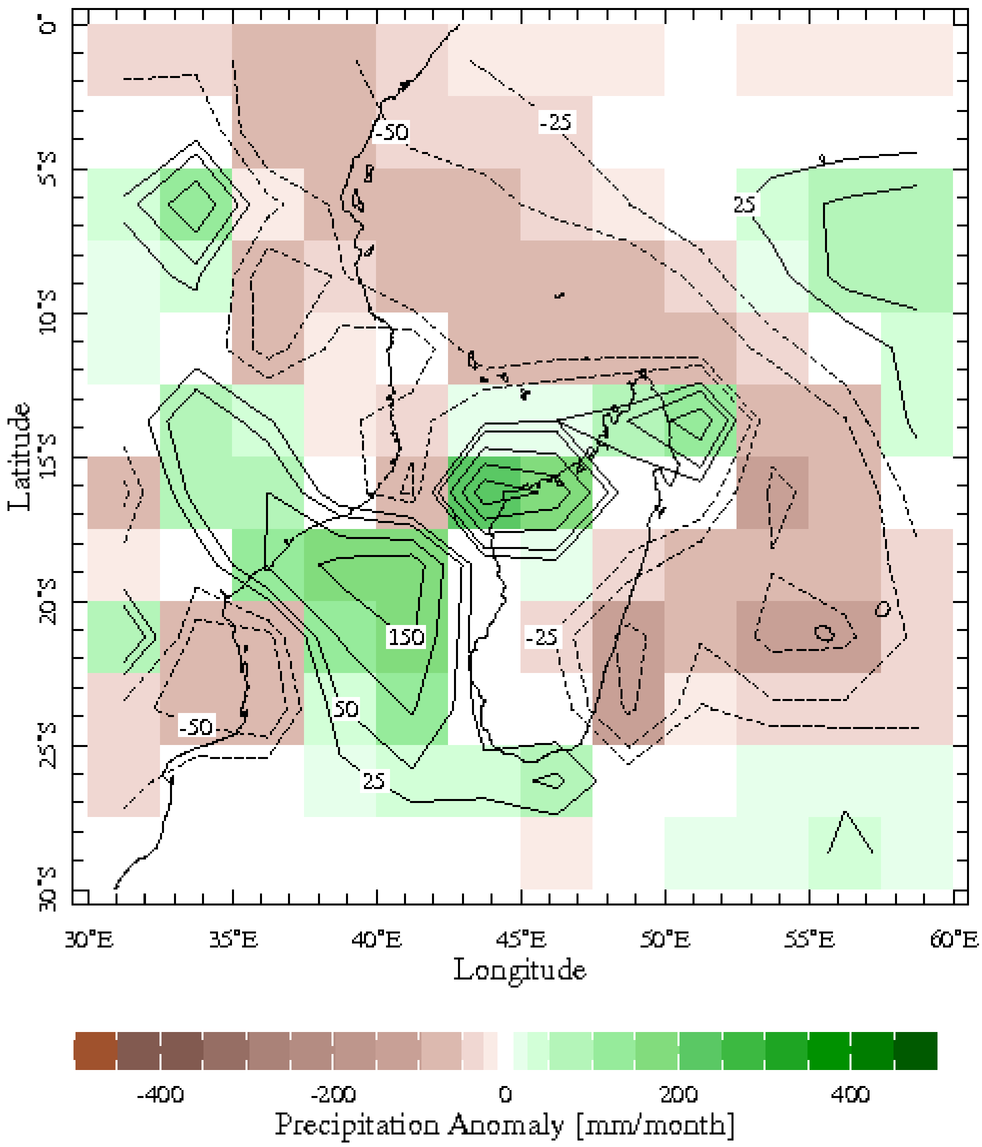

Figure S5: ARGO float trajectory (Plate-form Code 2902142) in the Mozambique Channel. Left: The map shows the float trajectory from Aug-2014 to Feb-2020. Right: Salinity at surface recorded when the float enters the Mozambique Channel in January 2017 (note the minimum in March 2019). Bottom: Salinity section (0-50m) recorded by the float in Jan-May 2019 showing the salinity minimum in late March 2019 after the Cyclone Event Idai. All figures produced with Ocean Data View, ODV (Schlitzer, 2013). Float data obtained from http://www.coriolis.eu.org/Data-Products/Data-Delivery/Data-selection. (Last access, 25-Feb-2020).

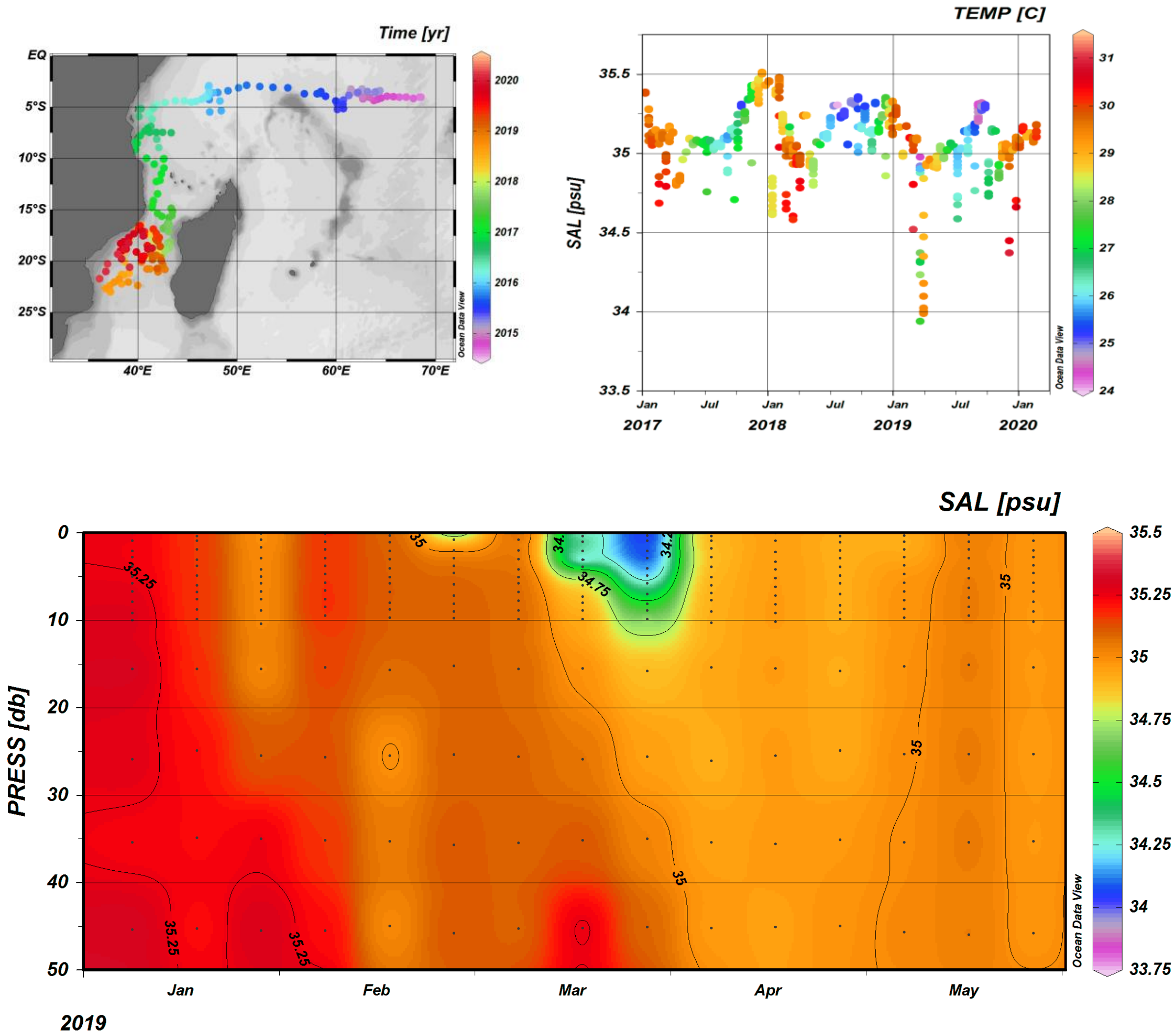

Figure S6: The annual cycle of SST (a), pCO2 (b) and C_T (c) in the Mozambique Channel (at 16°S, 20°S and 24°S) from the climatology (Takahashi et al 2014).

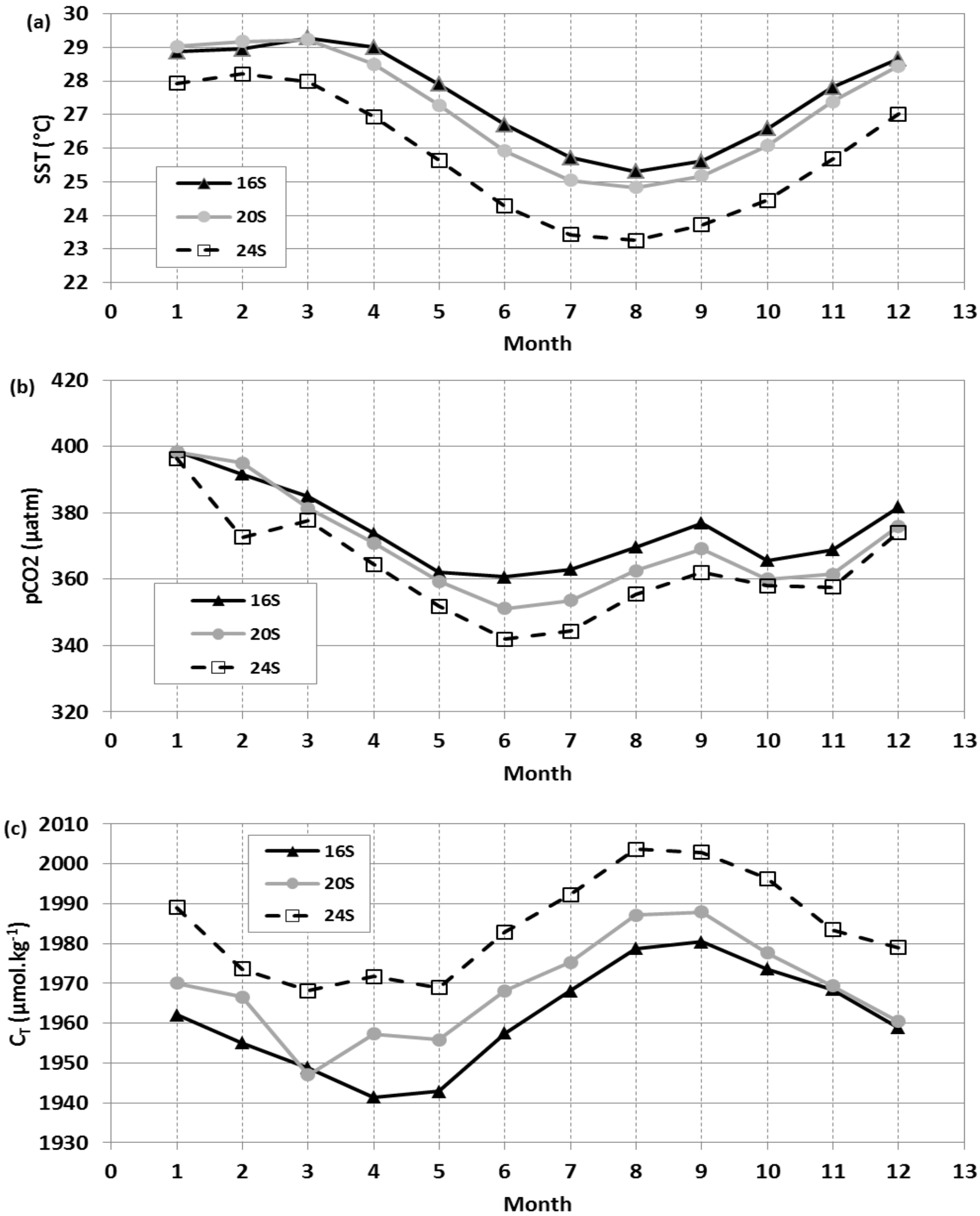

Figure S7: fCO_2 (µatm) versus SST (°C) for January 2004 (orange circles) and April 2019 (blue triangles) in the Mozambique Channel. The green ellipse identifies data in the vicinity of Juan de Nova Islands.

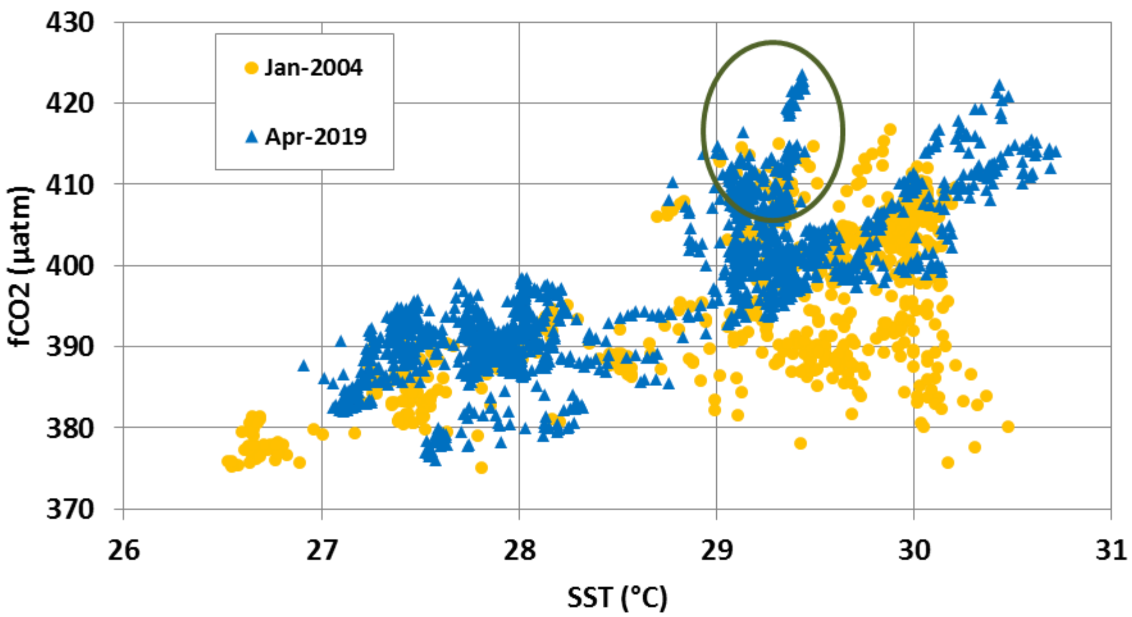

Figure S8: Top: Surface Chl-a (mg.m^{-3}) observations in the Mozambique Channel measured at several locations in January 2004 (orange) and April 2019 (blue). In 2004, the higher Chl-a values at 14-15°S and 22°S explain the low fCO_2 and departure from fCO_2/SST relation (fig S7). In 2019 a minimum in C_T was observed at 15.5°S where Chl-a reached a maximum. Bottom: Map of monthly surface Chl-a (mg.m^{-3}) in the region for January 2004 and April 2019 derived from MODIS data, highlighting the maximum around 22°S in 2004 extended from the coastal zone of Madagascar. In April 2019, MODIS data show higher Chl-a over the central region. Map produced with ODV (Schlitzer, 2013) from data downloaded at http://marine.copernicus.eu/services-portfolio/access-to-products/ (OCEANCOLOUR_GLO_CHL_L4_REP_OBSERVATIONS_009_082), last access, 20-Oct-2020. In both figures the Chl-a scale is 0-0.5 mg.m^{-3}.

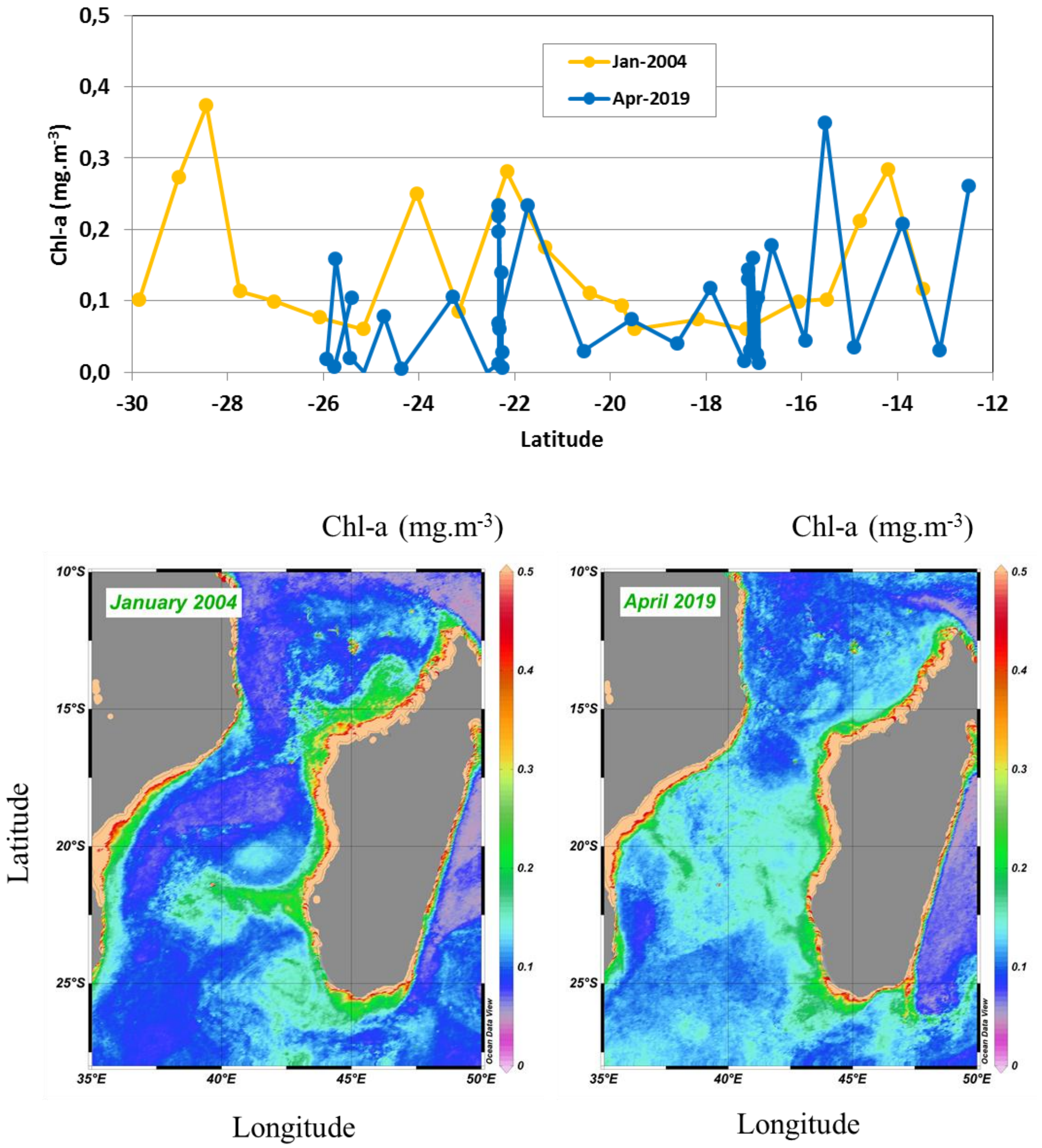

Figure S9: Top: Time-series of monthly sea surface Chl-a concentration (mg.m^{-3}) averaged in the Mozambique Channel (mean in bounding Box: 38E/26S-43E/15S). Data extracted from MODIS (Giovanni/NASA, last access 31/5/20). Bottom: Mean annual cycles of monthly Chl-a (from data in the top figure) and of N-C_T climatology at 20°S/42°E (open triangles, from Takahashi et al 2014). The N-C_T decrease from January to April is in part linked to biological activity.

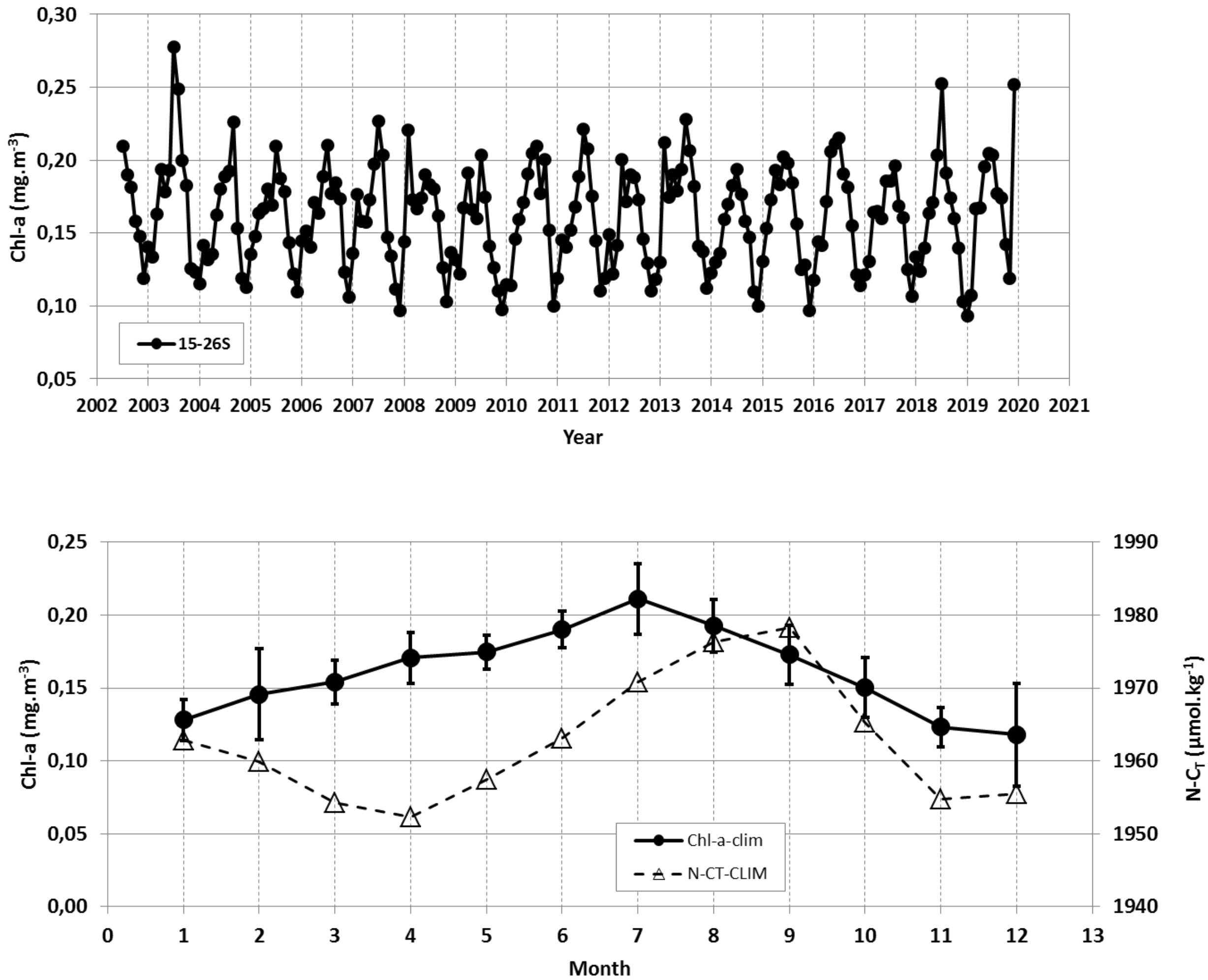

Figure S10: Difference of A_T calculated with different A_T/SSS relationships and measured A_T (January 2004 and April 2019, total 505 data) versus salinity. Only A_T samples from open ocean waters are included (i.e. samples measured closed to Islands are not used). A_T/SSS relationships are from Millero et al. (1998) for the Indian Ocean (open squares), from Lee et al. (2006) for the subtropical oceans (open circles), from January 2004 data (orange circles), from April 2019 data (blue triangles) or using Jan-2004 + Apr-2019 data (noted AT-MOZ, black squares). All relationships lead to the same results with no clear statistical differences. Therefore, in this analysis, we use the relationship derived from January 2004 + April 2019 data: A_T= 73.841* S – 291.02 (as shown in Figure 5, see main text).

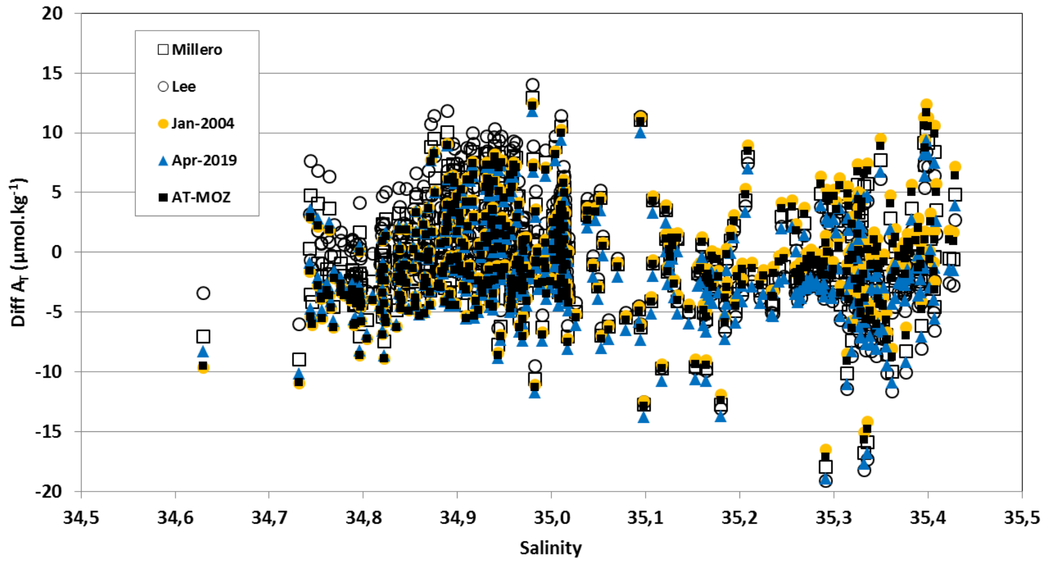

Figure S11: Monthly SST in the Mozambique Channel for the period 1981-2019 The dashed-line is the estimated annual SST trend of +0.011 (+/-0.007) °C.yr^{-1}. Data from Reynolds et al (2002). http://iridl.ldeo.columbia.edu/SOURCES/.NOAA/.NCEP/.EMC/.CMB/.GLOBAL/.Reyn_SmithOIv2/.monthly/ (Last access 1/4/2020).

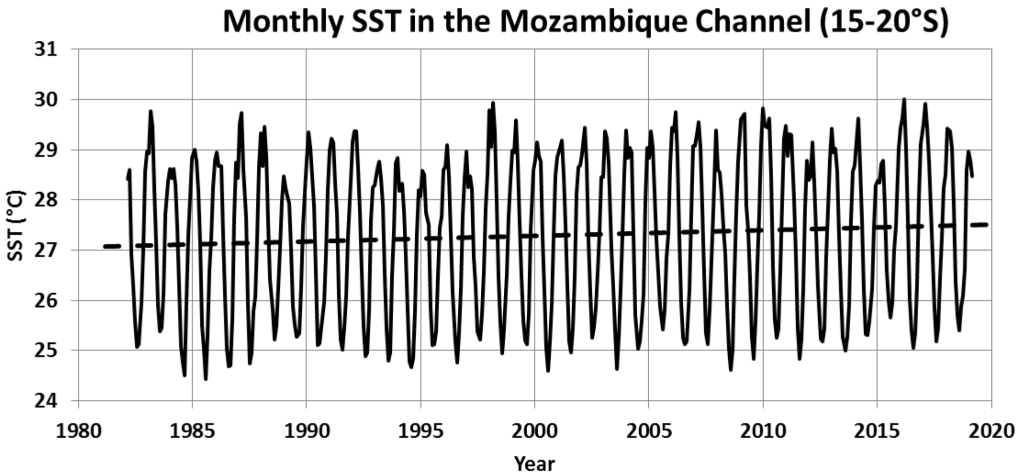

Figure S12: Sea surface distribution of (a) Ω_{Ca} and (b) Ω_{Ar} in the Mozambique Channel calculated from fCO_2 observations in May 1963 (grey), January 2004 (orange) and April 2019 (blue).

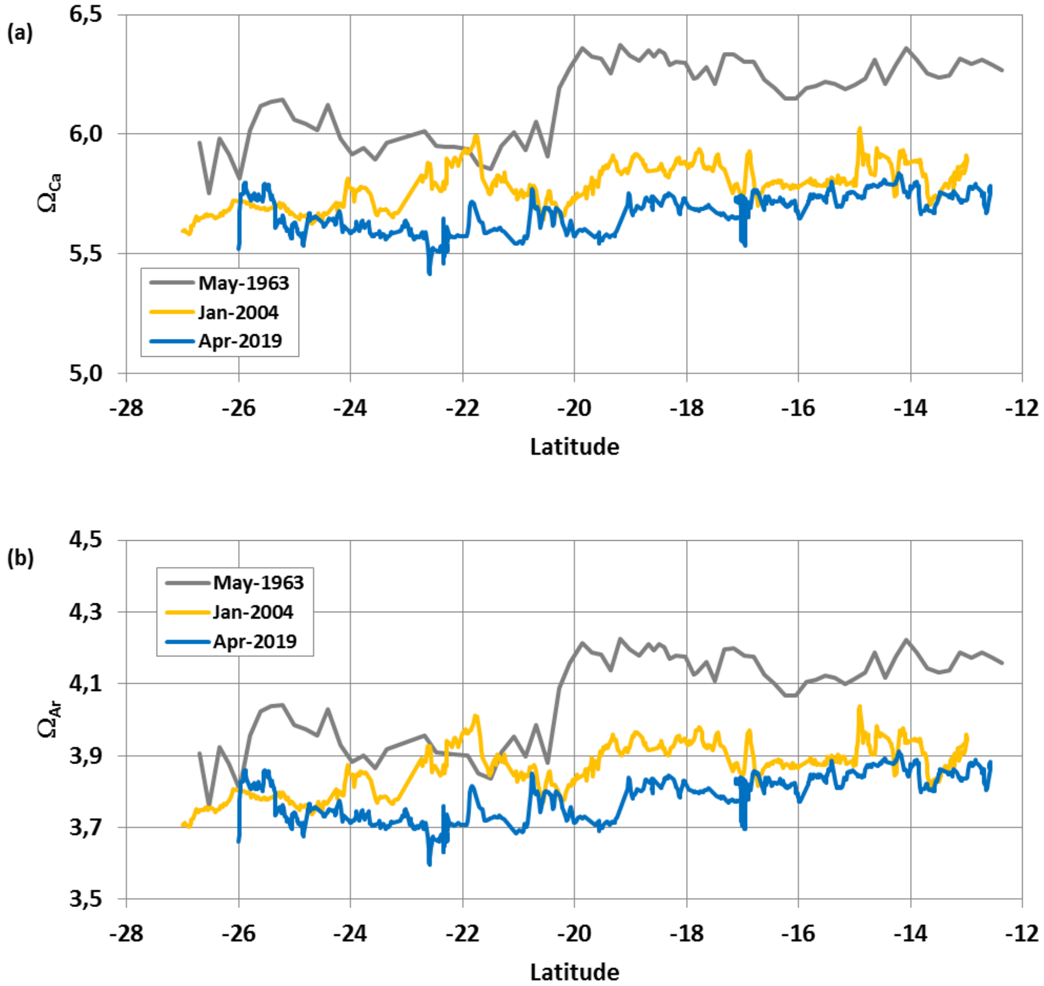

Figure S13: Top: Sea surface water [H+] concentrations around 25°S in the Mozambique Channel based on fCO_2 data in May 1963, June 1995, December 2003, January 2004, July 2014 and April 2019. Bottom: Temporal evolution of [H+] around 25°S in the Mozambique Channel based on data shown on top. [H+] concentrations calculated with fCO_2 and A_T are indicated by black circles (listed in Table 4). Values adjusted to the month of June indicated by grey diamond and used for trend estimates (dashed grey lines). Trends for 1963-1995 and 1995-2019 are respectively +0.0212 $nmol.kg.yr^{-1}$ and +0.0409 $nmol.kg.yr^{-1}$.

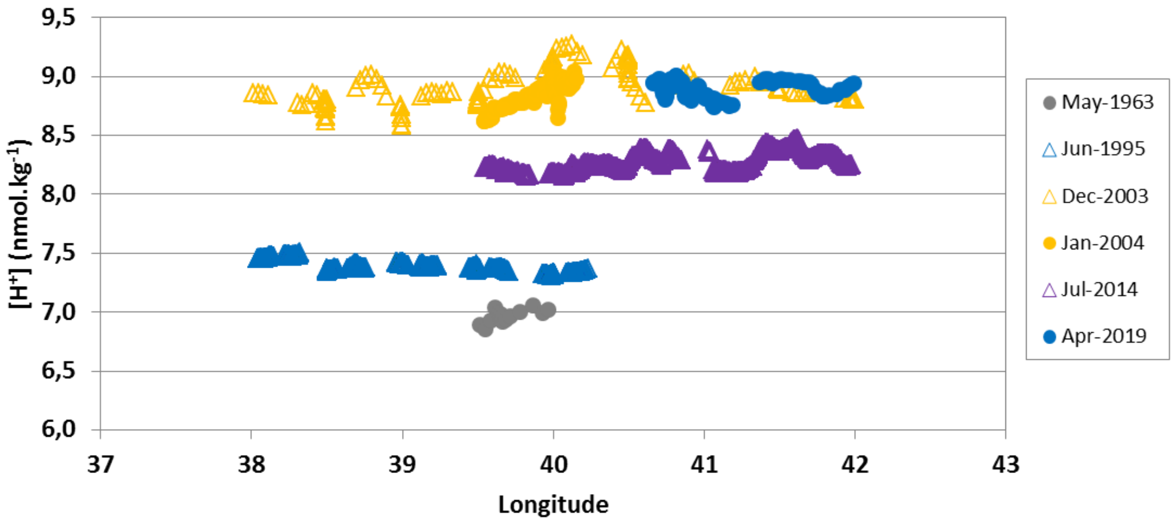

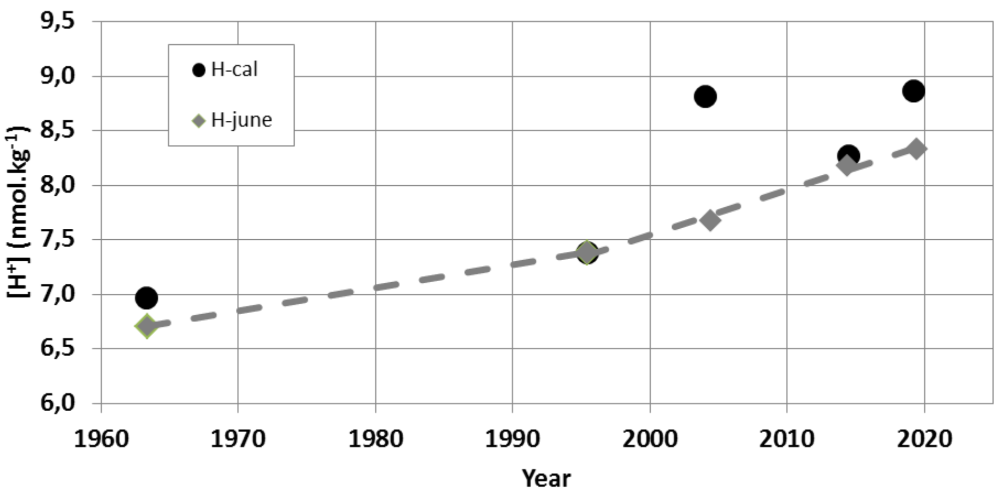

Figure S14: Distribution in the top 1000m of C_{ant} accumulated between 1994 and 2007 (Delta-C_{ant} in μmol.kg^{-1}) in the Mozambique Channel. Data are from Gruber et al., (2019b). Figure produced with Ocean Data View, ODV (Schlitzer, 2013).

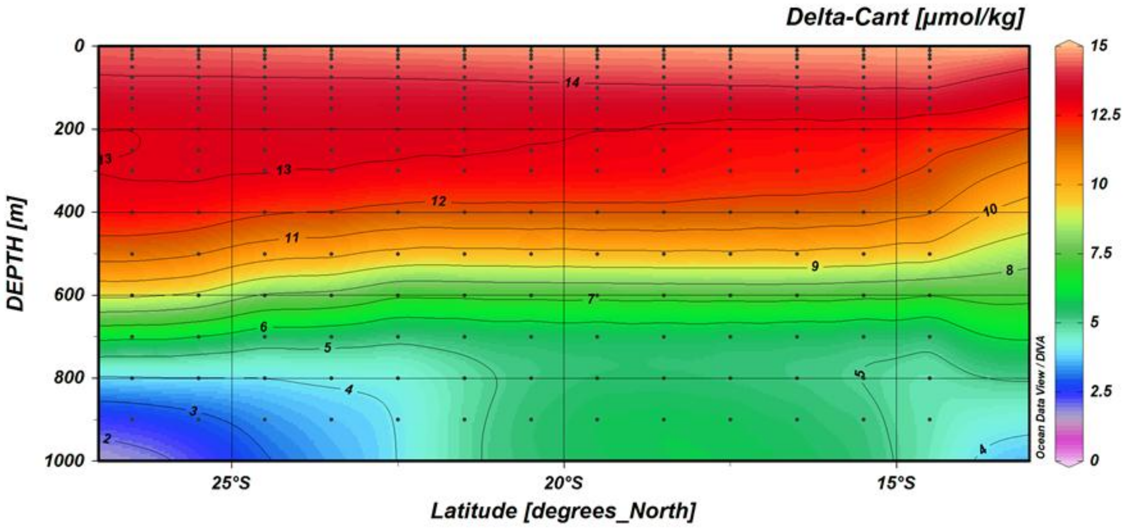

Figure S15: Reconstructed Aragonite saturation state (Ω_{Ar}) based on atmospheric xCO_2 historical data for seasonal fCO_2 (grey line) or assuming equilibrium (orange line). Calculated values from fCO_2 and A_T/SSS observations in 1963 to 2019 are also shown (blue triangles). The Orange circle identifies Ω_{Ar} = 3 in 2040 if the observed trend in recent decade is projected.

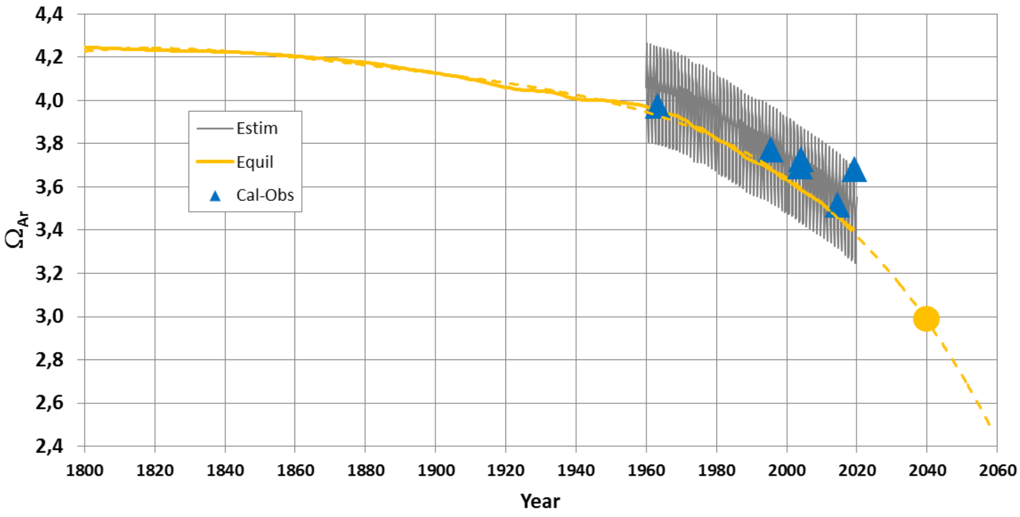

Methods for trends and uncertainties estimates

Trends and associated uncertainties provided in Tables 2, 3, 5 and in the main text are estimated as the means of slopes and standard deviation derived from the computation of linear least-squares regressions on Monte Carlo simulations. In general, 100000 samples are drawn from the Gaussian distribution with empirical means and standard deviation calculated from the observations (see in Tables 2, 3, 4) or the CMEMS-LSCE-FFNN model. The *stats.linregress* function in the *scipy* python package is used to fit a linear least-squares regression for two sets of data (e.g., measurements against datetime values) for each sample and for different time periods. Illustrations of this Monte Carlo approach on fCO_2 and pH, and other statistics to assess the significance of the regression analysis for all variables are shown in this Supplementary Materials (Tables S1, S2, Figures S16 and S17). These statistics include the 68% confidence interval (CI, mean ± uncertainty) of all slope estimates, the root mean square deviation (RMSD, the standard error between the target sample and the fit), and coefficient of determination (r^2, the degree of linear correlation between the target sample and the fit). Details of the regression analysis based on the observations and the model outputs are described as follows:

a. Trends evaluated from observations/calculations:

Given the means of observations or calculated variables, their standard deviations and measurement/calculation errors (see in Tables 2, 3, 4), we first compute the total uncertainty for each variable (e.g., pH) in each year (e.g., 1963). This total uncertainty is defined as the square root of the sum squared of the two sources of observation/calculation uncertainty. The individual observations are not used directly for the analysis but their mean values after adjustment to the month of June. For each iteration of 20 bootstrapping cycles, we generate, for each year, Nb pseudo-data (the corresponding number of observations in the year of interest, e.g., Nb= 15 in 1963) based on the calculated mean and uncertainty. This step allows recreating a set of individual pseudo-observations for the month of June which is statistically equivalent to the original data set. Then, these data are resampled to create a new ensemble of data with the size N = 5000, the slope and intercept as well as other statistics for different period are calculated for each realization in this ensemble. Figure S16 illustrates the method for the 1963-2019 and a sub-period (2004-2019).

b. Trends evaluated from the CMEMS-LSCE-FFNN model outputs

The CMEMS-LSCE-FFNN model provides a reconstruction of fCO_2 and pH from an ensemble-based approach. Monthly mean and model uncertainty are available at 1°x1° resolution. June data or the monthly data in the Mozambique Channel are extracted for the trend analysis and for comparison to those from the observations. The annual trend and uncertainty reported in Table 5 are calculated on the annual mean of the monthly data. Here we directly generate 100000 samples and fit linear functions among them. Figure S17 shows an illustration of the regression on only 500 realizations for fCO_2 and pH in June 1985-2019 and 2004-2019.

Table S1: Statistics for regression analysis on trends of surface properties and pH (see Tables 2, 3) in the band 14°S-25°S in May 1963, January 2004 and April 2019. These statistics include the 68% confidence interval (CI, mean ± uncertainty) of all slope estimates, the root mean square deviation (RMSD, the standard error between the target sample and the fit), and the coefficient of determination (r^2, the degree of linear correlation between the target sample and the fit).

Periods	fCO_2 $\mu atm.yr^{-1}$			$N\text{-}C_{Tca}$ $\mu mol.kg^{-1}.yr^{-1}$			$N\text{-}C_{Tmes}$ $\mu mol.kg^{-1}.yr^{-1}$		
	[68% CI]	RMSD	r2	**[68% CI]**	RMSD	r2	**[68% CI]**	RMSD	r2
2004-2019	[0.94, 2.56]			[0.19, 1.81]			[0.25, 1.83]		
1963-2004	[1.26, 1.81]			[0.61, 1.40]					
1963-2019	[1.40, 1.76]	0.22	0.98	[0.72, 1.29]	0.22	0.94			
	pH (fCO_2) $TS.yr^{-1}$			pH (A_T-C_T) $TS.yr^{-1}$					
2004-2019	[-0.00255, -0.00054]			[-0.00309, -0.0001]					
1963-2004	[-0.00193, -0.00115]								
1963-2019	[-0.00182, -0.00126]	0.00026	0.97						

Table S2: Statistics for regression analysis on trends observed around 25°S in the Mozambique Channel evaluated from observations and from the monthly reconstructed pCO_2 and pH values based on a neural network model (CMEMS-LSCE-FFNN, Denvil-Sommer et al 2019; Chau et al 2020) between 1963 and 2019 adjusted to June (as shown in Figure 10 and Tables 4,5). These statistics include the 68% confidence interval (CI, mean ± uncertainty) of all slope estimates, the root mean square deviation (RMSD, the standard error between the target sample and the fit), and the coefficient of determination (r^2, the degree of linear correlation between the target sample and the fit). For CMEMS-LSCE-FFNN the trends are computed for the month of June or using the annual mean of all months over 1985-2019.

	Periods	fCO_2(µatm.yr^{-1})			H+ (nmol.kg^{-1}.yr^{-1})			pH (TS.yr^{-1})			N-C_T (µmol.kg^{-1}.yr^{-1})		
		[68% CI]	RMSD	r2	**[68% CI]**	RMSD	r2	**[68% CI]**	RMSD	r2	**[68% CI]**	RMSD	r2
Observations	1963-2019	[1.44, 1.66]	0.21	0.95	[0.0255, 0.0326]	0.0049	0.92	[-0.00188, -0.00147]	0.00026	0.93	[0.83, 1.25]	0.20	0.89
	1963-1995	[0.90, 1.37]			[0.0144, 0.0283]			[-0.00171, -0.00087]			[0.41, 1.23]		
	1995-2004	[0.90, 2.51]			[0.0076, 0.0559]			[-0.00329, -0.00004]			[-0.10, 2.40]		
	1995-2019	[1.93, 2.46]	0.30	0.96	[0.0327, 0.0497]	0.0089	0.91	[-0.00275, -0.00179]	0.0049	0.91	[0.95, 1.79]	0.44	0.82
	2004-2019	[1.98, 2.84]	0.50	0.96	[0.0307, 0.0597]	0.0152	0.89	[-0.00322, -0.00164]	0.00083	0.89	[0.77, 2.14]	0.76	0.78
CMEMS-LSCE-FFNN	1985-2019 June	[1.74, 2.03]	0.16	0.82				[-0.00220, -0.00172]	0.00025	0.66			
	1995-2004 June	[0.74, 2.65]	0.88	0.34				[-0.00349, -0.00023]	0.00158	0.22			
	1995-2019 June	[2.04, 2.51]	0.25	0.78				[-0.00272, -0.00195]	0.00040	0.60			
	2004-2019 June	[1.94, 2.96]	0.51	0.62				[-0.00325, -0.00169]	0.00078	0.42			
	1985-2019 Annual	1.71, 1.89]	0.08	0.93				[-0.00189, -0.00165]	0.00011	0.88			
	1995-2004 Annual	[1.55, 2.50]	0.47	0.69				[-0.00274, -0.00132]	0.00072	0.50			
	1995-2019 Annual	[1.74, 2.03]	0.14	0.89				[-0.00199, -0.00161]	0.00019	0.80			
	2004-2019 Annual	[1.50, 2.10]	0.29	0.73				[-0.00203, -0.00127]	0.00037	0.60			

Figure S16: Trend analysis on a Monte Carlo simulation of fCO_2 and pH observed around 25°S in the Mozambique Channel, and adjusted to June (blue stars: mean values of observations, light blue bars: mean ± total uncertainty, black points: pseudo samples, grey and light blue lines: linear functions fitted to the samples and mean observations).

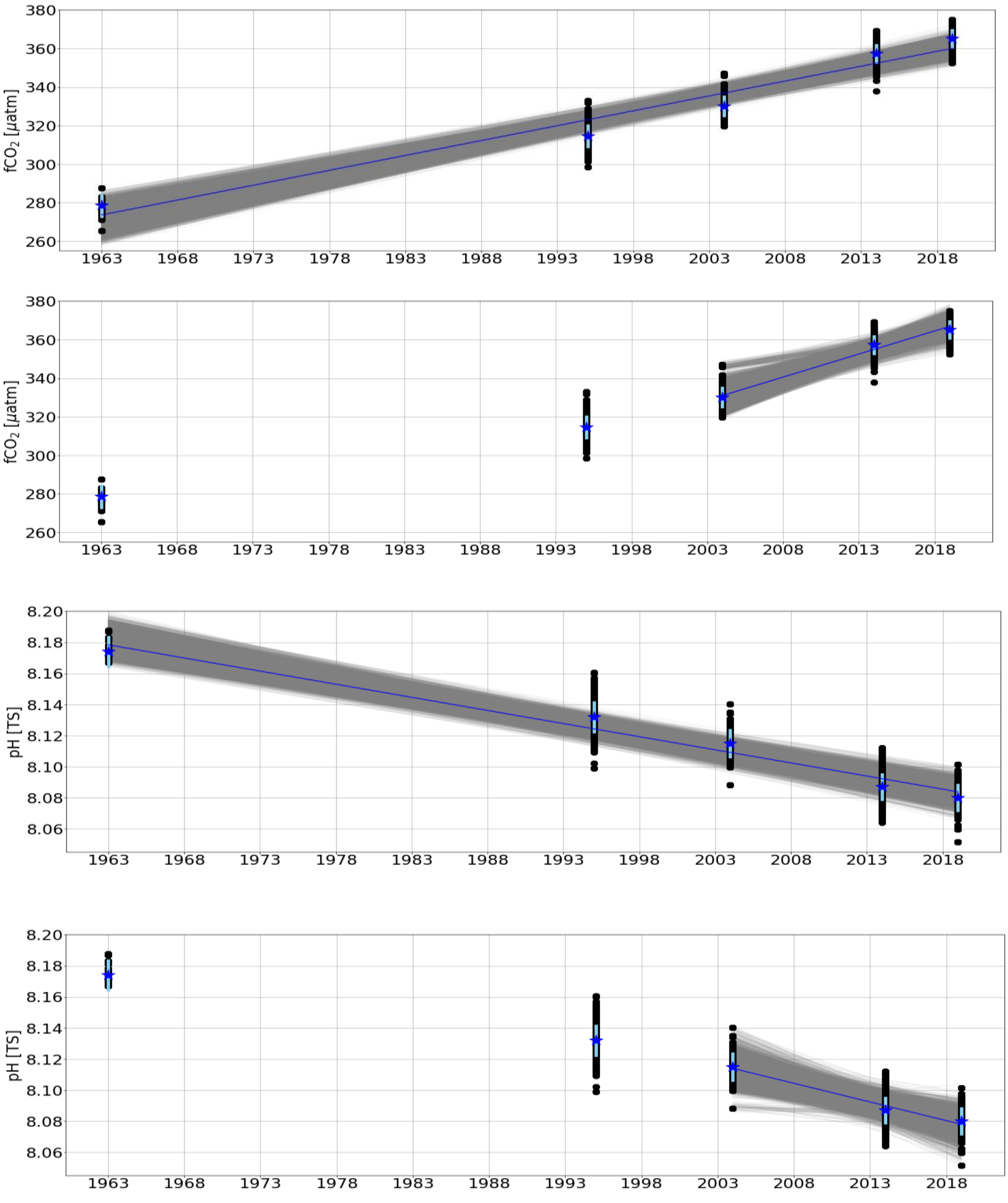

Figure S17: Trend analysis on a Monte Carlo simulation of the CMEMS-LSCE-FFNN estimates for fCO_2 and pH around 25°S in the Mozambique Channel in June for 1985-2019 or 2004-2019 (blue stars: mean values of observations, light blue envelop: mean ± model uncertainty, black points: pseudo samples, grey and light blue lines: linear functions fitted to the samples and mean observations).